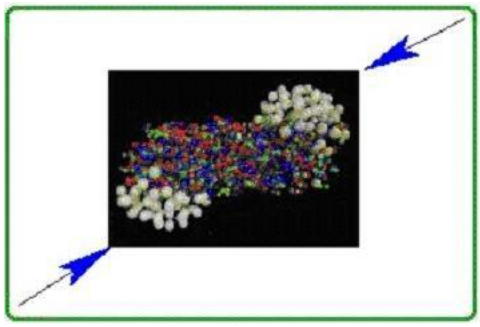

High Energy

High Intensity

Hadron Beams

Proceedings of 5th CARE-HHH-ABI Workshop on

"Schottky, Tune and Chromaticity Diagnostic (with real time feedback)"

Chamonix Mont-Blanc, 11-13 December, 2007

Edited by K. Wittenburg

DESY, Hamburg, Germany

Abstract

This report contains the final proceedings of the 5th meeting in the framework of the CARE-HHH-ABI networking, held 11. -13. December 2007, in Chamonix Mont-Blanc, with the subject: "Schottky, Tune and Chromaticity Diagnostic (with real time feedback)".

Proceedings of 5th CARE-HHH-ABI Workshop on

"Schottky, Tune and Chromaticity Diagnostic (with real time feedback)"

Chamonix Mont-Blanc, 11-13 December, 2007

The European Community reinforces the communication between scientific laboratories of similar nature in the field of high energy high intensity hadron beams.
For this reason a so called "networking" program has been defined, which over the next five years will join experts in the field of beam instrumentation and related controls activities. The principle purpose of these meetings is to exchange knowledge on well defined subjects. (CARE-N3 networking for HHH, i.e. for high energy, high intensity hadron beams). These events are not in concurrence with more general instrumentation workshops like DIPAC or BIW.
The 5th event of this nature is proposed by Kay Wittenburg (DESY), Peter Forck (GSI) and H. Schmickler (CERN) with the following topic:

"Schottky, Tune and Chromaticity Diagnostic (with real time feedback)".

December 11th-13th 2007 in Hotel Prieuré, 74404 Chamonix Mont-Blanc, (France).
The purpose of the event was:
- To discuss in detail technology issues related to the subjects.
- To understand the specifications for upcoming new hadron facilities
- To propose concrete work packages for the coming years in order to meet the specified objectives. For these objectives the experts from the major three European laboratories working with hadron beams (DESY; GSI; CERN) and experts from other institutes were brought together.

List of participants:

- CERN:Rhodri Jones, Marek Gasior, Ralph Steinhagen, Andrea Boccardi, Fritz Caspers, Eugenia Hatziangeli, Maria-Elena Angoletta,Mike Lamont, Jocelyn Tan,Tom Kroyer, M. Giovannozzi, Hermann Schmickler
- GSI: Peter Forck, V.Kornilov, Piot Kowina, Udo Rauch
- DESY: Kay Wittenburg, Jens Klute, Hans-Thomas Duhme
- FZ Jülich: Jürgen Dietrich
- BNL : Pete Cameron
- FNAL: C.Y.Tan, Andreas Jansson, Ralph Pasquinelli
- PSI: Micha Dehler

The schedule:

1 day: Tuesday 11. Dec.: ("Schottky Diagnostics"; Chairman: Peter Forck)
2 day: Wednesday 12. Dec.: ("Tune and Chromaticity Diagnostics"; Chairmen: H. Schmickler and K. Wittenburg)
3 day: Thursday 13. Dec: ("Real Time Feedback on Tune and Chromaticty; Handling Machine Coupling"; Chairman: Rhodri Jones)

Contents:

1st day: Schottky Diagnostics

Chair: P. Forck (GSI)

Speaker	Affiliation	Title	Page
F. Caspers	CERN	Schottky Tutorial : Schottky signals for longitudinal and transverse bunched beam diagnostics	5
R. Pasquinelli	FNAL	LARP LHC Schottky	11
V. Kornilov	GSI	Transverse Schottky Signals and BTF with Space Charge	13
J. Tan	CERN	Experimental results from LEIR	17
M-E. Angoletta	CERN	The AD Schottky System	24
A. Jansson	FNAL	Schottky Observations at the TEVATRON	37
T. Kroyer	CERN	The LHC Schottky System	40
P. Cameron	BNL	Schottky Observations at RHIC	withdrawn
P. Forck	GSI	**Discussion**	43
		(Add. DESY-HERA report: Longitudinal Schottky Signal Monitoring for Protons in HERA, EPAC 2000	44

2nd day: Tune and Chromaticty Diagnostics

Chairs: H. Schmickler (CERN) and K. Wittenburg (DESY)

Speaker	Affiliation	Title	Page
P. Forck	GSI	Requirements for the FAIR Project	47
M. Giovannozzi	CERN	Tune, Chromaticity & Coupling Observables	49
C.Y. Tan	FNAL	Tune Measurement at the Tevatron	53
J. Dietrich	Juelich	Tune measurements at COSY with noise excitation	56
U. Rauch	GSI	Investigations on BaseBand tune measurements using direct digitized BPM signal	58

M. Gasior	CERN	The BaseBand Tune (BBQ) System	63
R. Jones	CERN	The Head-Tail Chromaticity Measurement Technique	66
C.Y. Tan	FNAL	Continuous Head-Tail chromaticity measurement	70
C.Y. Tan	FNAL	The Tevatron PLL System for Q Measurement	73
H. Schmickler, K. Wittenburg	CERN, DESY	**Discussion** Topic assigned: HERA tune measurments: Tune Measurement with Chirped Excitation, by S. Herb, -DESY-; CERN Tune/PLL Workshop, June 10,11 2002	77

3rd day: Real Time Feedback, Handling of Coupling, Details of Implementation

Chair: R. Jones (CERN)

Speaker	Affiliation	Title	Page
R. Steinhagen	CERN	Introduction to Beam-based Feedback Design, Actuators for Tune, Chromaticity and Coupling Feedback	84
M. Dehler	PSI	Requirements for Tune, Coupling and Chromaticity Feedbacks for Light Sources	93
J. Klute	DESY	Tune Measurement & correction at HERA-p	97
A. Boccardi	CERN	The LHC PLL System for Q, Q' and |C| Measurement	101
P. Cameron	BNL	RHIC Tune and Coupling Feedback Results, and Plans for Chromaticity Measurement and Feedback during Run 8	withdrawn
H. Schmickler	CERN	**Closing**	

SCHOTTKY SIGNALS FOR LONGITUDINAL AND TRANSVERSE BUNCHED BEAM DIAGNOSTICS

Fritz Caspers, Jocelyn Tan, CERN, Geneva, Switzerland

Abstract

Following a brief historical overview on the origin and the evolution of Schottky noise we discuss applications in the field of beam diagnostics in particle accelerators. A very important aspect of Schottky diagnostics is the fact that it is a non perturbing method. Essentially statistics based, it permits to extract beam relevant information from rms (root mean square) noise related to the movement of the individual particles. This is also the basis for stochastic cooling. Schottky diagnostics permits one to extract a considerable number of important beam parameters such as the revolution frequency, momentum spread, incoherent tune, chromaticity and emittance.

INTRODUCTION

In the year 1918 the German physicist Walter Schottky (* 23 July 1886 in Zurich) published a paper describing the mechanism of spontaneous current fluctuations in different conductors. This is the origin of the term Schottky noise. The term Schottky noise refers both to thermal noise in resistors and noise in charged particle beams. Additional important contributions from Walter Schottky are the Schottky diode, Schottky defects (in semiconductors) and the Schottky equation (Langmiur – Schottky equation for space charge). In 1915 Schottky invented the tetrode and in 1918 he pioneered the superhet concept. In 1928 the thermal noise in resistors was first measured by J.B Johnson (Bell Labs) and he discussed his findings with Harry Nyquist who worked at the same laboratory. This is the origin of the term Johnson-Nyquist noise which is more frequently used in the English literature when referring to thermal noise.

An important milestone in accelerator technology was the invention of the stochastic cooling concept in 1968 by Simon van der Meer (Nobel price shared with Carlo Rubbia in 1984). Clear Schottky noise signals from a strong coasting (unbunched) beam of protons were observed in 1972 in the CERN–ISR (Intersecting Storage Rings) followed in the same year by the first publication of the cooling idea by Simon van der Meer [1]. In 1975 schemes for pbar accumulation were developed and tested experimentally with protons in 1976 (ICE = Initial Cooling Experiment). Over the following years a rapid worldwide evolution of beam diagnostics with Schottky noise took place, both for bunched and unbunched beams. Nowadays Schottky diagnostics is a vital element in nearly all large circular machines operating with hadrons and also to a certain extent for electron rings and even linacs. The information extracted this way allow continuous monitoring of important beam parameters and the control of a number of related machine settings.

SHOT NOISE IN A VACUUM DIODE

Consider a simple vacuum diode (fig 1) where a small number of electrons pass from a heated cathode to the anode [2].

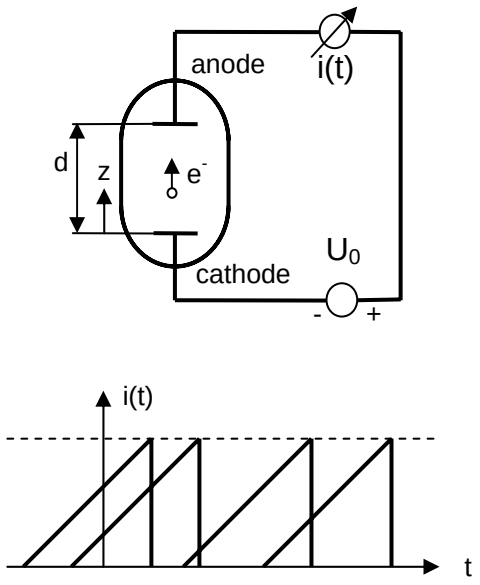

Fig. 1 a: Vacuum diode with two electrodes (from [2])
Fig. 1 b: Anode current related to individual electrons

When a single electron is emitted from the cathode and starts moving to the anode (due to the acceleration voltage U_0) an approximately linear increase of current at the anode is measured. This is due to the dD/dt (D = dielectric displacement) related displacement current which continues as a conducting current when the electron approaches the flat anode. Each of these saw tooth like signals (fig 1b) has a length τ which is the travel time of the electron from the cathode to the anode. As the individual electrons are emitted in a random manner, those saw tooth like signals occur as a non periodic time function. This is very similar to the time function of acoustic noise originating from little grains falling on a metal plate and is the origin of the term “shot noise”.

If we assume this diode to be working in the saturated regime (i.e. the anode voltage is high enough that all emitted electrons are accelerated to the anode and there is no space charge cloud near the cathode) then, after some

derivation, the "low "frequency spectral density $S_i(\omega)$ of the short circuit current can be expressed as

$$S_i(\omega) = 2I_0 e \qquad (1)$$

where e is the elementary charge of an electron with $v_{mean} = N/\tau$ and I_0 stands for the mean current as defined by $I_0 = e\, v_{mean}$.

Obviously the travel time τ plays a very important role for the range of validity of this formula. Typical τ values for vacuum diodes operated at a few 100 volts and a cathode anode spacing of around a cm are in the order of a fraction of a nanosecond. This translated to maximum frequencies in the GHz range (fig 2).

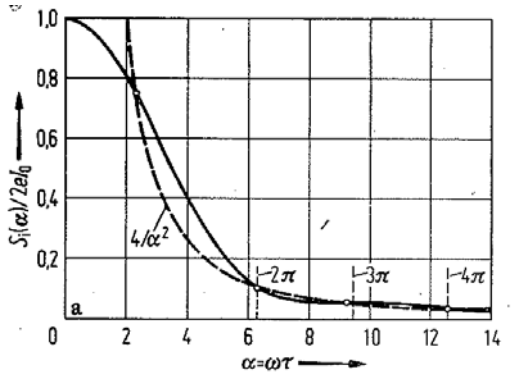

Fig. 2: Normalized spectral density as a function of the transit time angle α (from [2])

In a similar manner, starting from the saturated high vacuum diode, via the vacuum diode in the space charge region and then applying the theory [2] to a biased and unbiased solid state diode one can finally arrive at the noise properties of a linear resistor. This general relation for the open (unloaded) terminal voltage u of some resistor in thermo dynamical equilibrium for a frequency interval Δf, which is also valid for very high frequencies f and/or very low temperatures T (K), is given by

$$\overline{u^2} = 4k_B TR \frac{hf / k_B T}{\exp(hf / k_B T) - 1} \Delta f \qquad (2)$$

Here h=6.62· 10^{-34} J·s is Planck's constant and k_B = 1.38·10^{-23}J/K equals Boltzmann's constant. From this general relation it is possible to write the low frequency approximation, which is still reasonably valid at ambient temperature up to 500 GHz, as (open terminal voltage)

$$\overline{u^2} = 4k_b T\Delta f\, R \qquad (3)$$

and for the short circuit current we get accordingly

$$\overline{i^2} = 4k_b T\Delta f / R \qquad (4)$$

Note that the factor 4 in equations (3) and (4) often leads to confusion. When **terminating** a noisy resistor with an "external load" consisting of a resistor of the same ohmic value (power match) but at 0K temperature one can visualize the "available noise power". This power delivered to an external load is given by

$$P = k_b T\Delta f \qquad (5)$$

and is independent of the value of R! For the power density p per unit bandwidth an even simpler relation is obtained

$$p = k_b T = -174 dBm/Hz \ @300\text{K} \qquad (6)$$

This relation is also valid for networks of linear resistors with a homogenous temperature between any two terminals. In fact a normal carbon resistor is already such a network of many tiny carbons grains. Equation (6) does not apply to resistors or resistor networks which are not at a homogeneous temperature. In particular, devices which are not in thermo dynamical equilibrium such as a DC biased diode or a transistor connected to some supply voltage are excluded. Such "active" resistors may have noise temperatures which are considerably below their physical temperature and can be used as a pseudo-cold loads in order to avoid bulky and costly cryogenics [3]. As an example one may take the typical TV satellite receiver front-end where the actual input amplifier has a noise temperature of about 50-70 K in the 10-12 GHz range. In the CERN LEIR machine the concept of pseudo-cold terminations in the 100 MHz range has been applied for strip-line type pick-ups [4].

THE FIELD SLICE OF FAST AND SLOW BEAMS

Similar to what has been shown for the planar vacuum diode, where the spectrum is a function of the electron velocity and the spacing between cathode and anode, particles in a particle accelerator produce $\beta = v/c$ related spectral modifications in the beam-pipe. This is linked to the fact that virtually all Schottky monitors interact in one way or the other with the image current on the inner surface of the beam-pipe. For slow beams the "field slice" has a certain opening angle (roughly ~1/γ) which causes a "smear out" of the spatial resolution and thus limits the maximum observable frequency as a function of beam-pipe diameter and γ-value. Figure 3 gives a nice impression how the "field slice" contraction for increasing beam velocity enhances the spectral content in the image current towards higher frequencies.

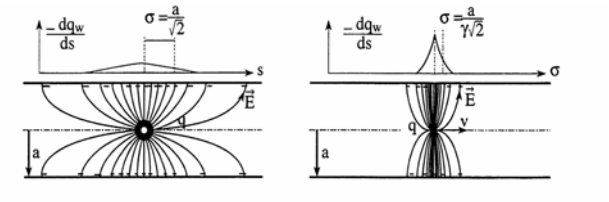

Fig. 3: Electromagnetic field of slow and fast beams (from [5])

SINGLE PARTICLE CURRENT

Consider a single particle circulating in some storage ring with a constant frequency $\omega_0 = 2\pi f_0 = 2\pi/T$. This particle will induce a certain signal on some pick-up at its passage time t_k

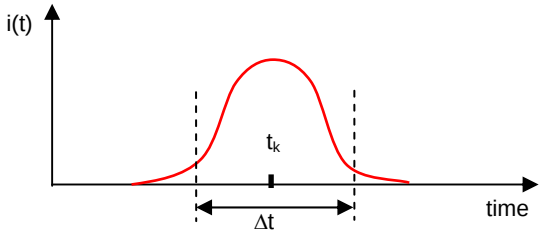

Fig 4 : Pick-up signal of a single particle

For a highly relativistic particle and a pick-up with infinite bandwidth this signal should have length $\Delta t \approx 0$ and can be approximated as a Dirac pulse. The signal over m ($m \to \infty$) revolutions can be expressed as:

$$i_k(t) = \frac{e}{T}\sum_m \delta(t - t_k - mT) \qquad (7)$$

Applying the Fourier expansion to $i_k(t)$ gives

$$i_k(t) = i_0 + 2i_0\sum_{n=1}^{\infty} a_n \cdot \cos n\omega_0 t + b_n \cdot \sin n\omega_0 t \qquad (8)$$

with $\begin{cases} i_0 = ef_0 \\ a_n = \cos n\varphi_k \quad \text{and} \quad b_n = \sin n\varphi_k \end{cases}$

This leads to a corresponding series of Dirac pulses in the frequency domain.
With a second particle at a slightly different frequency $f_1 = f_0 + \Delta f$ with

$$\Delta f = f_0 \times \eta \frac{\Delta p}{p} \qquad (9)$$

one obtains the situation shown in Fig 5. The frequency difference Δf at each harmonic of the revolution frequency f_0 then increases proportionally to the harmonic number n.

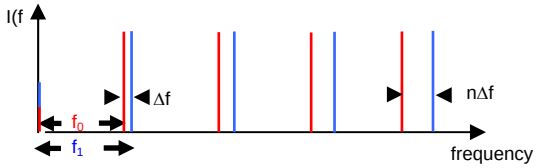

Fig. 5: Two particles with a slight frequency offset Δf

LARGE NUMBER OF PARTICLES IN LONGITUDINAL PHASE SPACE

Now we have to deal with the problem that we have a large number N of particles with (for the moment) equal revolution frequency, but random initial phase $\varphi_k = \omega_0 t_k$. This will result in some amount of mean current $I_0 = Ni_0$, which is proportional to the number of circulating particles in the machine and which does obviously not depend on the initial phase of each individual particle, and fluctuations caused by the random phases

$$I(t) = I_0 + \Delta I$$

where the fluctuations are given by

$$\Delta I = \sum_{n=1}^{\infty} I_n = 2i_0 \sum_{n=1}^{\infty} A_n \cdot \cos n\omega_0 t + B_n \cdot \sin n\omega_0 t \qquad (10)$$

$$A_n = \sum_k^N \cos(n\varphi_k) \qquad B_n = \sum_k^N \cos(n\varphi_k)$$

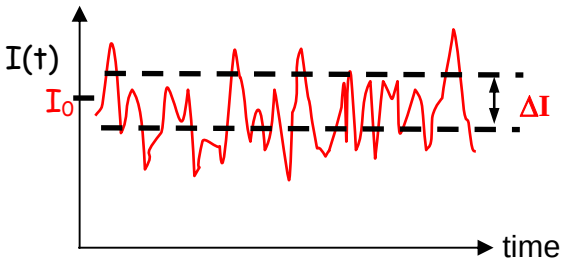

Fig. 6 : Illustration of mean current and fluctuations ΔI

In the total current $I(t)$ the n-th harmonic contains the contributions of all N particles. On a time display one can only recognize a noise trace with some DC offset. But in the frequency domain distinct bands (Fig. 5) occupied with noise would become visible. Notice that for the current fluctuations the amplitude ΔI shown in Fig. 6 is a ± 1σ value and that the peak excursions seen on a scope will be much higher due to the fact that we have a Gaussian amplitude density distribution [6].

Omitting a few intermediate steps in the derivation, one obtains the following expression for the mean square current fluctuations contained in the n-th harmonic

$$\langle I_n \rangle^2 = \frac{(2i_0)^2}{2} \sum_{k=1}^{N} \cos^2 n\varphi_k + \sin^2 n\varphi_k = 2e^2 f_0^2 N$$

or

$$\langle I_n \rangle^2 = 2e^2 f_0^2 N = 2eI_0 f_0 \quad [\mathrm{A}^2] \qquad (11)$$

In this relation, which describes the probable power contribution to the n-th Schottky band for a group of N **mono-energetic** particles, results in a set of equal lines in the frequency domain, spaced by f_0. There is no dependency on the harmonic number. The current fluctuations (Fig 6) now appear as:

$$\Delta I = I_{rms} \sum_{n=1}^{\infty} \cos(n\omega_0 t - \varphi_n)$$

$$\text{with } I_{rms} = 2ef_0\sqrt{\mathrm{N}} \qquad (12)$$

In the case of ions with charge number Z (i.e. each ion presenting a "macro-particle" with charge $Z\,e$), the e in the above equation is replaced by $Z\,e$:

$$\langle I_n \rangle^2 = 2(Ze)^2 f_0^2 N \qquad (13)$$

Note that the power in the fluctuations is proportional Z^2 which means that a single fully stripped uranium ion gives the same signal as about 8500 protons.
Of course it is not realistic to assume that all particles have the same revolution frequency as this would imply either an η-value of 0 or a vanishing momentum spread. Thus we assume a distribution of revolution frequencies as

$$f_0 \pm \frac{\Delta f}{2}$$

For a subgroup of particles over a very narrow range df the total number of particles N turns to $\left(\frac{dN}{df_r}\right)df_r$, and

$$d\langle I_n \rangle^2 = 2e^2 f_r^2 \left(\frac{dN}{df_r}\right) df_r$$

$$\Rightarrow \frac{d\langle I_n \rangle^2}{df_r} = 2e^2 f_r^2 \left(\frac{dN}{df_r}\right) \qquad (14)$$

The spectral **density** of the noise in the n-th band returns as:

$$\left(\frac{d\langle I_n \rangle^2}{df_r}\right) \quad \text{in units of } [\mathrm{A}^2/\mathrm{Hz}]$$

integrating over the band $f_0 \pm \Delta f$ we obtain the total noise power per band

$$\langle I_n \rangle^2 = 2e^2 f_0^2 N = 2eI_0 f_0 \qquad (15)$$

As an immediate implication we see that the total noise power in each "Schottky" band is constant. But we also know that the width of the Schottky band is increasing proportional to the harmonic number, and thus the height must decrease with 1/n.
It is very clear from Fig 7 that when we continue increasing the harmonic number and thus the frequency, that at a certain point there will be Schottky band overlap.

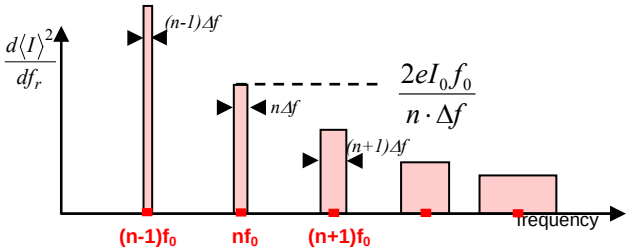

Fig. 7: A realistic picture of longitudinal Schottky bands

From what has been deduced so far for the longitudinal phase space we can already state that the following important beam parameters are measurable with Schottky noise:

- The mean revolution frequency
- The frequency distribution of particles
- The momentum spread
- The number of particles

TRANSVERSE PHASE SPACE

A single, highly relativistic particle in a storage ring passing through a position sensitive pick-up with infinite bandwidth generates a series a Dirac pulses. (Fig 8)

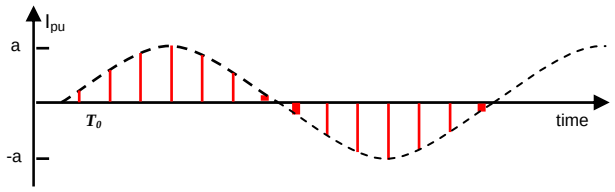

Fig. 8: A single particle with betatron oscillation of amplitude a as seen by a transverse pick-up

The betatron motion results in the particle wobbling around some reference orbit and thus the transverse position changes every turn. This transverse signal is not seen in the sum output of any pick-up structure (e.g. a pair of strip-lines) but is observed in the Delta, or difference, output. The output signal of such a pick-up has two contributions, one related to the longitudinal phase space and another related to the betatron oscillations.

$$i_{pu}(t) = \frac{e}{T}\sum_{n}^{\infty}\delta(t - nT + \varphi_k) \times a_k \cos(q\omega t + \phi_k) \qquad (16)$$

The first term under the sum sign is just the same as already seen in the longitudinal phase space discussion. In addition, however, there is an amplitude modulation of this signal due to the betatron motion. This has a frequency of qω/(2π), with q being the non-integer part of the betatron frequency and an amplitude a_k representing the oscillation amplitude. The difference response of the pick-up, Δi_{PU} , can therefore be written as

$$\Delta i_{PU} = S_\Delta \times a_k(t) \times i_k(t)$$

$$= S_\Delta \times a_k \cos(q\omega_0 t + \phi_k)$$

$$\times\left[i_0 + 2i_0 \sum_{n=1}^{\infty} \cos(n\omega_0 t + n\varphi_k) \right] \qquad (17)$$

with the term S_Δ defining the transverse sensitivity of the pick-up.
The equation for the n-th harmonic then becomes

$$\Delta(i_{PU})_n = S_\Delta \cdot a_k \cdot i_0 \cdot \begin{bmatrix} \cos\left((n-q)\omega_0 t + n\varphi_k - \phi_k\right) \\ +\cos\left((n+q)\omega_0 t + n\varphi_k + \phi_k\right) \end{bmatrix} \qquad (18)$$

.
For N particles in the beam, randomly distributed both in azimuth and betatron phases, averaging equation (18) gives

$$\left\langle \Delta i_{PU}^2 \right\rangle = S_\Delta^2 a_{rms}^2 i_0^2 \frac{N}{2} = S_\Delta^2 a_{rms}^2 e^2 f_0^2 \frac{N}{2} \qquad (19)$$

representing the total power (in a 1Ω resistor) in each sideband.

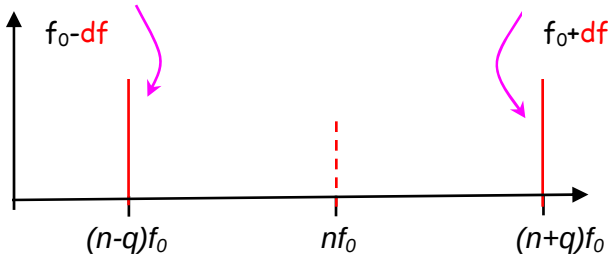

Fig. 9: Illustration of the fractional tune

It can be seen from equation (19) that the total power in each band is constant and proportional to the term a_{rms}^2 , which for an ensemble of particles is nothing more than the rms transverse beam size and is proportional to the transverse emittance.
The width of the sidebands is given by

$$\Delta f_\pm = (n \pm q) \times df \pm f_0 dq \qquad (20)$$

where q stand for the fractional tune and *dq /Q* is the tune spread.

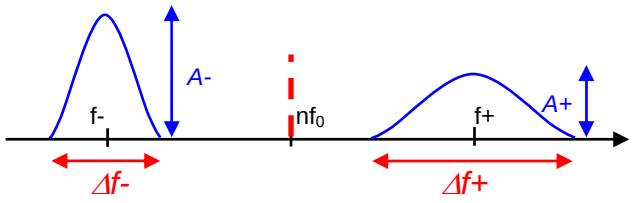

Fig. 10: Example of a Schottky signal with non-zero chromaticity

The fractional part of the tune, *q,* (Fig 9,10) can be measured using equation (20)

$$q = \frac{1}{2} + \frac{f_+ - f_-}{2f_0} \qquad (21)$$

The tune spread *dq/Q* is obtained from equation (20)

$$\frac{dq}{Q} = \frac{\Delta f_+ - \Delta f_-}{2f_0 Q} \qquad (22)$$

With the momentum spread *dp/p* given by

$$\frac{dp}{p} = \frac{1}{\eta} \times \frac{\Delta f_+ + \Delta f_-}{2nf_0} \qquad (23)$$

Combining equations (22) and (23) it is then possible to calculate the machine chromaticity, ξ :

$$\xi = \left(\frac{dq}{Q}\right) / \left(\frac{dp}{p}\right) \qquad (24)$$

BUNCHED BEAMS

So far the discussion has been limited to the Schottky noise properties of coasting i.e. unbunched beams. For bunched beams it is necessary to convolute the transverse spectra obtained in the case of an unbunched beam with the synchrotron spectrum related to the motion of particles in the RF bucket. When particles are oscillating in an RF bucket the revolution period $T = T_0$ is no longer constant but modulated periodically in time with a deviation Δt from T_0 given as

$$\Delta T(t) = A_s \sin(2\pi f_s t + \psi) \qquad (25)$$

Here A_s stands for the amplitude of the synchrotron oscillation, f_s is the synchrotron frequency and ψ is some initial phase. Introducing this time dependence into equation (1) one obtains, after some manipulations [7]:

$$i(t) = e\, f_o + 2\, e f_0 \sum_{n=0}^{\infty} \cos\{2\pi n f_0 [t + A_s \sin(2\pi f_s t + \psi)]\} \qquad (26)$$

In other words, each single line (c.f. Fig. 5) is split up into an infinite number of modulation lines by this synchrotron oscillation related phase modulation. The spacing between adjacent lines is equal to f_s .Their amplitude is given by

$$\sum_{p=-\infty}^{n} Jp(2\pi n f_0 t A_s) \cos(2\pi n f_0 + 2\pi n f_s + p\psi)$$

with Jp being the Bessel Function of order p.
In a similar way it is possible to obtain an expression [5] for the dipole moment D of a single particle travelling in an RF bucket of a circular machine

$$D = a \cos(q 2\pi f_0) e f_0 \cos[2n f_0 t + T(t) \sin(2\pi f_0 t + \psi)] \qquad (27)$$

It can be seen that the first cosine term in this equation is related to the amplitude modulation caused by the transverse movement, while the and the second cosine term represents the phase modulation with f_s. Equation (27) can be further expanded [7] leading to a rather lengthy expression for the amplitude of each particular line.
In short one can say that for case of bunched beams each line in the transverse spectrum of the unbunched beam has to be convoluted with the synchrotron motion related spectrum. This leads to a fine structure within the distribution shown in Fig. 10. However, the total integrated power is not affected by this synchrotron motion related modulation.

ACKNOWLEDGEMENTS

The authors would like to thanks Rhodri Jones and Trevor Linnecar for inspiring discussions, reading the manuscript and for support.

REFERENCES

[1] S. van der Meer, Stochastic Damping of Betatron Oscillation in the ISR, CERN-ISR-PO/72-31, Aug. 1972
[2] O.Zinke, H. Brunswig, Lehrbuch der Hochfrequenztechnik, Vol 2, Springer 1974
[3] R.H. Frater, D.R. Williams, An Active „Cold“ Noise Source, IEEE Trans.on Microwave Theory and Techn., pp 344-347, April 1981
[4] J.Tan, Experimental Results From LEIR Schottky System, CERN AB-Note-2008-013, 2008
[5] A.Hofmann, Physical Phenomena Used in Beam Observation, Proc. Frontiers of Particle Beams; Observation, Diagnosis and Correction, Eds M.Month & S.Turner, p.368, Springer-Verlag, 1988
[6] S.Chattopadhyay, Some Fundamental Aspects of Fluctuations and Coherence in Charged-Particle beams in Storage Rings, CERN Yellow report 84-11, October 1984
[7] Linnecar, T, Schottky Beam Instrumentation, CERN-PE-ED 001-92, Geneva, CERN, 1992

Report from the CARE NA3 workshop at Chamonix, France December 11-13, 2007

Ralph J. Pasquinelli
Fermilab

The focus of the workshop was on tune measurement, use of Schottky diagnostics, and discerning other beam parameters from such instruments i.e. chromaticity, momentum spread, and emittance. My talk centered on the history and technical details behind the 4.8 GHz Schottky System for the LHC.

The use of broadband pickups for Schottky tune measurements had it beginnings in the stochastic cooling systems of the Antiproton Source at Fermilab. In the mid 1990's a program was started to improve performance of the Debuncher stochastic cooling systems. The original cooling systems operated at 2-4 GHz with phased array quarter wave loops. The operational temperature of the pickups was 80 degrees Kelvin due to the low signal to noise associated with antiproton production. New higher frequency pickups were envisioned and even contemplation of plunging pickups similar to those used at CERN in the ACOL in the late 1980s. Dave McGinnis of Fermilab came up with the design of a new slotted waveguide pickup that could achieve 4-8 GHz coverage in 8 separate frequency bands with high sensitivity. In addition, it was decided to have a front-end operational temperature of 4 degrees Kelvin as the cryogenic infrastructure for cooling the Tevatron was in place and the spare capacity to cool these pickups could be implemented within reasonable cost limits.

With the successful implementation of the Debuncher cooling, the team that built those systems was now available for a new project. It was decided to rebuild the Accumulator core transverse cooling systems with this new style of pickup/kicker. Signal to noise in the Accumulator ring is significantly higher than the Debuncher; hence there was no added complexity of a cryogenic system. Here the 4-8 GHz frequency coverage was accomplished in three bands due to space limitation in the ring.

No longer an R&D effort, the slotted waveguide pickups could now be designed with a high degree of accuracy. It was at this time, 2002, which I proposed building a Schottky pickup that could be used in both the Recycler and Tevatron rings. These would be designed to operate at a frequency centered around 1.7 GHz with a bandwidth exceeding 100 MHz. This frequency allowed the waveguide structure to be large enough so as to not be an aperture restriction in either ring. The bandwidth would allow seeing individual bunches in the Tevatron. In addition, the bidirectional nature of the pickup would allow forward or reverse direction particles to be detected. In the Recycler, reverse tune up protons and forward antiprotons could be measured. For the Tevatron, an added feature was the simultaneous measurement of both protons and antiprotons during a collision store. With bunch spacing of 396 nanoseconds in the Tevatron and 100 MHz pickup bandwidth, a gating system could easily pick the two signal apart from the pickup, which has only 15 dB directivity. This means the pickup needed to be placed in the Tevatron at a location where the passage of protons and pbars are separated spatially in time.

The Schottky pickups are used daily in Fermilab operations of both the Recycler and Tevatron since January 2003. Detection of individual antiproton bunch tunes in the Tevatron has provided the operations group with the ability to correct beam-beam tune shifts, something that was not possible before this instrument became available. These Schottky pickups also have the added advantage that they are totally non invasive to the beam, i.e. requiring no external beam excitation to see signals, an advantage for long stores.

In the fall of 2004 I proposed the building of a Schottky system for the LHC under the auspices of the LARP collaboration. The project was approved in the spring of 2005 and design of the system started in earnest. A frequency of operation was chosen to be 4.8 GHz as the dimensions for such a pickup would not pose an aperture restriction and still fit in the tight space between the two LHC beam pipes. Fermilab designed the pickup structures, which were fabricated at CERN due to limited funding for the LARP contributions. Signal processing was designed, built, and tested at Fermilab with significant contributions from the CERN staff. As of the summer of 2007, all the hardware has been installed in the LHC tunnel. A control interface is now being designed at Fermilab and will be installed in the spring of 2008 before beam commissioning commences in the LHC.

The presentation for this CARE workshop can be found on line at

http://adweb.desy.de/mdi/CARE/chamonix/abi_workshop_2007.htm

Complete system documentation is located on line at

http://larpdocs.fnal.gov/LARPpublic/DocDB/ShowDocument?docid=482

The following published papers contain more details of performance of the systems at Fermilab and the proposed CERN system.

A 1.7 GHz Waveguide Schottky Detector System, Pasquinelli et al, Fermilab, 2003 PAC IEEE Nuclear Science, June 2003, Portland, Oregon

THPLT135 Experience with the 1.7 GHz Schottky Pick-ups in the Tevatron 2774
* A. Jansson, P. Lebrun, R. Pasquinelli
Fermilab, Batavia, Illinois, EPAC 2004 proceedings Lucerne, Switzerland

The 4.8 GHz LHC Schottky Pick-up System, Caspers, Pasquinelli et al, 2007 PAC IEEE Nuclear Science, June 2007, Albuquerque, New Mexico

Transverse Schottky Noise and BTF (Beam Transfer Function) with Space Charge

Vladimir Kornilov, Stefan Paret, Oliver Boine-Frankenheim
GSI Darmstadt, Planckstr. 1, 64291 Darmstadt, Germany

Transverse Schottky noise [1] and the Beam Transfer Function (BTF) belong to the most powerful beam diagnostics methods, providing direct measurements of beam stability properties, impedances and various beam and lattice parameters. Observations of the side bands $f^{\pm} = f_0(n \pm Q_0)$ at a harmonic n provide the betatron tune Q_0, chromaticity ξ and particle momentum spread δp. BTF signals [2] are obtained by exciting a beam with a periodic signal and measuring the resulting beam response (amplitude and phase). On the other hand, space charge effects [3] modify transverse Schottky and BTF signals. The role of space charge is especially important for the envisaged operation with high quality and high intensity ion beams in the FAIR synchrotrons [4]. In this study we consider distortions of transverse Schottky bands and BTF by space charge in coasting beams.

In order to characterize space charge effects in the transverse plane, we define the space charge parameter

$$\chi_{\rm sc} = \frac{\Delta Q_{\rm sc}}{\delta Q_\xi} \ , \tag{1}$$

which is a ratio between the space-charge tune shift

$$\Delta Q_{\rm sc} = -\frac{Nq^2}{m\gamma^3 C\, Q_0\, \omega_0^2\, r_{\rm kv}^2} \ , \tag{2}$$

and the chromatic tune spread $\delta Q_\xi = |\eta(n - Q + Q\frac{\xi}{\eta})|\, \delta p/p$ for a lower side band and $\delta Q_\xi = |\eta(n + Q - Q\frac{\xi}{\eta})|\, \delta p/p$ for an upper side band. C is the ring circumference, $r_{\rm kv}$ is the full radius, N is the particle number and $\omega_0 = 2\pi f_0$ is the revolution frequency. BTF is given by the response of the beam to the excitation divided by the exciting force amplitude, $R_0(\Omega) \propto \hat{\overline{y}}/\hat{G}$ and can be calculated as

$$R_0(\Omega) = \mathcal{A} \int \frac{\rho(f) {\rm d}f}{f - \Omega} \tag{3}$$

with ρ the particle distribution function and $\mathcal{A}$ a normalisation constant. An external impedance in the accelerator modifies the BTF signal as

$$\frac{1}{R(\Omega)} = \frac{1}{R_0(\Omega)} + iZ^{\perp} \ , \tag{4}$$

but space charge is an internal force which moves with the beam and thus changes BTF in a different way. For linear space charge, which shifts the betatron frequency of all the particles by $\Delta Q_{\rm sc} f_0$, the integral of R_0 includes incoherent tune shifts and BTF is given by

$$\frac{1}{R(\Omega)} = \frac{1}{R_0^{\Delta}(\Omega)} + \chi_{\rm sc} \ . \tag{5}$$

where $R_0^{\Delta}(\Omega)$ is the intrinsic BTF with the space-charge effect, which appears in the denominator of Eq. (3) as $(f + \Delta Q_{\rm sc} f_0)$. For linear space charge, it can be reformulated as $R_0^{\Delta}(\Omega) = R_0(\Omega - \Delta\omega_{\rm sc})$. As we see, effects of space charge cannot be described here as an impedance. Modifications of BTF due to space charge are illustrated in Fig. 1.

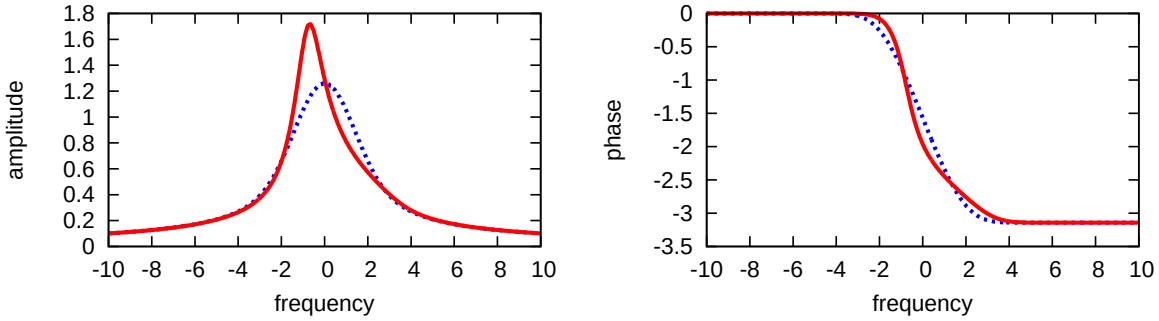

Figure 1: BTF amplitude (left) and phase (right) from Eq. (5) with space charge $\chi_{\rm sc} = -0.85$ (red solid line) and without (blue dashed line), the example is for a lower side band, the frequency is normalized by $\delta Q_\xi f_0$.

Schottky noise for a slow wave $f^- = (n - Q_0) f_0$ (which is called the lower side band) in the case without collective distortion is described by the power spectrum density,

$$P_0(\Omega) = \mathcal{D}\ \Psi\left(\frac{\Omega}{n - Q_0}\right) \ , \tag{6}$$

where $\Psi(\omega)$ is the particle distribution in revolution frequencies and the constant $\mathcal{D}$ depends on the beam intensity and emittance.

In the case where collective effects are important, Schottky noise can be formulated [1, 3, 5] as

$$P(\Omega) = \frac{P_0^{\Delta}(\Omega)}{|\varepsilon(\Omega)|^2} \ , \tag{7}$$

where P_0^{Δ} is the distribution with actual incoherent betatron frequencies. This means that for space charge $P_0^{\Delta}(\Omega)$ contains corresponding tune shifts and can be reformulated as $P_0^{\Delta}(\Omega) = P_0(\Omega - \Delta\omega_{\rm sc})$, but in the case of an external impedance $P_0^{\Delta}(\Omega) = P_0(\Omega)$, because

it affects only coherent beam oscillations. The dielectric function $\varepsilon(\Omega)$ is also treated in different ways for coherent and incoherent effects,

$$\text{external impedance (coherent)} \qquad \varepsilon(\Omega) = 1 + iZ^{\perp}R_0(\Omega), \tag{8}$$

$$\text{space charge (incoherent)} \qquad \varepsilon(\Omega) = 1 + \chi_{\rm sc}R_0^{\Delta}(\Omega)\ . \tag{9}$$

We would like to stress that for both BTF and Schottky noise, space charge effects can not be treated in the same way as an external impedance. Difference between these two collective distortions is illustrated in Fig. 2.

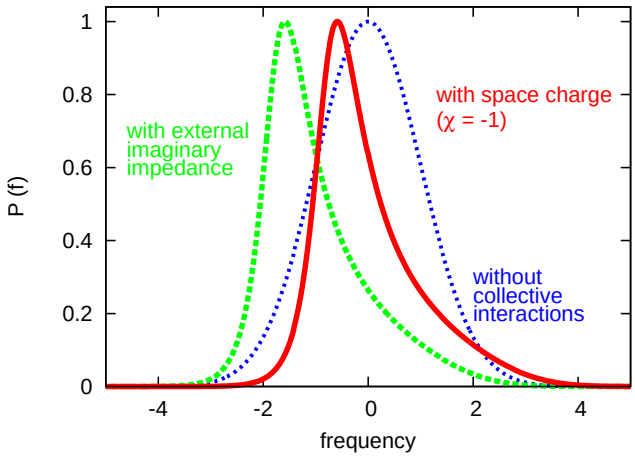

Figure 2: Transverse Schottky noise from Eqs. (7)-(9) distorted by the space-charge effect ($\chi_{\rm sc} = -1$, the red line) and by an external impedance which causes coherent tune shift $\Delta Q_{\rm coh}/\delta Q_{\xi} = +1$ (the green line). The example is for a lower side band, the unperturbed band is also shown.

Schottky noise has been measured during high-current experiments in the SIS 18 synchrotron at GSI Darmstadt in August 2007, with coasting Ar^{18+} beams at the injection energy (11.4 MeV/u) and $N = 7 \times 10^9$ particles. Figure 3 demonstrates a vertical Schottky signal with the black line. The side band is strongly unsymmetric, without distortions it would have the form of the red line for Gaussian momentum distribution. We explain the asymmetry by the space-charge effect and fit the experimental band by the model discussed above [Eq. (7)]. This yields the space charge parameter $\chi_{\rm sc} = -1.03$, which is in a reasonable agreement with the estimated (using measured emittance, momentum spread) parameter ≈ -0.8. The green line in Fig. 3 shows the incoherent betatron tune shifted by the space charge effect.

In a conclusion, a linear space-charge theory for distortions of transverse BTF and Schottky signals has been discussed, the space-charge effects has been successfully verified using measurements at the SIS 18 heavy ion synchrotron. Two practical consequences for beams with strong or moderate space charge should be mentioned:

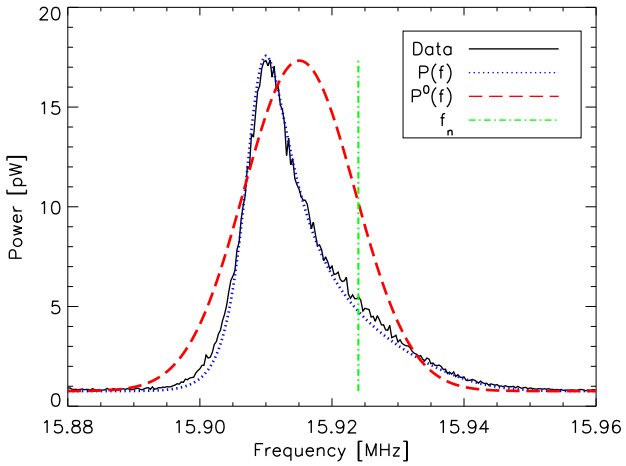

Figure 3: Schottky side band measured at SIS 18 during high-current experiments. Experimental data (vertical lower side band for $m = 75$) is shown with the black line. The dashed blue line is a fit with Eq. (7) for the space-charge effect with $\chi_{\rm sc} = -1.03$. The red line corresponds to the Schottky band without collective distortions.

(1) for distorted Schottky side bands, the distance between two peaks does not provide the bare tune Q_0 and the band width does not provide a direct measure for the momentum spread δp. However, a fit with the corresponding model can yield these parameters.

(2) analysis of distorted Schottky side bands provides a direct measure for the space-charge tune shift.

References

[1] S. Chattopadhyay, CERN 84-11 (1984)

[2] J. Borer, et al, CERN-ISR-RF-TH-BOM/79-20, presented at PAC1979, San Francisco

[3] D. Möhl and H. Schönauer, Proc. IX Int. Conf. High Energy Acc., Stanford, 1974, p. 380 (1974)

[4] FAIR Baseline Tech. Report 2006: http://www.gsi.de/fair/reports/btr.html

[5] D. V. Pestrikov, Nucl. Inst. Methods A 562, 65 (2006)

EXPERIMENTAL RESULTS FROM LEIR SCHOTTKY SYSTEM

J. Tan, CERN, CH-1211 Geneva 23, Switzerland.

5th Workshop in the framework of CARE-N3-HHH-ABI
"Schottky Diagnostics and Real Time Tune and Chromaticity Control"
11th - 13rd December 2007, Chamonix, France

Abstract

The high density Lead ion beams, needed for LHC, are obtained in the Low Energy Ion Ring (LEIR) at CERN by multi-turn injection followed by electron cooling and stacking. During this injection and stacking phases, where the circulating beam is unbunched, diagnostics with Schottky noise are used for probing essential beam parameters, such as tune, momentum spread, emittance and their evolution with time… LEIR is presented in the frame of the LHC ion accelerator chain. Schottky noise physics is briefly introduced and signal-to-noise estimates are given. Then the hardware facility and some results obtained since the machine commissioning in 2005 are described.

THE LEAD ION FILLING SCHEME OF LHC

A number of 0.7×10^8 ions/bunch at 2.7 TeV/u within normalised emittances ($\beta\gamma\sigma^2/\beta_{h,v}$) smaller than 1.5 μm is required to reach the desired luminosity of 10^{27} cm^{-2} s^{-1} for the lead experiments in LHC [1]. The emittance budget has been set to 1.2 μm at the exit of the SPS, 1 μm at the end of the stripper in the TT2 line, and 0.7 μm at the exit of the accumulator ring LEIR [2]. An improved ECR ion source (from 100 μA to 200 μA of Pb^{27+}) feeds the Linac3, pulsing at up to 5 Hz. At the end of the Linac3, a first stripping takes place to obtain a beam of Pb^{54+} (50μA, 200μs), Lead ion energy is then 4.2 MeV/n. Besides beam delivered for LEIR, studies of the source were made: the extraction and acceleration of Pb^{29+} was tested with a similar ion current out of the Linac3 [3]. As a consequence RF tanks operate at lower fields with Pb^{29+} ion, x-ray emission is reduced accordingly.

The LEIR machine is an essential part of the LHC injection chain for supplying high brightness ion beams. Multi-turn injection and phase-space cooling are the keys elements: long and low density Linac pulses are thus transformed into short and dense bunches. Two bunches of $4.5 \cdot 10^8$ ions each are accelerated up to 72 MeV/n within 3.6 s. The chosen transfer energy is a compromise between the limitations by space charge at the PS injection ($\Delta Q_{incoherent} < 0.25$), the gap needed between two consecutive bunches for the rise of the extraction kicker (150 ns, kick error <1%), the cycle length, and the minimum frequency available with the basic PS RF system.

The PS circumference being 8 times longer than LEIR, the 2 bunches are captured by an RF voltage at harmonic 16. Following a first acceleration step, the 2 bunches are gradually transferred from h=16 to h=12, then they are split into 4 bunches (h=24) and finally there is another transfer from h=24 to h=21. After a last acceleration to 5.9 GeV/u, a transfer from h=21 to h=169 (42 MHz cavities) takes place. In short: the PS transforms two dense bunches of $4.5 \cdot 10^8$ ions/b into four bunches of $2.25 \cdot 10^8$ ions/b, having 100 ns bunch spacing, within 3.6 seconds.

In the TT2 transfer line between PS and SPS the ions are fully stripped. About thirteen PS cycles are needed to fill up the SPS. The high transfer energy combined with the low bunch population decreases the space charge effect and the intra-beam scattering during the long SPS injection flat-bottom. The 100ns bunch spacing is compatible with the SPS RF system (around 200 MHz). This procedure is repeated until the two LHC rings are filled with 592 bunches each. The filling takes about 10 min per LHC ring.

The lead ion filling scheme for LHC is summarized in Figure 1 :

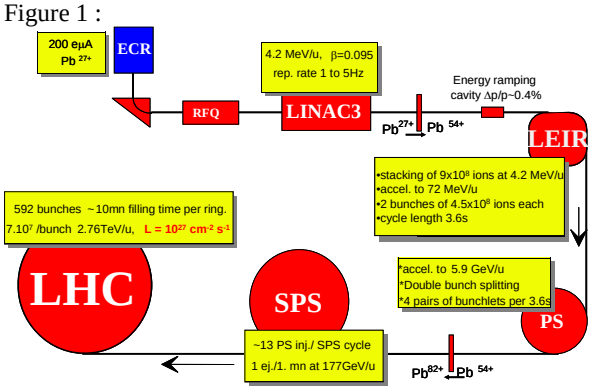

Figure 1 : Lead ion filling scheme for LHC

LEIR MACHINE

The lattice

The layout of the LEIR ring is depicted in Figure 2. The beam circulates anti-clockwise in the square-shaped machine of 78.54m circumference. The lattice features a two-fold symmetry with zero dispersion in the opposite straight sections, which contain respectively the extraction point and the electron cooling device. The quadrupole positions are re-arranged into four doublets and four triplets.

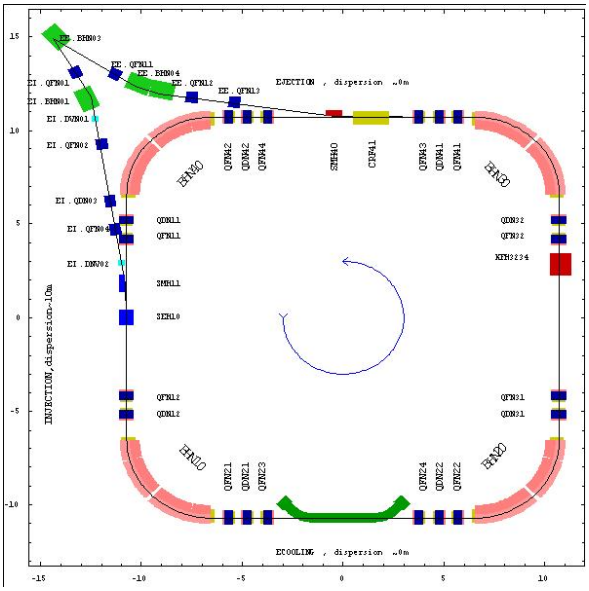

Figure 2 : LEIR machine layout.

In the upper left corner of Figure 2, the beam coming from Linac 3 (at β = 0.095) and the one extracted towards the PS (β = 0.37) enter a 60 m long common line where they travel in opposite directions and at very different (factor ~4) magnetic rigidities.

The nominal working points are Q_h = 1.72 and Q_v = 2.82. This lattice leads to a momentum acceptance of 8‰ together with (A_h, A_v) = (100, 50) π mm.mrad when using the actual vacuum chamber dimension. To avoid losses by charge-exchange with the residual gas, the vacuum has to be very good and the outgassing of the chamber walls by the lost ions has to be minimised. A typical vacuum pressure of a few 10^{-12} mb is achieved after baking the whole ring at 300°C.

LEIR nominal cycle

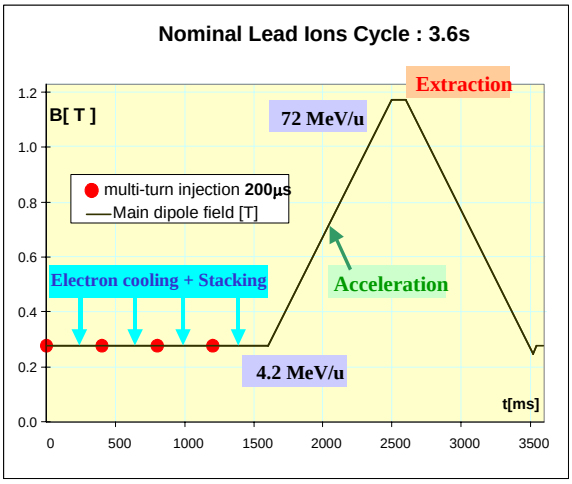

Figure 3 : Nominal Lead ion cycle showing the main B field and the sequence of events within 3.6 seconds.

Basically the LEIR ring transforms a series of low intensity and long Linac pulses into dense and short bunches by phase-space cooling and stacking (see Figure 3) thanks to the state-of-the-art electron cooler (built by BINP-Novosibirsk) [4]

The accumulation principles involving multi-turn injection [5] and electron-cooling have been successfully tested in the past [6]. Each Pb^{54+} pulse is injected during 70 turns then cooled for 400ms. About four to five Linac pulses are required for accumulating $9{\cdot}10^8$ un-bunched ions. At the end of the 1.6s injection step, electron cooling is stopped. Two bunches are adiabatically accelerated on the second harmonic from 4.2MeV/u up to 72MeV/u, then ejected towards the PS.

SCHOTTKY NOISE BASICS

Longitudinal Signal

Widely used in circular machines Schottky pick-ups (PUs) extract beam parameters from the analysis of the random component of the coasting beam current. A detailed derivation of the Schottky theory is not within the scope of this paper. Basic concepts on this topic can be found in the following short list of papers [7, 8, 9, 10].

In a storage ring, a single particle of charge *Ze* circulating at a revolution frequency $f_k = 1/T$ induces a series of δ functions onto a short PU placed somewhere around the ring. With a passage time t_k given by initial conditions, the current created and its Fourier expansion are:

$$\begin{aligned} i_k(t) &= Zef_k \sum_m \delta(t - t_k - mT) \\ &= Zef_k \left(1 + 2\sum_{n=1}^{\infty} \cos n\omega_k (t - t_k)\right) \end{aligned} \quad (1)$$

The so-called longitudinal spectrum consists of a DC part $i_{k0} = Zef_k$ which is the circulating beam current, and an infinite series of lines at all harmonics of f_k. Now assume an un-bunched beam of N individual particles with random initial phases φ_k and revolution frequency f_k within a distribution $f_0 \pm \Delta f/2$. Averaging $i_k(t)$ over N particles gives the circulating beam current $I_0 = N(Zef_0) = N \cdot i_0$. Further, each particle contributes to its own series of harmonic lines. The latter are indistinguishable for an observer who instead will see at the harmonic $n \cdot f_0$ a Schottky band of width $n \cdot \Delta f$, as the mean square current fluctuations is not zero. The spectral line at $n \cdot f_0$ can be written as :

$$< I_n^2 >= (2i_0)^2 \left(\frac{1}{2}\left[\sum_{k=1}^{N} \cos n\varphi_k\right]^2 + \frac{1}{2}\left[\sum_{k=1}^{N} \sin n\varphi_k\right]^2 \right) \quad (2)$$

The initial phases being randomly distributed, the sums over cross-terms cancel and

$$< I_n^2 >= (2i_0)^2 \left(\frac{1}{2}\sum_{k=1}^{N} \cos^2 n\varphi_k + \sin^2 n\varphi_k \right) = 2(Ze)^2 f_0^2 N \quad (3)$$

From Eq.(3), it turns out that the total noise power per band (dissipated in a 1Ω resistor) is constant and not

harmonic dependent. However the power spectral density scales as *1/(n×df)*. Thus longitudinal Schottky spectra give the mean revolution frequency and the momentum spread

$$\frac{df}{f_0} = \eta \frac{dp}{p} \tag{4}$$

where $\eta = \left|1/\gamma^2 - 1/\gamma_{tr}^2\right|$ is the off momentum parameter of the machine. With a calibrated system, the number of particles can also be deduced [11].

Transverse Signal

The betatron motion of amplitude a_k, of a single particle at a fixed observation point is described as

$$x_k(t) = a_k \cos(\omega Q t + \phi_k) \tag{5}$$

A position PU is sensitive to the dipole moment $d_k(t)$ which can be interpreted as the amplitude modulation of the longitudinal current :

$$d_k(t) = x_k(t) \cdot i_k(t) = a_k \cdot i_0 \cdot \sum_n^{\infty} \cos((n \pm q)\omega t + n\varphi_k \pm \phi_k) \tag{6}$$

where q is the fractional part of the tune Q. The spectrum at a given harmonic n of the revolution frequency features two sidebands at $(n \pm q)f$. As for the longitudinal case, the total noise power per transverse band is not harmonic dependent. The average power in each sideband is the same for uncorrelated particles with random phase :

$$< D_{n\pm q}^2 >= \frac{a_{rms}^2}{2} (Ze)^2 f_0^2 N \tag{7}$$

where a_{rms}^2 is the r.m.s beam size, proportional to the transverse emittance. The widths of the sidebands at $(n \pm q)f_0$ are obtained by substituting q by $(q+dq)$ and f_0 by (f_0+df) :

$$df_{n\pm q} = (n \pm q)df \pm f_0 dq \tag{8}$$

Hence transverse Schottky spectra provide a large set of fundamental beam parameters: the fractional part of the tune, the tune and momentum spreads, the transverse emittance and the mean revolution frequency.

SCHOTTKY PICK-UPS

Stripline transfer function

The working principle of a stripline electrode and the time domain signals are depicted in Figure 4. Consider the stripline as a matched transmission line, of length L, and place two observers A and B on each end side. A single particle travelling from left to right at a speed $v=\beta c$ induces a pulsed image current i_0 which splits into two pulses of half amplitude, travelling in opposite directions. The signal reflected towards R_A is seen at initial time zero by the observer A, whereas the observer B gets later the forward pulse at $t_1 = L/c$. The particle transit time from A to B is $t_2 = L/v$. The sign of pulsed image current induced in B is inverted due to the reverse boundary conditions. The forward signal towards R_B is seen at t_2 by the observer B, whereas the observer A gets later the reflected pulse at $t_1 + t_2$.

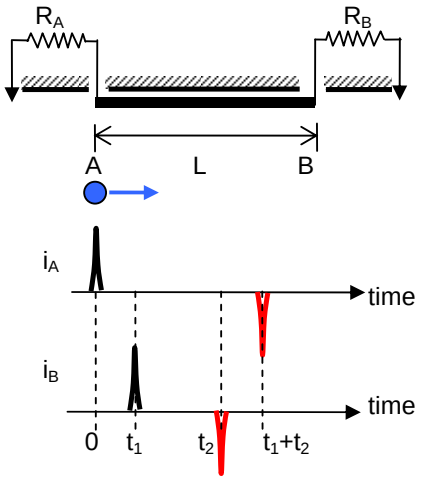

Figure 4: Stripline signals in the time domain.

These current pulses can be approximated by delta-functions, then the time signal can be written as

$$\begin{aligned} i_A(t) &= \frac{i_0}{2}(\delta_0 - \delta_{t_1+t_2}) \\ i_B(t) &= \frac{i_0}{2}(\delta_{t_1} - \delta_{t_2}) \end{aligned} \tag{9}$$

The Fourier transformations of i_A and i_B give the transfer functions in the frequency domain :

$$\begin{aligned} I_A(\omega) &= K \frac{I_0}{2} \sin\left(\frac{\omega}{2}(t_2 + t_1)\right) \times e^{j\Phi} \\ I_B(\omega) &= K \frac{I_0}{2} \sin\left(\frac{\omega}{2}(t_2 - t_1)\right) \times e^{j\Phi} \end{aligned} \tag{10}$$

where $\Phi = \frac{1}{2}(\pi - \omega(t_1 + t_2))$, $\omega = 2\pi f$, $t_1 = \frac{L}{c}$, $t_2 = \frac{L}{\beta c}$.

An additional coupling factor K should be included if only a fractional part of the image current is picked-up by the stripline. It contains many hidden construction details and has to be measured or calculated.

Some remarks about the transfer function:

i/ I_0 contains implicitly the spectral components of the particle beam.

ii/ the frequency bandwidth and phase are β-dependent,

iii/ modulus and phase are periodic (half sine function),

iv/ although the signals can be picked-up from any end-side of the stripline for low β particles, I_B cancels out for relativistic particles, as $t_1 \cong t_2$. In this case only the reflected signal on port A provides valuable information.

LEIR Schottky pick-ups

Two existing systems, inherited from the former Low Energy Antiproton Ring (LEAR) at CERN have been brought back to operation. Both consist of a succession of short strip-line PUs. However they differ by the way the signals from the individual strip-lines are combined:

In Figure 5 a/ the "Travelling wave" system is suitable only for low energy particles at injection (β = 0.0947). The striplines are connected in series, with appropriate electrical delays so that the currents from all electrodes are added. The signal is extracted at the downstream electrode, amplified and processed. There is one PU per transverse plane. The horizontal one yields also longitudinal information.

In the second configuration (see Figure 5 b/), the backward signal from each individual strip-line is directly amplified, delayed then summed using power combiners. Although this scheme yields a poorer signal to noise ratio than the travelling wave system, it can be applied for any particle velocity if the PU is equipped with variable delays. One PU is used for measuring signals in both longitudinal and horizontal planes, and a second one serves for the vertical plane.

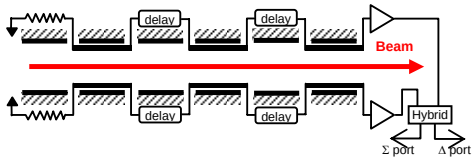

a/

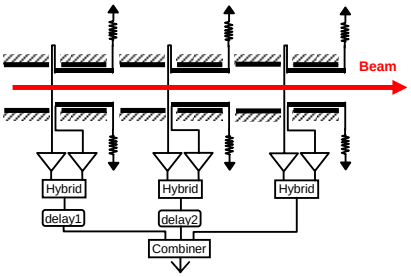

b/

Figure 5 : Schottky PUs used in LEIR. a/ At injection energy, the "travelling wave PU", which adds currents, yields a power signal proportional to the squared number of electrodes. b/ At extraction energy, power combining from another set of striplines is used. The power signal is proportional to the number of electrodes.

Figure 6 : Assembling of the vertical travelling wave PU.

The longitudinal/horizontal PU consists of 24 pairs of striplines and 74 dB amplification is enough for beam observations. The vertical PU having 6 pairs due to lack of space inside the triplet upstream the bending magnet 20, needs an amplification gain of 102 dB. Figure 6 shows the vertical PU during assembling. The signal cables are plugged onto a remotely controlled spectrum analyser.

Thermal noise sources and models

An impedance R_S at temperature T_S can be considered as a thermal noise source, whose mean square noise voltage in a narrow frequency band Δf is given by the Nyquist's noise theorem [12]:

$$\overline{u^2} = 4kT_S R_S \Delta f \qquad [V^2] \qquad (11)$$

where k is the Boltzmann constant. The equivalent model of a real (noisy) resistor is then an ideal (noise-free) impedance coupled with a zero-impedance voltage generator, and is illustrated by Figure 7 a/.

Similarly in a real amplifier the noise figure NF (generally expressed in dB) reflects the intrinsic noise generated by passive and active components. When the external noise source at the input of the amplifier is due to R_S as shown in Figure 7 b/, the total mean square output noise is given by :

$$\overline{V_{out}^2} = \overline{u^2} G^2 \times 10^{\frac{NF}{10}}$$

The total mean square input noise before amplification is then deduced from the ratio

$$\frac{\overline{V_{out}^2}}{G^2} = \overline{u^2} \times 10^{\frac{NF}{10}} = 4kT_S R_S \Delta f \cdot 10^{\frac{NF}{10}} \equiv \overline{u_e^2} \qquad (12)$$

$\overline{u_e^2}$ contains the contributions of the external noise u and of the amplifier noise. An external noise source (R_S, T_S) connected to a real amplifier can be replaced by an external noise source (R_S , $T_S \times 10^{NF/10}$) connected to a noise-free amplifier (see Figure 7 c/). $\overline{u_e^2}$ is the figure of merit of the system with respect to low noise performance as it is used for evaluating the signal-to-noise ratio, prior to any amplification.

From [Eq 12], one can also deduce the contribution of the amplifier itself. Assume an ideal noise-free amplifier which has $NF = 0\ dB$, one gets then $\overline{u_{e,ideal}^2} = \overline{u^2}$. The difference

$$\overline{u_e^2} - \overline{u_{e,ideal}^2} = \overline{u^2}(10^{\frac{NF}{10}} - 1) = 4kT_E R_S \Delta f$$

can be interpreted as the internal contribution of the amplifier to the total mean square input noise. Hence a real amplifier characterized by its noise figure NF is modelled as an external noise source R_S at T_E coupled to the input of a noise-free amplifier (see Figure 7 d/). T_E is the so-called effective input noise temperature [13] :

$$T_E = T_S \times (10^{\frac{NF}{10}} - 1) \qquad [K] \qquad (13)$$

Note that all three models b/, c/ and d/ are equivalent as they produce the same mean square output noise voltage $\overline{V_{out}^2}$.

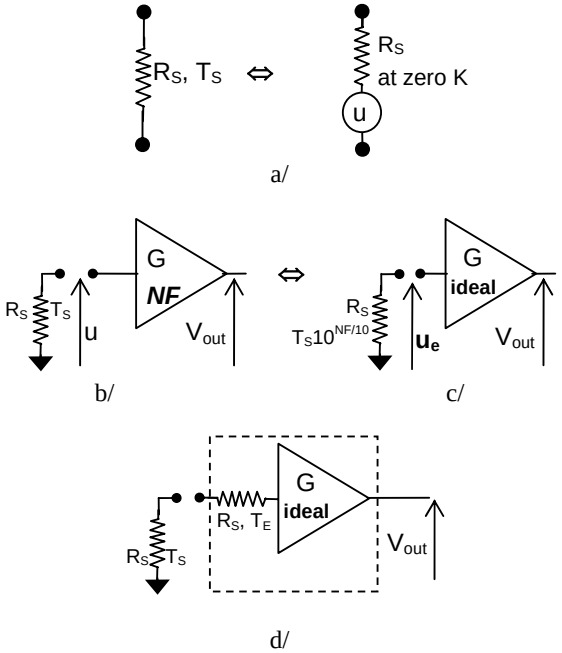

Figure 7 : Equivalent models of noise sources : a/ A resistor; b/ an external noise source at the input of a real amplifier; c/ d/ two equivalent models which produce the same mean square output noise voltage $\overline{V_{out}^2}$ as b/.

Improvement of the signal-to-noise ratio

In LEIR Schottky PUs, each stripline electrode can be considered as a matched transmission line, terminated with a physical load R_S at room temperature T_S on one side and terminated by the input impedance of an amplifier on the other side (see Figure 8 a/). Replacing the matching load R_S by the input impedance of a very low noise amplifier, as depicted in Figure 8 b, is equivalent to changing the noise temperature of R_S from T_S to T_E. Putting numbers in [eq.13] with T_S*=293K* and *NF'=1.2dB* gives an effective input noise temperature T_E as low as 93 Kelvins. The left amplifier then acts as a pseudo-cold load.

Note that the factor 4 in $\overline{u_e^2}$ vanishes when the amplifier input impedance R_{in} (with $R_{in} = R_S = 50\Omega$) is taken into account. Finally one gets also the equivalent mean square input noise density from [Eq. 12]:

$$\frac{I_e^2}{\Delta f} = \frac{kT_E}{R_S} 10^{\frac{NF}{10}} \qquad [A^2/Hz] \qquad (14)$$

For *NF= NF'=1.2dB* the total input noise density in the case of Figure 8b is 5.8 $pA/Hz^{1/2}$ which means a noise reduction of 5dB as compared to the configuration of Figure 8a. All matching impedances of LEIR Schottky systems are pseudo-cold loads in real life.

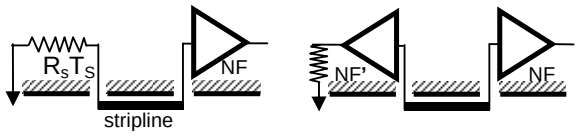

Figure 8: a/Basic stripline electrode configuration. b/ A low noise amplifier replaces the load resistor for noise reduction purposes.

The signal-to-noise ratio *U* can now be estimated. The power spectral density of a given longitudinal Schottky band is given by [Eq. 3] and [Eq. 4]. Taking into account the transfer function in [Eq. 10], one obtains:

$$\left(\frac{d<I_n^2>}{df}\right)_{band} = (Ze)^2 f_0^2 \left(\frac{dN}{df}\right) \frac{K^2 \sin^2(\pi f_0 (t_2 \pm t_1))}{2} \qquad (15)$$

Then *U* is defined as :

$$U = \left(\frac{d<I_n^2>}{df}\right)_{band} / \left(\frac{I_e^2}{\Delta f}\right) \qquad (16)$$

The above equation is valid for a single electrode. For "travelling wave PUs" which add the current from n_{PU} individual plates connected in series (see Figure 5 a/), *U* is proportional to $n_{PU}^2 \sin^2(\pi f_0 (t_2 - t_1))$. In the other configuration where the reflected power from n_{PU} electrodes is added using power combiners (see Figure 5 b/), *U* is proportional to $n_{PU} \sin^2(\pi f_0 (t_2 + t_1))$.

RESULTS

First circulating beams

In October 2005, the initial commissioning phase of the LEIR ring has been carried out with O^{4+} ions instead of Pb^{54+}[14]. The choice of oxgen ions was first motivated by a lower cross section for charge exchange processes with the residual gas. A longer vacuum life-time than with Lead ions is then expected. Secondly, the beam rigidity is very close for both ions species as their ratio *Z/A* are nearly equal. Furthermore, the oxgen ions are easier to create than Lead ions, and the source was available.

The first machine run showed that the gain on life-time was not so significant. Some possible causes are: high local pressure induced by beam losses, and few vacuum leaks from recuperated bellows. Coupling impedances would also yield fast losses. The latter were in good correlation with transverse "activity" observed from Schottky signals. Consequently, beam cooling interpretation was not straightforward, since no significant increase of density was observed.

From [Eq. 15, 16] it appears that the signal-to-noise ratio is much lower with light ions than with heavy ions. This limiting factor could be overcome with active loads (Table 1).

Table 1: Signal-to-noise ratio obtained with O^{4+} .

plane	Longitudinal	Horizontal	Vertical
U with O^{4+}	10	4.5	2.3

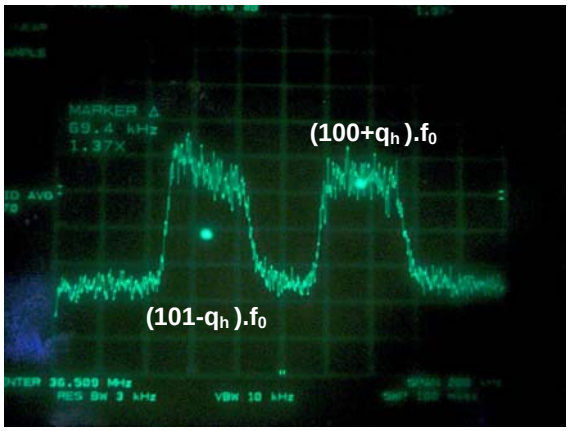

Figure 9 : Horizontal spectrum measured with O^{4+} ions. Side bands are observed at harmonics 100±q.

With about 1 to 2 mA of circulating beam [15], some fundamental parameters were deduced from the first Schottky spectra, as shown in Figure 9 : the average revolution frequency of 363.3kHz, the initial momentum spread of ~ 4×10^{-3}, and the tune Q_h/Q_v = 1.795 / 2.604 not far from the expected one.

Towards the nominal beam

Since the machine start-up in 2006, the injection scheme with Pb^{54+} ions has been successfully tested. During the runs 2006 and 2007, the next phase of LEIR commissioning attained its goal of providing the so-called "early ion beam" needed for the first LHC ion runs with reduced luminosity. A single Linac pulse was sufficient to produce the early beam which consists one bunch of 2.25×10^8 Lead ions with normalized transverse emittances of about 0.3μm, and longitudinal emittance of ~ 0.04 eV·s/n [16].

In parallel with the previous scheme, studies for generating the nominal beam as described in section 1 were undertaken. A typical cycle is shown in Figure 10 where only 80% of the nominal intensity is extracted. Studies are on-going to reach the goal: increasing the Linac current closer to the design value of 50μA, injection mismatch reduction, lattice improvement, achieve cooling studies…

The longitudinal spectrum shown in Figure 11 a/ has been recorded during the injection phase, at the 100th harmonic of the revolution frequency f_0=*360.45 kHz*. The horizontal axis spans 1% of the momentum spread. Time is represented on the vertical axis, with the start of the acquisition time on top. Multi-turn injection with a 200μs Linac pulse takes place first. The coasting beam is placed onto a stacking orbit during electron-cooling. After five injection-cooling sequences every 300ms, the dense ion beam is brought back to the nominal orbit for adiabatic bunching and acceleration.

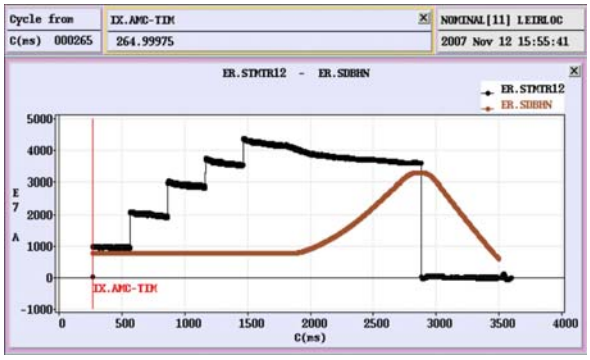

Figure 10 : The LEIR nominal cycle (500ms/div.). The brown trace is the magnetic cycle, and the black trace is the number of charges (10^{10}/div.). About 7.7×10^8 Lead ions are accumulated before acceleration, and there are 6.6×10^8 left at extration.

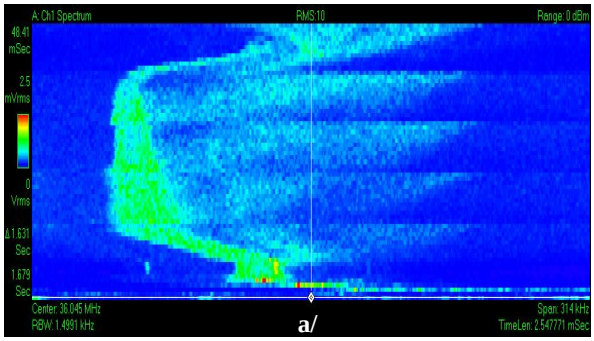

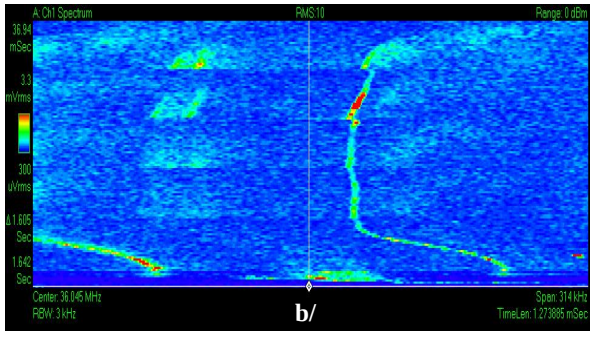

Figure 11: Nominal scheme studies: waterfall plots at harmonic 100 of: (a) the longitudinal spectrum and (b) the vertical spectrum during five injection-cooling sequences. The horizontal axis scales 1% of Δp/p, and the vertical axis represents 1.6s.

The momentum spread of the stacked ions is widening along the injection process, from the second Linac pulse onwards. This effect is purposely obtained by longitudinal modulation of the electron beam for limiting intra beam scattering and space charge phenomena. From the FWHM measurements of the spectrum lines, one could deduce a drop of the full momentum spread from 4×10^{-3} down to $\sim10^{-3}$ when the beam is fully stacked.

In Figure 10 the maximum number of incoming ions per pulse does not exceed 1.8×10^8. From the ionisation

profile monitor, one deduces the vertical beam size of ~18 mm at the PU location, which corresponds to an measured signal-to-noise ratio of about 1.5. Before RF capture, there are ~ 7.7×10^8 stacked cold ions. The vertical beam size and was reduced down to 13 mm, so that U raised up to 5. These measurements of the signal-to-noise ratio from the spectrum analyser (Figure 11 b/) are in good agreement with the theoretical estimates.

The low number of striplines (only six pairs) is the main limiting factor for the sensitivity of the vertical PU. Improvement of the injection efficiency and observation at higher harmonics might enhance U by a factor 2. The case of horizontal monitor is not an issue, and yields $U \sim 20$ for a single Linac pulse thanks to the combination of 24 pairs of electrodes.

Sudden jumps of the transverse signals are sometimes observed (e.g. during the cooling of the second pulse in Figure 11 b/). This phenomenon is interpreted as a coupling of the beam with the machine impedance which induces transverse coherent oscillations.

Tunes, tune spreads are obtained from transverse spectra acquisitions and equation (8) giving the sideband frequencies. The results are summarised in Table 2. The normal setting of the machine is to compensate the natural chromaticity with sextupoles to cancel out the tune spread.

Table 2: Beam parameters during the injection phase, without compensation.

	tune	dq/Q	ξ
Horizontal	1.82	7.7×10^{-3}	-1.92
Vertical	2.72	4.4×10^{-3}	-1.06

CONCLUSIONS

Schottky pick-ups have been routinely used during the three successive commissioning phases of LEIR. Combining travelling-wave structures and active loads allows a significant gain of the signal to noise ratio. Essential machine parameters have been measured from coasting beams, and spectra showed evidence of dynamic phase space cooling. Further studies and optimizations are one the way to improve the monitors' sensitivity. An application with graphical user interface should be implemented and provide the evolution of the tune and of the beam size with time.

ACKNOWLEDGMENTS

The author is very grateful to M. Chanel and F. Caspers for numerous fruitful discussions and for advice. The constant support of U. Raich is warmly acknowledged.

REFERENCES

[1] M.Chanel, Ion Accumulation for LHC, CERN PS-2001-054 (AE), 2001

[2] LEIR, LHC Design Report, Ed. : M.Benedikt et al., Vol. 3, Chap. 35, CERN-2004-003, 2004

[3] D. Manglunki et al., Ions for LHC : Status of the injection chain, Proc. of APAC 2007, pp. 226-228, Indore, India, 2007

[4] A.Bubley, V.Parkhomchuk, V.Prieto, R.Sautier, G.Tranquille, LEIR Electron Cooler Status, Proc. of EPAC 2006, pp. 1651-1653, Edinburgh, Scotland, 2006

[5] C.Carli, S.Maury, D.Möhl, Combined Longitudinal and Transverse Multiturn Injection in a Heavy Ion Accumulator, Proc. of PAC, p. 976, Vancouver, May 1997

[6] J.Bosser et al. The Production of Dense Lead ion Beams for the CERN LHC, CERN PS-99-042 (BD), 1999

[7] D.Boussard, Schottky Noise and Beam Transfer Function Diagnostics, CERN SPS 86-11 (ARF), 1986

[8] S.van der Meer, Diagnostics with Schottky Noise, CERN PS-88-60 (AR), 1988

[9] D.Möhl, Stochastic Cooling for Beginners, Proc. CERN Acc. School : Antiprotons for colliding beam facilities, p. 126, Geneva, October 1983

[10] F.Nolden, Instrumentation and Diagnostics Using Schottky Signals, Proc. 5th DIPAC, p. 6, Grenoble, May 2001

[11] J.Bosser, Measurements on the Low Intensity Beams of LEAR and the Antiproton Accumulator, CERN PS-95-28 (BD), 1995

[12] P.A.H. Hart, Standard Noise Sources, Philips Tech. Rev, Vol 23, pp. 293-309, 1961/1962

[13] C.K.S.Miller, W.C.Daywitt, M.G.Arthur, Noise Standards, Measurements, and Receiver Noise Definitions, Proc. IEEE, vol 55, p. 865, 1967

[14] P.Belochitskii et al., LEIR Commissioning, Proc. of EPAC 2006, pp. 1876-1878, Edinburgh, Scotland, 2006

[15] C.Carli, M.Chanel, Private Communication

[16] M.Chanel et al., LEIR : Towards the Nominal Lead Ion Beam, Proc. of APAC 2007, pp. 229-231, Indore, India, 2007

THE AD SCHOTTKY SYSTEM AND FUTURE EVOLUTIONS

Maria Elena Angoletta, CERN, Geneva

Abstract

An innovative system to measure antiproton beam intensity, momentum spread, mean momentum and tune in CERN's Antiproton Decelerator (AD) is described. This system is based on a state-of-the-art Digital Receiver (DRX) board, consisting of 8 Digital Down-Converter (DDC) chips and one Digital Signal Processor (DSP), and on ultra-low noise pick-ups. The system provides real-time information characterising the machine performance; it has been used for troubleshooting and to fine-tune the AD, thus allowing further improved performance. This paper gives an overview of the system hardware and software, together with hints on its possible future evolution.

CARE-N3-HHH-ABI Workshop

Chamonix, December 11-13, 2007

1. INTRODUCTION

A new CERN machine for low energy antiprotons production, named the Antiproton Decelerator AD [1], is operational since 2000. Antiprotons from a target, bombarded with an intense beam from the 26 GeV Proton-Synchrotron (PS), are fed to the AD where they are decelerated in several ramps to a momentum p of about 100 MeV/c. Figure 1 shows the basic AD cycle; bunched-beam deceleration ramps are interspersed with plateaus, where the beam is cooled at fixed p and revolution frequency f_{REV}.

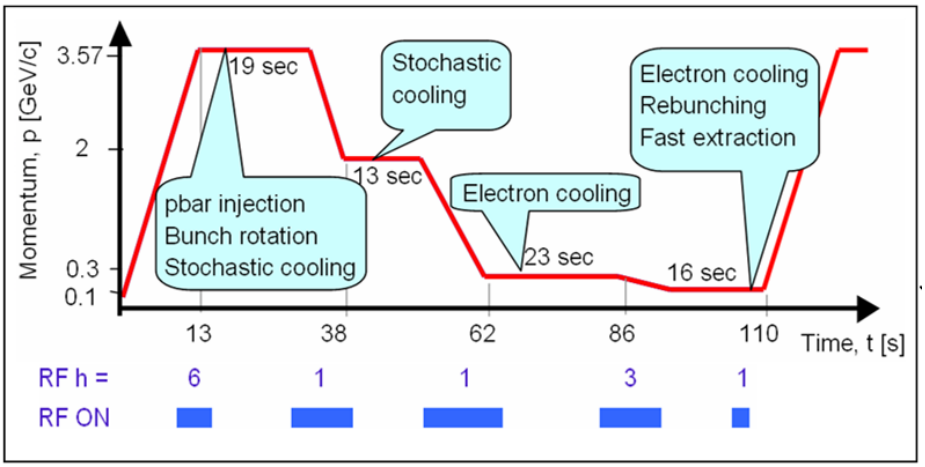

Figure 1: *The momentum p during the AD basic cycle (2002 version).*

The intensity of its antiproton beam varies from some 5×10^7 particles at 3.5 GeV/c to some 3×10^7 at 100 MeV/c. Traditional DC beam transformers do not work at these low intensities, hence ultra-low-noise longitudinal [2] and transverse [3] pick-ups are used.

The new digital-receiver-based AD beam-diagnostic system acquires and processes the data generated by these pick-ups. The system measures beam current intensity, momentum spread, mean momentum and transversal tunes throughout the AD cycle. It therefore enables a real-time evaluation of cooling and deceleration performance during the AD cycle.

2. SYSTEM OVERVIEW

On the magnetic plateaus the beam is debunched for stochastic or electron cooling and longitudinal beam properties (intensity, momentum spread and mean momentum) are measured by FFT-based spectral analysis of Schottky signals. For bunched beams, the intensity is obtained by measuring the amplitude of the fundamental and second RF Fourier components; the bunch length is also derived. The tune is measured by the Beam Transfer Function (BTF) method [4]. Additional information can be found in [5,6].

Figure 2 gives an overview of the system. The inputs from the two longitudinal pick-ups (LPUs), optimised respectively for high (HF LPU) and low frequency (LF LPU), are filtered and added together by a summing unit to give the total input over the whole frequency range. The resulting signal is amplified by a variable-gain, remotely-controlled second-stage amplifier. After a low-pass filter stage, the signal is digitised by an ADC VME board. The data are digitally down-converted and processed by a Digital Receiver (DRX) board, which is

set up before each measurement. The horizontal and vertical (TPUH/V) transversal PUs are devoted to tune measurement by the BTF method. The noise generator MG produces the analogue excitation used for BTF measurements.

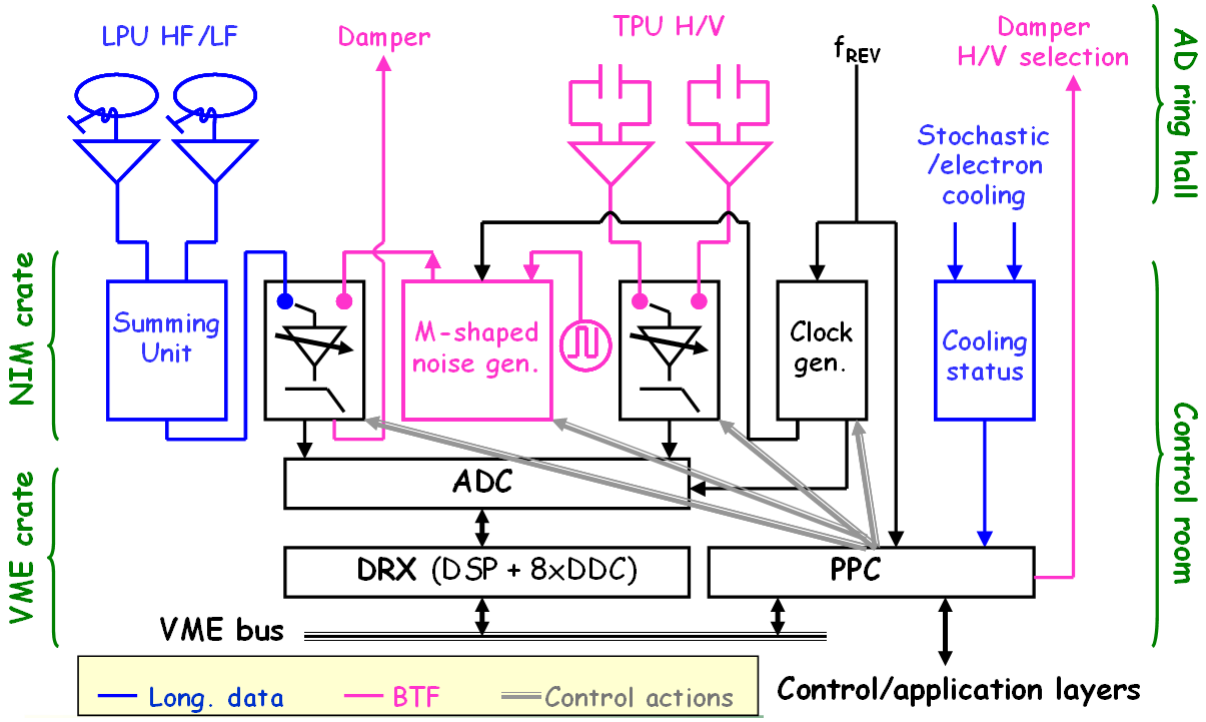

Figure 2: *Schematic view of the new digital-receiver-based system for the measurement of antiproton beam parameters.*

Finally the software task running in the PowerPC (PPC) VME board collects, post-processes and stores the data for later display. Additionally, the PPC acquires from the RF and the stochastic cooling systems the information needed to optimise the choice among various user settings. Users access the system, to evaluate data and to set various parameters, through the standard Control and application layers.

3. HARDWARE

3.1 Longitudinal pick-up

Two LPUs provide the frequency bandwidth 0.1 MHz to 16 MHz required for the measurement of Schottky signals and beam intensity. They also improve the S/N ratio by lowering the overall noise floor. The noise power spectral densities of the two LPUs are given in Figure 3 and Figure 4 as functions of frequency and are summarised in Table 1.

	Total response bandwidth/MHz	**Low noise bandwidth/MHz**	**Low noise value / pA/Hz^½**
HF LPU	0.25 – 30	[1 - 3]	1.5
LF LPU	0.02 - 3	[0.1 – 1]	2

Table 1: *Nominal characteristics of the HF and LF LPUs.*

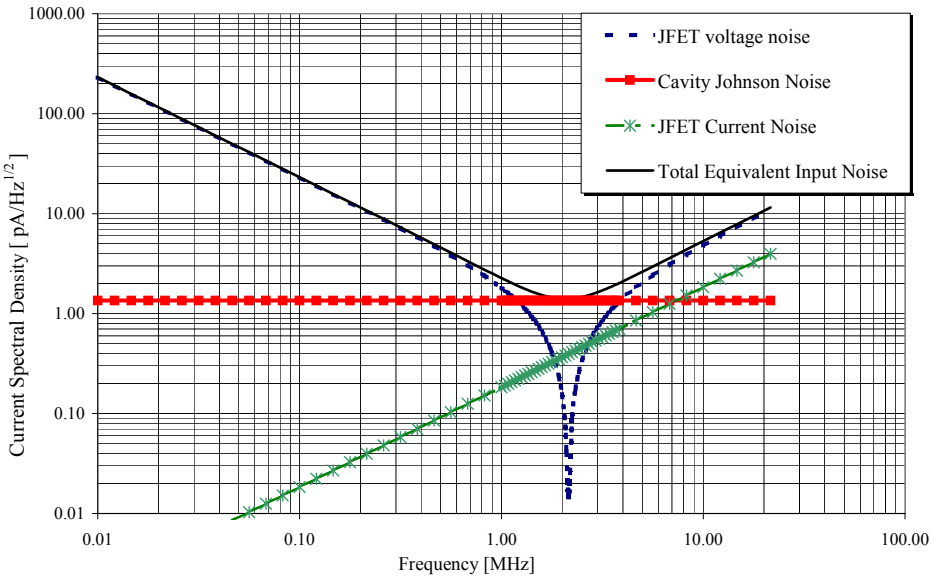

***Figure 3**: Equivalent input current noise for the HF LPU.*

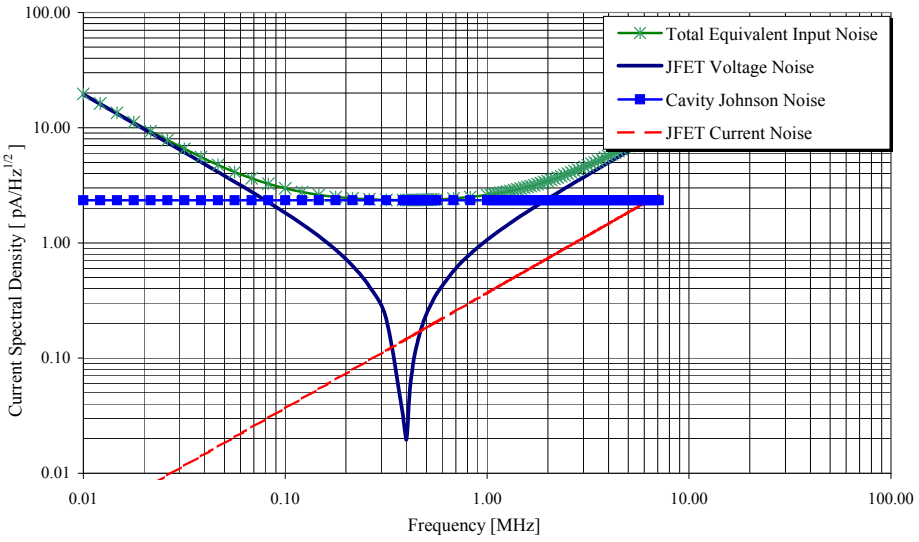

***Figure 4**: Equivalent input current noise for the LF LPU.*

The LPUs are high-Q resonant devices, hence with a minimised Johnson noise. They are broad-banded by an active feedback, around the head amplifier, which simulates a "noise-free" resistor in parallel with the resonant circuit, as shown in Figure 5. The design of the LPUs and the corresponding head amplifiers ensures that the total equivalent input noise, in a part of the bandwidth, is dominated by the cavity Johnson noise. This can be seen in Figure 3 and Figure 4. Such bandwidth is indicated as the low-noise bandwidth in Table 1.

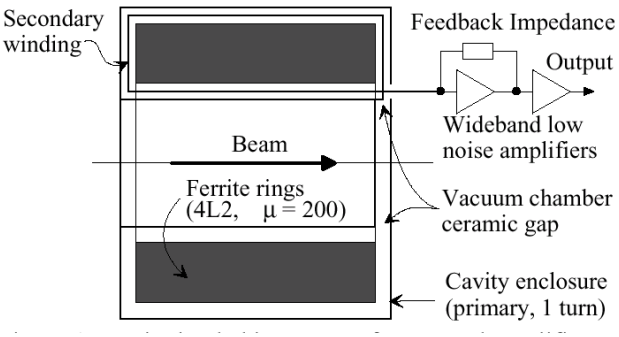

Figure 5 *The HF LPU ferrite-loaded beam transformer and amplifier.*

The outputs of the two LPUs are filtered and added together by the PU Summing Unit, to give a flat frequency response over the 0.02-30 MHz bandwidth. The low frequency pick-up signal is low-pass-filtered, the high frequency pick-up signal high-pass-filtered, giving the required bandwidth when the two are summed.

3.2 Transversal pick-up

Two electrostatic, transversal pick-ups have been constructed, for the vertical and for the horizontal plane, respectively. Each 1m long electrostatic PU is resonant at 5.6 MHz. The pre-amplifier has been designed so that, in a band around the resonance frequency, the Johnson noise from the losses in the coil is the dominant noise source of the system. To achieve the highest possible Q (low losses) of the resonant circuit, the PU has been designed with the coil inside the vacuum chamber. The high Q resonant circuit is detuned by a feedback around the pre-amplifier, making the input impedance appear like a 350 Ω resistor working at a temperature of less then 13 K. The principle of the same as that used in the longitudinal pick-ups, described in paragraph 3.1. Detuning the resonant circuit makes the PU broad-banded enough to always have a betatron sideband in the low noise part of the response from 5.3 MHz to 6.2 MHz. Figure 6 shows the construction details of a transversal pick-up and Table 2 gives their nominal characteristics.

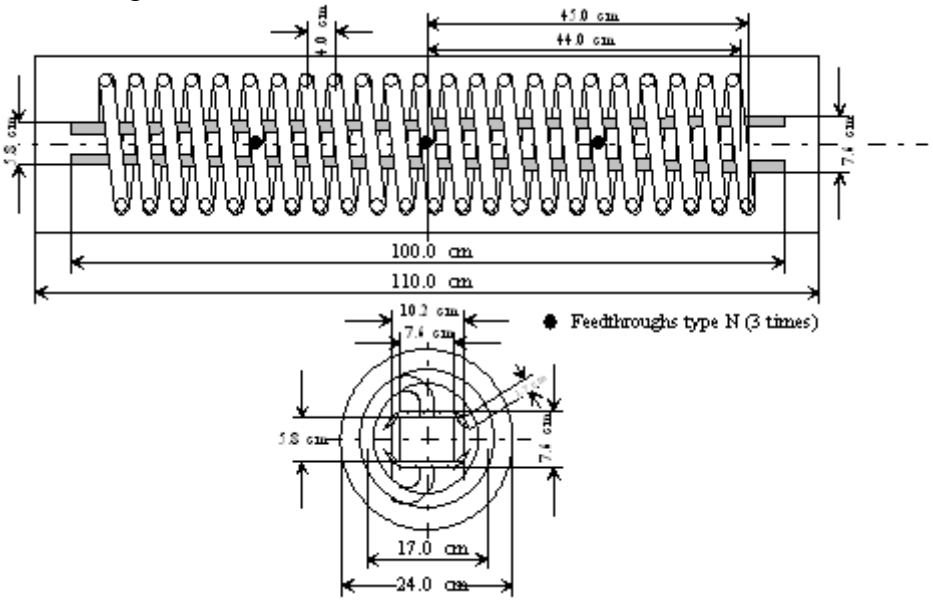

Figure 6*: Transversal pick-up – construction overview.*

	Low noise bandwidth/MHz	Low noise value / pA/Hz^½
TPU H/V	[5.3 – 6.2]	1 pA/Hz $^{1/2}$

Table 1: *Nominal characteristics of the TPU PUs.*

3.3 Digital Signal Processing Hardware

3.3.1 ADC Board

The ADC board is a customised version of the Pentek 6441 model, a dual channel, 12-bit, board that operates at sampling rates of up to 41 MHz. Two analogue input signals are first amplified and then low-pass filtered prior to being fed to the Analog Devices 12-bit A/D chip. The digital signal is multiplexed so that both signals are made available on two different flat cables (Upper and Lower). An external clock controls the board, so as to change the ADC sampling frequency f_S according to the beam state.

Initial off-line testing of the 6441 ADC showed that the measured S/N ratio was over 15 dB worse than what was listed in the original manufacturer specifications. It was found that the additional noise came from the board analogue input front-end. This major drawback was overcome by developing an in-house front-end which bypassed the input amplifier and the low-pass filter. The trade-off was the need to add an external filter on the analogue signal path before its digitisation. In this way, the S/N ratio was improved by 13 dB on average. Based on this solution, the ADC board manufacturer later developed a “low-noise” version of the board analogue front-end, which is now commercially available.

3.3.2 Digital Receiver Board

The digital receiver board is a commercial off-the-shelf VME board [7,8] that hosts 8 Harris HSP50016 Digital Down Converters (DDC) and one TI TMS320C40 Digital Signal Processor (DSP). This board is in charge of parallel data acquisition, independent digital down conversion and processing of up to 4 digitiser inputs. Figure 7 gives a schematic version of the board. The digitised inputs are pre-processed by the DDC chips, by digitally translating (*downmixing*) the input signal to DC, then zooming (*decimation*) on the frequency window of interest. Both the bandwidth and the centre f_{LO} of the frequency window are user-selectable. Each DDC is connected to a FIFO memory where data are stored. From the FIFOs the data are then retrieved and processed by the DSP. The board is equipped with several memory banks, of which the Global Memory is visible from the VMEbus and is used to retrieve processed data.

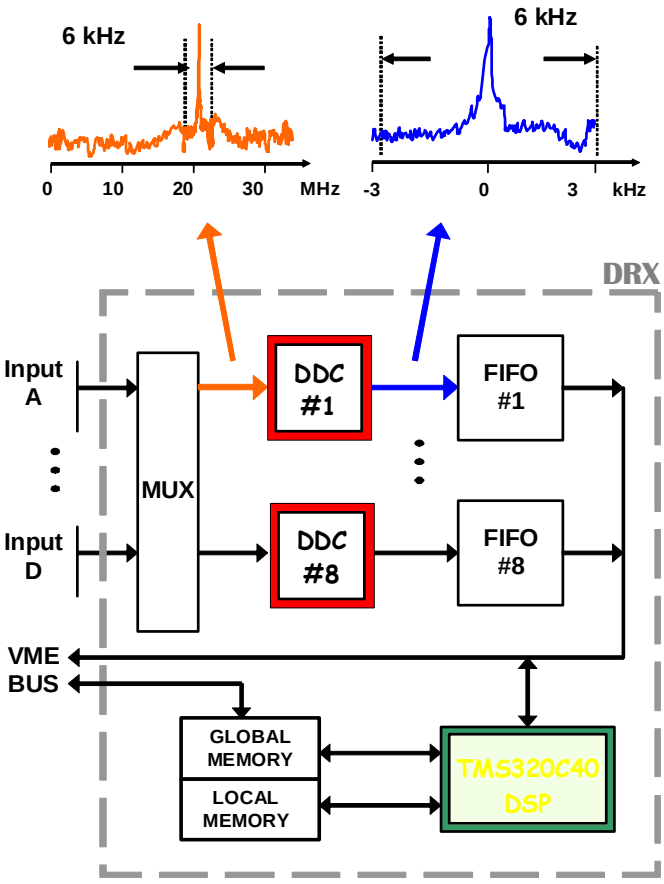

***Figure 7**: Schematics of Pentek's 6510 DRX board. Shown at the top is an example of digital zoom on the window of interest and DDC sample decimation.*

4. DIGITAL SIGNAL PROCESSING

4.1 Longitudinal bunched signals

For bunched beams, the intensity is obtained by measuring the amplitude of the fundamental and second RF Fourier components. The bunch length is also derived from this measurement. Figure 8 gives an overview of the data processing method.

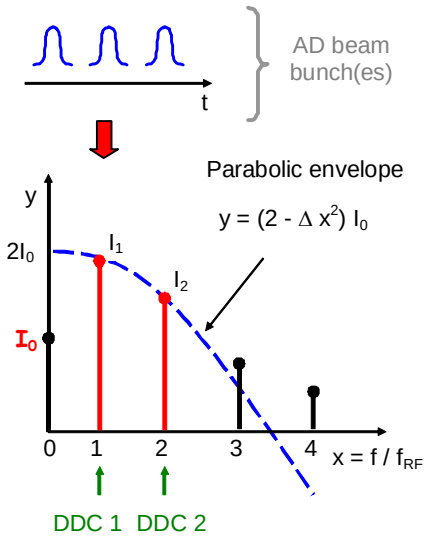

***Figure 8**: Longitudinal bunched processing: RF harmonics Fourier analysis with a parabolic bunch approximation..*

The ADC f_S is proportional to f_{REV}, thus allowing to track the beam when its revolution frequency changes. At each turn m = 0,1,2 .., the intensity time profile $I(t)$ of a single bunch is approximated, in the interval [(m-½)/f_{REV} ; (m+½)/f_{REV}], by a parabola:

$$I(t) = \frac{3}{4\sqrt{2}} \frac{I_0}{\tau \cdot f_{REV}} \cdot \left(1 - \frac{t^2}{2\tau^2}\right) \qquad (1)$$

where I_0 is the DC current intensity per bunch and 2τ is the FWHM.

The experimental Fourier coefficients J_k (k=1, 2, ...) are calculated and then fitted with a truncated series of f/f_{RF}

$$J_k = I_0 \cdot h \cdot \left\{2 - \Delta \cdot \left(\frac{f}{f_{RF}}\right)^2\right\} \qquad (2)$$

where $h = f_{RF}/f_{REV}$ is the RF harmonic number. I_0 and Δ are therefore obtained, and thus the bunch size τ :

$$\tau = \frac{1}{2 \cdot \pi \cdot f_{REV}} \cdot \sqrt{\frac{5\Delta}{2}} \qquad (3)$$

Integration of the beam profile over time gives the total number N of particles circulating in the machine, i.e. the beam intensity:

$$N = \alpha_B \cdot \frac{I_0 \cdot h}{f_{REV}} \qquad (4)$$

The DRX actually uses only two data points $A_k = J_k/G$ with k=1,2. These are labelled DDC1 and DDC2, respectively, in Figure 8. The A_k are then fitted with a truncated series of $x = f/f_{RF}$

$$y = A_0 \cdot (2 - \Delta \cdot x^2) \qquad (5)$$

hence I_0 and the bunch size can be derived.

4.2 Longitudinal debunched signals

On the magnetic plateaus the beam is debunched for stochastic or electron cooling and longitudinal beam properties (intensity, momentum spread and mean momentum) are measured by FFT-based spectral analysis of Schottky signals. Figure 9 shows the data processing method.

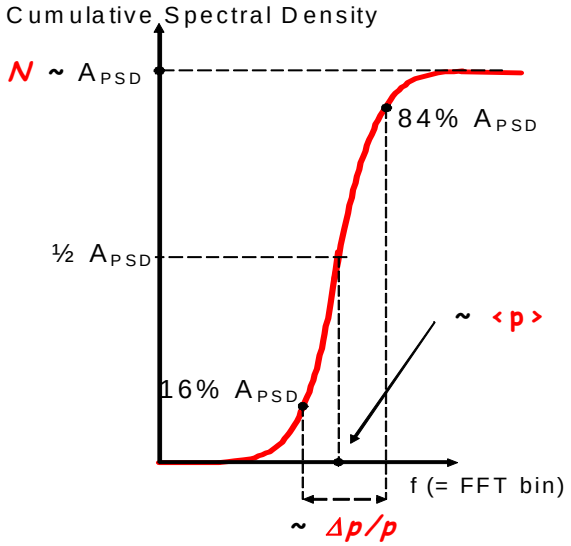

***Figure 9**: Longitudinal Schottky integrated power.*

The number of coasting particles N is found from f_{REV} and the area A_{PSD} under the peak of the *PSD* vs. *f* curve:

$$N = \frac{\alpha_U}{G_U^{\,2}} \cdot \frac{A_{PSD}}{f_{REV}^{\,2}} \qquad (6)$$

where α_U is a calibration constant and G_U is the global system gain. From the width Δf of the PSD curve at a 2σ height, the momentum spread $\Delta p/p$ is:

$$\frac{\Delta p}{p} = \frac{1}{n \cdot f_{REV} \cdot \eta} \cdot \Delta f \qquad (7)$$

where $\eta = (\gamma_{TR}^{\,2} - \gamma^{\,2})/(\gamma_{TR}\,\gamma)^2$, $\gamma = E/E_0$, $\gamma_{TR} = 4.75$ and n is the harmonic number.

4.3 Transversal signals

The beam is excited with a band-limited M-shaped noise, by means of a transverse damper deflector, and recording the deflector excitation and the transverse beam response. These are then FFT-processed to yield the tune. Figure 10 gives an overview of the data processing method.

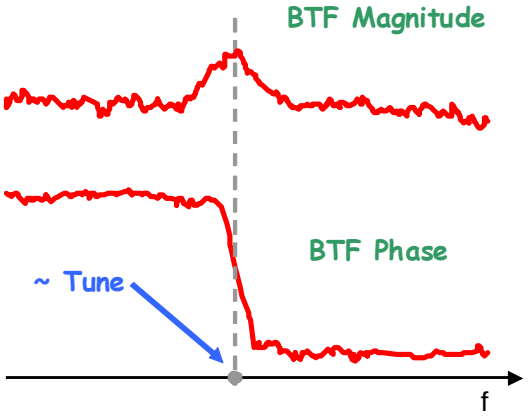

***Figure 10**: Principle of the BTF measurement. The tune is determined mainly from the BTF phase spectrum.*

It is possible to measure tunes at lower intensities and during the ramps, by keeping the sampling frequency f_S equal to a multiple of f_{REV}. The M-shaped excitation is chosen so as to minimise transverse beam blow-up, by setting f_C very close to a betatron frequency. The system calculates five spectra: the transfer function (magnitude and phase), the coherence function and the power spectral density of the beam and of the noise. The user uses a dedicated application program to determine the machine tune from these spectra, thus the tune is measured in a semi-automatic way.

5. MEASUREMENT EXAMPLES

Figure 11 shows typical intensity and momentum spread $\Delta p/p$ measurement over an AD cycle, together with the RF status. When the RF is ON the beam is bunched and the intensity is measured with the method described in paragraph 4.1. On the contrary, when the RF is OFF the beam is debunched and intensity and $\Delta p/p$ are measured with the method described in paragraph 4.2. Measurements carried out during the bunched-debunched beam transition are intrinsically inaccurate. Debunched beam data are more affected by noise, whereas bunched beam signals, which are much larger, are less influenced. Towards the end of the cycle, instabilities and/or bad statistics generate an “explosion” of the measured power, thus generating overestimations of the beam intensity.

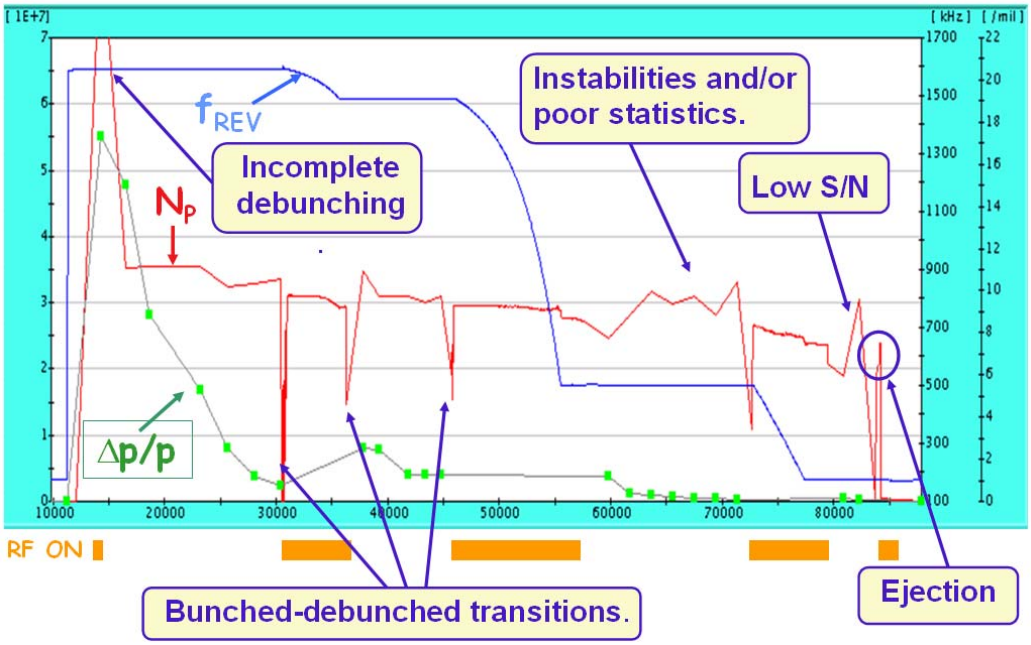

***Figure 11**: Intensity (red trace), revolution frequency (blue trace) and Δp/p (green trace) in a typical AD cycle (screenshot taken in 2002). The RF status (ON/OFF) is shown in orange at the bottom of the picture.*

Figure 12 shows a typical screenshot of the BTF application program. The five spectra available to the user are shown in the figure bottom part, as a function of the FFT bin number. The setup parameters or each measurement are shown in the top part. The user clicks on the bin corresponding to the tune and the application calculates the corresponding tune from the bin number and from the measurement setup parameters.

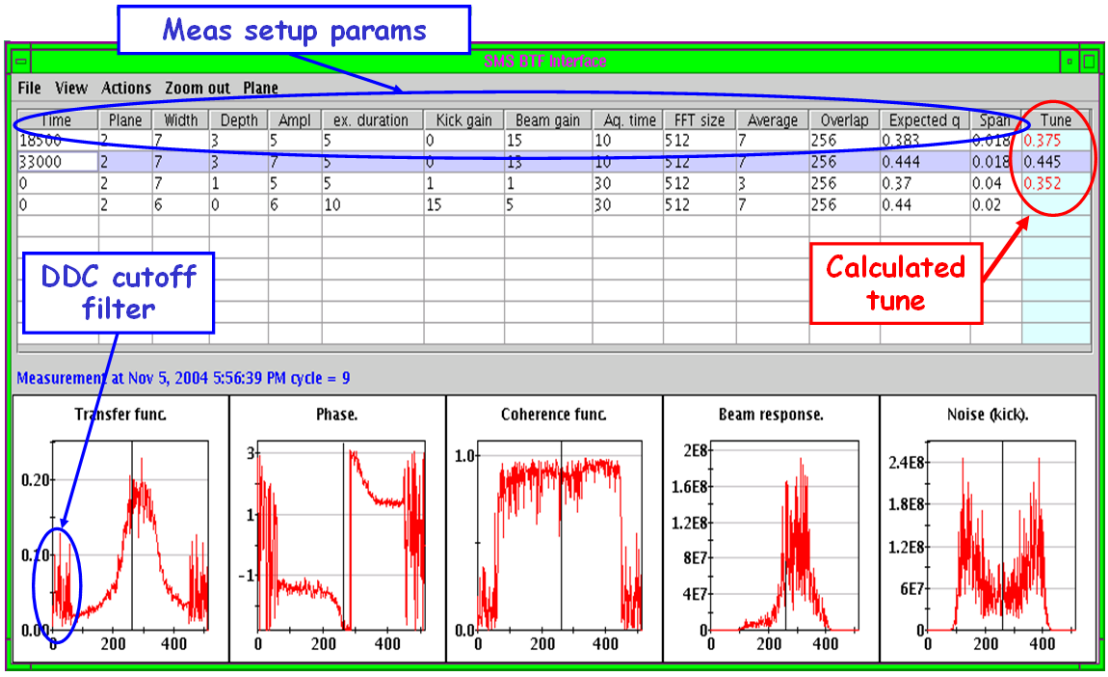

***Figure 12**: BTF on bunched beam @ ramp 2 (screenshot taken in 2004).*

6. FUTURE EVOLUTION

A new compact ring for post-AD antiproton deceleration & cooling has been proposed. This ring is called Extra Low ENergy Antiprotons (ELENA) ring and its preliminary cost and feasibility study report can be found in [9]. A system with the same capabilities of the AD Schottky system is needed; its implementation has been proposed based upon the same hardware successfully deployed in Low Energy Ion Ring (LEIR) LLRF [10, 11]. Its basic building blocks are a DSP/FPGA motherboard and several daughtercards (MDDS, SDDS, DDC) and the proposed system, implementing LLRF as well as and diagnostic systems is shown in Figure 13. Advantages over the AD Schottky system implementation include a reduced cost per channel. Additionally, the BTF noise is generated digitally instead of with a dedicated analogue hardware.

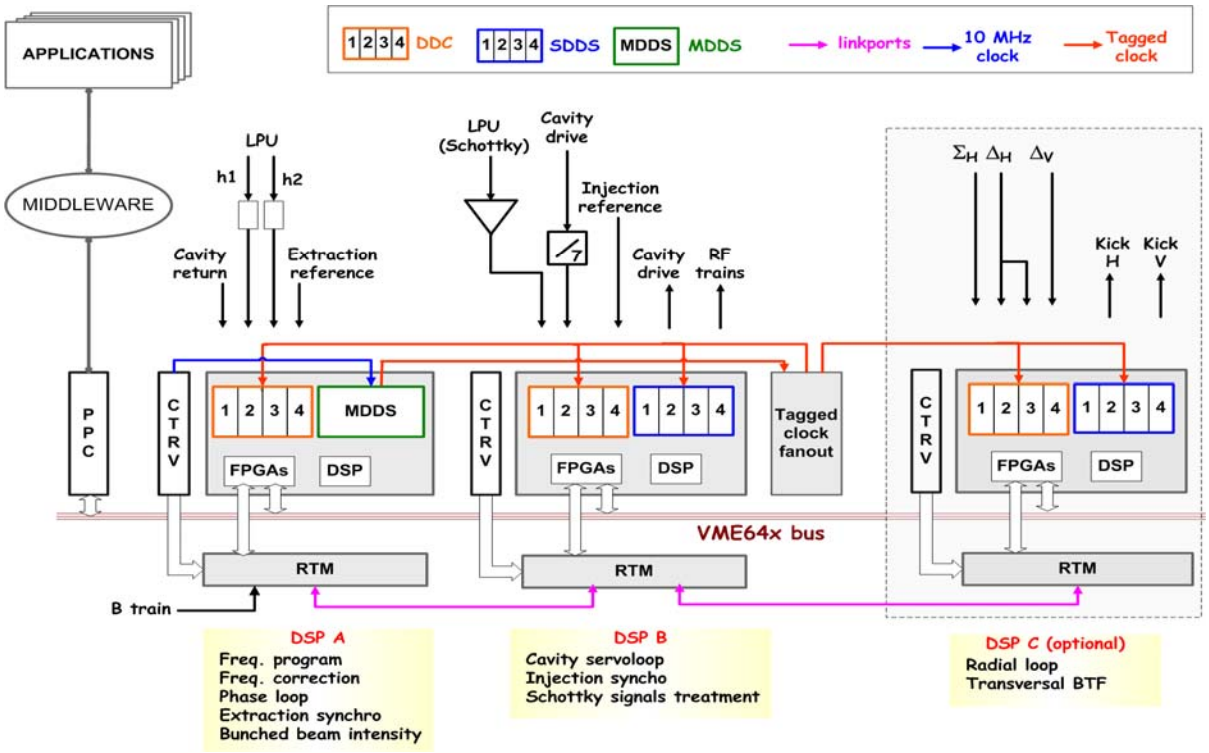

***Figure 13**: LLRF and intensity-tune measurement systems proposed for the ELENA ring.*

A similar system can be envisaged for the AD, if a consolidation plan is required.

7. CONCLUSION AND FUTURE WORK

The AD Schottky system described in this note provides data that are essential for a smooth AD operation as well as for the experimental users. The same data processing on a more flexible hardware is proposed for the new compact ring for post-AD antiproton deceleration & cooling, ELENA. A similar system can be envisaged for the AD, if a consolidation plan is required.

REFERENCES

[1] S. Baird et al., "*The antiproton decelerator: AD",* Proc. 1997 Particle Accelerator Conference, Vancouver, Canada (1997).

[2] C. Gonzales, F. Pedersen, "*An ultra low-noise AC beam transformer for deceleration and diagnostics of low intensity beams",* PAC '99, NY, 1999.

[3] O. Marqversen at al., *"'Real-time Tune Measurements On The CERN Antiproton Decelerator"*, DIPAC 2001, Grenoble, France.

[4] D. Boussard, "*Schottky Noise and Beam Transfer Function Diagnostics"*, CERN SPS/86-11 (ARF), 1986.

[5] M. E. Angoletta at al., "*The New Digital-receiver-based System For Antiproton Beam Diagnostics"*", PAC '01, Chicago, US.

[6] M. E. Angoletta at al., "*Upgrades To The Digital-receiver-based Low-intensity Beam Diagnostics For CERN AD"*", PAC '03, Portland, US.

[7] Pentek, *Model 6441 Operating manual*.

[8] Pentek, *Model 6510 Operating manual*.

[9] T. Eriksson [ed.], *"' ELENA: A Preliminary Cost And Feasibility Study'",* CERN-AB-2007-079.

[10] M. E. Angoletta at al., *"Beam Tests Of A New Digital Beam Control System For The CERN LEIR Accelerator*", PAC '05, Knoxville, US

[11] M. E. Angoletta et al., *"First Experience With The New LEIR Digital Beam Control System"*, AB-Note-2006-003-RF.

Schottky Observations in the Tevatron

CARE NA3 Workshop

Chamonix, France, December 11-13, 2007

Andreas Jansson
Fermilab

Introduction

The Tevatron has two Schottky systems that are used in operation. One system works at a relatively low (21.4MHz) frequency, while the other works in the microwave regime (1.7 GHz). Both systems are integral parts of day-to-day collider operation, but they are used in different ways. This note gives a brief overview of the systems, and their operation. More in-depth information is available in the references.

21.4 MHz Schottky

The 21.4 MHz Schottky system consists of resonant pick-ups (horizontal and vertical) connected to spectrum analyzers in the main control room. The pick-ups were originally designed with movable plates in order to maximize sensitivity, although this functionality is no longer used. Also, the initial system had two pick-ups in each plane, and the signals could be combined with appropriate delays to separate protons from the counter-rotating pbars.

Due to the low frequency, the spectrum is dominated by coherent signal. To enhance the signal, the beam is usually 'tickled" using band-limited white noise injected through a vertical BPM. This limits use of the system to tune-up and dedicated studies. Without excitation, the signals are usually too weak and can difficult to interpret.

The system is primarily used for tune measurements. In particular, the 21.4 MHz Schottky is the workhorse for machine tune-up before each collider shots, as well as for various beam studies. Operation is purely manual, with the operator determining the tune by moving the cursor on the spectrum analyzer to determine the central peak of spectrum. Attempts were made to automate this process, but it was found to be very hard to develop and algorithm that consistently would find the central synchrotron line.

1.7 GHz Schottky

The 1.7GHz consists of two slotted waveguide microwave structures (horizontal and vertical). The signals are down-converted to baseband in three steps (Ifs are 400MHz and 21MHz), and connected to vector signal analyzers. The pick-ups are a directional, which provides for some (~20dB) differentiation between protons and pbars. In addition, the signals are gated after initial amplification (but before

down-conversion), which cleanly separates the two species and also allows for single bunch operation. The gating also improves the signal to noise ratio, by shutting out the thermal noise from the front end amplifier when there is no signal.

Because of the high frequency, the Schottky bands are very wide and the synchrotron satellites are not resolved. This lends itself easily to automated data analysis. The VSA spectra are read every few seconds by a stand-alone program running on a separate data analysis server. For each trace, a Gaussian curve is fitted to the upper and lower Schottky bands. Tune is determined from the position of the Schottky peaks, momentum spread is determined from their average width, and chromaticity is given by the difference in width between the upper and lower Schottky bands. Emittance can be calculated from the total power in the band, using an empirical calibration constant. All of these results are published to the control system and logged through the general logging system. This enables the long term evolution of the tune and other parameters to be tracked.

In addition, the measured tunes are plotted in real time in the control room, and an alarm will post when the values are outside of a pre-determined range, requesting the operators to make corrections to bring it back. The available tune space in the Tevatron is quite restricted, and incorrect tunes may lead to high losses or emittance growth. Corrections are usually required on the scale of every half hour to an hour. The 1.7 GHz Schottky is the only device available to measure tunes during HEP stores.

Due to the broad Schottky peaks at 1.7 GHz, the horizontal and vertical normal modes overlap and cannot be separated by frequency. Therefore, in the presence of coupling, the observed tunes are a weighted average of the two tunes, with the weights determined by the amount of local coupling. This tends to underestimate the tune separation. It can be shown that in a simple model, this effect exactly cancels the “pushing apart” of the tunes caused by the coupling itself, leading to the popular notion that the “1.7 GHz approximately measured the uncoupled tunes”.

The primary operational use of the microwave Schottky is to measure average tunes. The bunch-by-bunch tune measurement capability is used primarily for studies of e.g. beam-beam effects and compensation. The emittance, momentum spread and chromaticity readings are generally not used directly in operation, partially because there are other established instruments available (at least for emittance and momentum spread).

The ”momentum spread” reading from the 1.7GHz Schottky is really a measure of tune spread. By comparing this reading with the momentum spread as measured from the bunch length, it is possible to directly measure the beam-beam contribution to the tune spread. For pbars early in stores, beam-beam gives a significant contribution to the width of the Schottky bands.

The emittance reading scales well with the flying wire measurements during stores, but an apparent variation of the calibration constant has been observed from store to store. The chromaticity readings have been found to follow changes in chromaticity settings well, although quantitatively there is not perfect agreement. It should be noted that all of these readings are also affected by local coupling, which probably explains these discrepancies.

A problem that has been observed with the 1.7 GHz system is that early in stores there is a lot of coherent power in the longitudinal Schottky bands. The total power in the signal may be two orders of magnitude higher for the first half hour to an hour, as compared to the power level a few hours into the store. The source of this longitudinal signal is not well understood, but it is believed to be due to meta-stable remnant structure (solitons?) within the bunch. Sometimes, the signal also rebounds briefly a few hours into the store. This effect usually is only seen by the 1.7 GHz Schottky, and does not appear to cause any noticeable harm to the beam. However, the strong longitudinal signal may saturate components in the signal chain, producing inter-modulation products which temporarily mask the transverse Schottky signal. Because of this, the 1.7 GHz Schottky sometimes has problems to produce reliable tune measurement very early in the stores. Work of reducing the sensitivity of the system to these power surges is underway.

Summary

Schottky diagnostics is critical to the Tevatron collider operation. Low frequency "Schottky" is used with noise excitation for tune-up and studies, and passive microwave frequency Schottky is used during stores. The high frequency Schottky data is continuously analyzed and the measured parameters, such as tunes, published to the control system. Based on these results, tune corrections are made on a roughly hourly basis, whenever the changing beam-beam effect causes the tunes go out-of predetermined limits.

References

[1] A 1.7 GHz Waveguide Schottky Detector System, Pasquinelli et al, Fermilab, 2003 PAC IEEE Nuclear Science, June 2003, Portland, Oregon

[2] Experience with the 1.7 GHz Schottky Pick-ups in the Tevatron, A. Jansson, P. Lebrun, R. Pasquinelli, EPAC 2004, Lucerne, Switzerland

[3] Effect of coupling on 1.7 GHz Schottky tunes, A. Jansson, Fermilab Beams-Doc-1576, http://beamdocs.fnal.gov/AD-public/DocDB/ShowDocument?docid=1576

THE 4.8 GHZ LHC SCHOTTKY PICK-UP SYSTEM

Tom Kroyer, Fritz Caspers, Jose Miguel Jimenez, Owain Rhodri Jones, Christophe Vuitton, CERN, Geneva, Switzerland.

Timothy W. Hamerla, Andreas Jansson, Joel Misek, Ralph J. Pasquinelli, Peter Seifrid, Ding Sun, David Tinsley, Fermilab, Batavia, Illinois

Abstract

The LHC Schottky observation system is based on traveling wave type high sensitivity pickup structures operating at 4.8 GHz. The choice of the structure and operating frequency is driven by the demanding LHC impedance requirements, where very low impedance is required below 2 GHz, and good sensitivity at the selected band at 4.8 GHz. A sophisticated filtering and triple down-mixing signal processing chain has been designed and implemented in order to achieve the specified 100 dB instantaneous dynamic range without range switching. Detailed design aspects for the complete systems and test results without beam are presented and discussed.

INTRODUCTION

In order to optimize the integrated luminosity of the LHC, the beam emittance must remain as small as possible during the collision runs. Since the synchrotron radiation damping times required for any reduction in emittance are very long (of the order of 10 hours), the use of beam instrumentation that needs an excitation of the beam, hence leading to an increase in emittance, has to be limited [1]. This applies in particular to standard methods for the measurement of coherent tune and chromaticity that require various sources of beam excitation. A Schottky monitor on the other hand allows the measurement of these parameters without any additional excitation of the beam.

This monitor must comply with the stringent beam coupling impedance limitations of the LHC (longitudinal Z/n of the total machine <0.1 Ω up to 2 GHz). At the same time a very high transverse sensitivity is required in order to provide a reasonable signal to noise ratio even for a pilot bunch circulating in the machine. In order to meet those seemingly contradictory requirements we chose a frequency range of operation close to 5 GHz, where the coherent bunch spectrum is low and the pick-up impedance does not have too large an impact. At this frequency we are not yet limited by Schottky band overlap and pick-up (PU) technologies exist that permit a very high transverse sensitivity over a 100 to 200 MHz bandwidth with an acceptable length of the structure and suitable aperture. This amount of bandwidth is required to assure the possibility of gating on single bunches, which is not possible with a high Q cavity pick-up. Taking all these boundary conditions into account the choice of the PU hardware as well as the subsequent triple down conversion analog signal treatment chain is justified and will be discussed in the following sections.

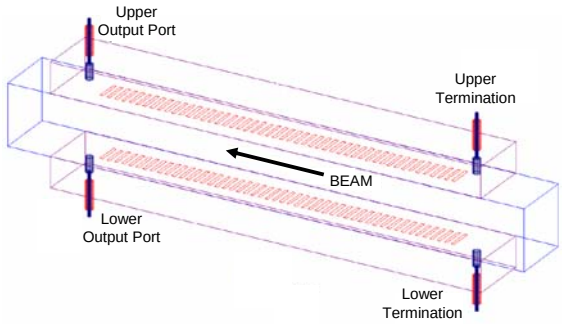

Fig. 1: The slotted waveguide slow-wave structure schematic for the LHC Schottky pick-up [4].

A detailed list of the LHC machine and beam parameters can be found in the literature [1, 2]. For the installation of this monitor in the tunnel a suitable location has been identified near point 4 in a normal conducting straight section meeting the required aperture of about 6 cm. Four monitors were installed, i.e. one for each plane of the two beams.

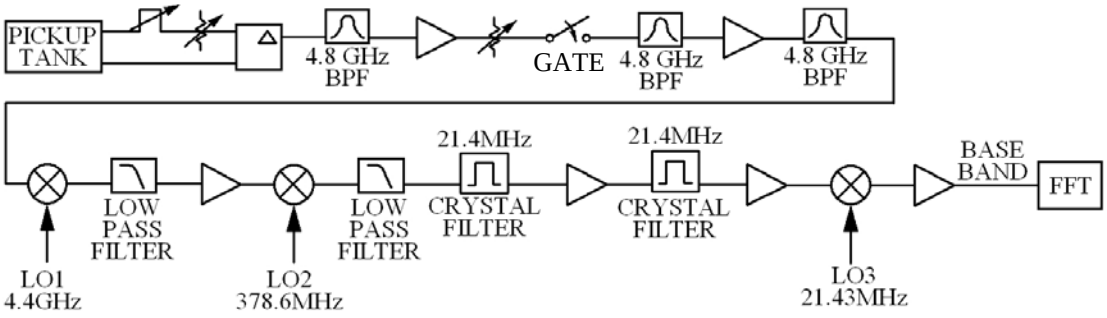

Fig. 2: Block diagram of the signal processing system

ANALOG SIGNAL TREATMENT CHAIN

A superheterodyne triple down conversion signal treatment chain has been designed and was implemented. This effort is required in order to provide a 100 dB instantaneous dynamic range without gain switching. Such triple down conversion concepts are also in use in high quality commercial instruments like certain spectrum analyzers for similar reasons. Such a large instantaneous dynamic range is required as there is a possibility that strong coherent signals may also appear in the bandwidth of interest. This is a typical phenomenon in large proton machines (SPS, Tevatron, RHIC). A simplified block diagram is shown in Fig. 2.

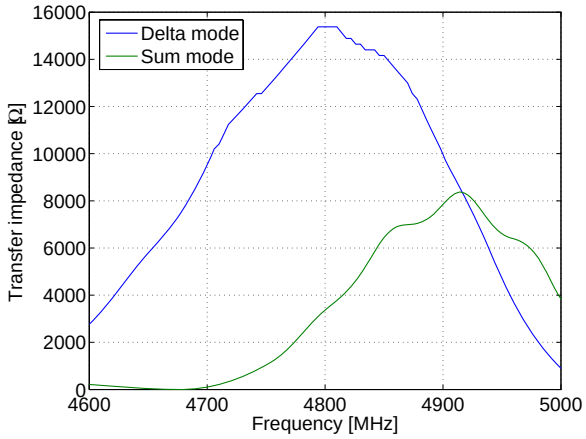

Fig. 3: Simulated transfer impedance for LHC Schottky monitor

Mechanical centering of the pick-up for maximizing common mode rejection was not an option as pickup motion could create an aperture restriction which is unacceptable in the LHC. Common mode signal reduction is therefore implemented by continuously adjustable mechanical attenuators and phase shifters before the signal recombination in the hybrids.

One important part of the RF front end is the gate to select single bunches or groups of bunches in the machine.

DETECTOR SENSITIVITY

The simulated transfer impedance of the LHC Schottky pick-up [7] is plotted in Fig. 3**Error! Reference source not found.**. The design has been centered at 4.8 GHz, which is an integer multiple of the 40 MHz revolution lines of the 25 ns bunch spacing of the nominal LHC beam. The transverse sensitivity of the pick-up has been designed to peak at this frequency. However, there is also a substantial longitudinal sensitivity at this frequency. From past experience it is estimated that the frequency offset between the simulated and the real pick-up response may be of the order of 50 MHz [6,7]. This was taken into account in the design of the signal treatment chain.

EXPECTED SIGNAL STRENGTH

The quantities of interest measured by the Schottky Monitor are the transverse Schottky sidebands. The signal to noise ratio (SNR) is given by the power of a Schottky sideband divided by the noise power in a relevant bandwidth. For this bandwidth several definitions are in use [2]; for the results presented below the +/- 1 sigma width of the Schottky bands is employed.

The signal to noise ratio after combination of the two arms in a perfect hybrid is given for the longitudinal signals (sum output) as [2]

$$SNR_L = \frac{e^2 N f_0^2}{kT\Delta f}\frac{Z_\Sigma}{N_f}, \qquad (1)$$

where e is the elementary charge, N the number of particles in the beam, f_0 the revolution frequency, k the Boltzmann constant, T the pick-up temperature, Δf the width of the Schottky band, Z_Σ the sum mode pick-up impedance and N_f the noise figure of the signal processing chain. The signal to noise ratio for the transverse signal (difference output of hybrid) is given as

$$SNR_T = \frac{e^2 N f_0^2 a_{rms}^2}{kT\Delta f}\frac{2Z_\Delta}{d^2 N_f}, \qquad (2)$$

where a_{rms} is the rms beam size, Z_Δ the Delta mode pick-up impedance and d the beam pipe diameter. The "old definition" of Z_Σ and Z_Δ are used here [5]. The expected sum and difference spectrum for a nominal LHC beam after combination in an ideal hybrid is shown in Fig. 4. The noise figure of the signal processing chain is not included and the chromaticity was neglected on account of its small effect on the bandwidth and SNR. A thermal noise floor of -174 dBm/Hz is assumed, which adds to the expected signal from the beam.

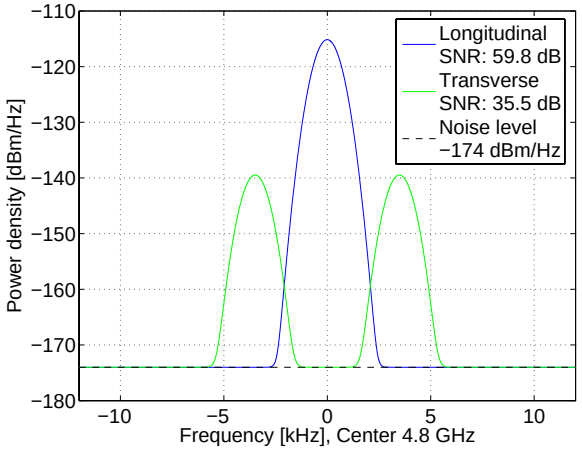

Fig. 4: The calculated spectrum for a nominal LHC proton beam at injection.

Tab. 1 shows the expected SNR for the different types of beams in the LHC. The noise figure of the signal processing chain and the possible improvements by gating

are not included. The range given for the pilot beam corresponds to minimum and maximum transverse emittance.

		Schottky SNR [dB]	
		longitudinal	transverse
Nom. p^+ beam	inj.	60	36
	coll.	64	28
Pilot p^+ beam	inj.	12	-17 to -13
	coll.	16	-25 to -20
Nom. Pb ion beam	inj.	58	34
	coll.	64	28
Early Pb ion beam	inj.	49	24
	coll.	54	18

Tab. 1: Calculated SNR of the incoherent Schottky band for nominal beam and pilot in the LHC.

GATING

When the beam fills only a small fraction of the machine circumference, the pick-up will detect noise for most of the time. In particular for the pilot beam the noise level may become comparable to, or even bigger than, the Schottky sidebands. In this case the effective noise level can be decreased by gating, where the input signal is switched "on" only for a relatively short time during the passage of the beam. In practice, however, the input signal cannot be totally switched "off" and there will always be thermal noise coming from the terminating load and/or the losses of the switch itself. A cryogenic load could be used as a low-noise termination together with a lossless switch. A load at 1 K would then reduce the noise power by a factor 300 or 25 dB. However, in reality switches typically have transmission losses of about 2 dB, which renders such a concept non-applicable.

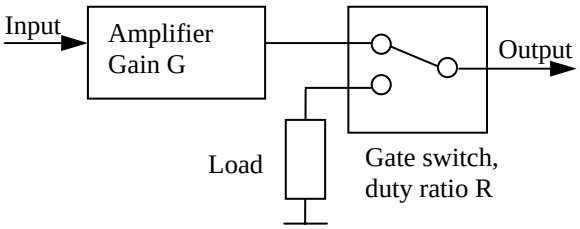

Fig. 5: Gating after pre-amplification can be used to reduce the effective noise level

The remaining option is to use sufficient pre-amplification before the gate (Fig. 5). This way *both* the input noise and the beam signal are boosted. After this amplification, the gate switch can be used to pick out the amplified beam signal plus noise during the passage of the beam. The amplified noise during the rest of the time is removed by the gate and is replaced by the thermal noise of the gate in the "off" position, so corresponding to an effective reduction of the overall noise level.

The increase in signal-to-noise ratio due to gating, *SNR'* can be derived as:

$$SNR' = \frac{SNR_{OUT}}{SNR_{IN}} = \frac{G}{RG + 1 - R}, \qquad (3)$$

with the amplifier gain G and the gate duty ratio R. For small *G* the gain in signal to noise is proportional to *G*, while for large *G* the gain in signal to noise converges to *1/R*. In LHC, with a gain before gating of 35 dB, it should be possible to improve the SNR through gating by about 30 dB for single bunch measurements.

CONCLUSION

In the framework of a LARP collaboration between FNAL and CERN a Schottky monitor system for the LHC has been designed and is now nearly completely installed. All test results can be found on a LARP web page [8]. Three stage down conversion has been implemented to achieve an instantaneous dynamic range of 100dB without gain switching, while a 24-bit Audio ADC followed by an FPGA implemented FFT algorithm [9] will be used to provide the continuous FFT spectra of the down converted baseband signals

ACKNOWLEDGEMENTS

The authors would like to thank the US Department of Energy Office of Science and LARP for financial support. Thanks also to Fermilab's Accelerator Division RF and Mechanical Support Departments and R. Garoby (CERN, AB-BI) and T. Linnecar (CERN, AB-RF) for their support. We would also like to acknowledge the work done by Andrea Boccardi, Marek Gasior and Krzysztof Kasinski in providing a superb system for the baseband acquisition of the Schottky signals.

REFERENCES

[1] LHC Design report, Vol. 1, CERN-2004-003, Geneva, CERN, 2004
[2] Kroyer, T., Incoherent High-Frequency Schottky Signals in LHC, CERN-AB-Note-2007-021 (2007)
[3] Linnecar, T, Schottky beam instrumentation, CERN-PE-ED 001-92, Geneva, CERN, 1992
[4] McGinnis, D, Slotted Waveguide Slow-Wave Stochastic Cooling Arrays, Particle Accelerator Conference PAC '99 , New York, USA, 1999
[5] McGinnis, D, 4-8 GHz Debuncher Upgrade Array Impedance Response, FNAL Pbar Note 580, 1998
[6] Pasquinelli, R J et al., A 1.7 GHz Waveguide Schottky Detector System, Particle Accelerator Conference PAC 2003, Portland, OR, USA
[7] Sun, D, McGinnis, D, Pasquinelli, R, Private communication, 2006
[8] http://larpdocs.fnal.gov/LARP-public/DocDB/ShowDocument?docid=482
[9] Boccardi, A et al, "The FPGA-based continuous FFT tune measurement system for the LHC and its test at the CERN SPS", these proceedings, PAC2007.

Schottky observation: Results of discussion

The use of Schottky systems at the different facilities has been complied in the following table:

	RHIC	**Tevatron**	**LEIR**	**AD**	**LHC**
Current I	Not foreseen	Not foreseen	Not foreseen	Yes	Not foreseen
Momentum spread Δp/p	Yes	Yes	Yes	Yes	Yes
Tune q	Yes	Yes	Yes	yes, but noisy BTF instead	Yes
Chromaticity ξ	First attempts	Possible	No	No	Under investigation
Trans. Emittance ε	Yes, measurements presented	Yes, measurements presented	Yes, First attempts	No, too much noise	

The use of Schottky in all facilities is very successful concerning the determination of momentum spread Δp/p for the longitudinal degree of freedom and for the tune determination using transverse observation. The chromaticity ξ seems to be difficult everywhere. A fit to the sideband width is required, at Fermi-Lab the value is extracted from the line-width of the left sideband W_1 and the right sideband W_2 of the narrow band Schottky 1.4 GHz pickup as $\xi \alpha (W_1-W_2)/(W_1+W_2)$ with sufficient accuracy. Also for the momentum spread, and the relative transverse emittance, the corresponding properties of both side bands are used at Fermi-Lab. If a broadband Schottky pick-up is used, a harmonics for the sidebands have to be chosen correctly to achieve a good resolution. A detailed comparison of the emittance results compared to the measurement with an ionization profile monitor has been presented for RHIC, but does not give conclusive results in all cases.
For space charge dominated beams, the Schottky sidebands are significantly deformed, as described by V. Kornilov. The deformation depends on the harmonic number and has to be taken into account for the determination of tune and chromaticity.
For bunched beams the suppression of the coherent lines required. This enables also the observation of bunch synchronous properties. A dedicated amplifier chain enhances the observation accurecy with even an effective noise temperature below the ambient value is described by Jocelyn Tan and confirmed by F. Caspers.

LONGITUDINAL SHOTTKY SIGNAL MONITORING FOR PROTONS IN HERA

Wilhelm Kriens, Michiko Minty, Deutsches Elektronen Synchrotron, DESY
Hamburg, Germany

Abstract

Stable longitudinal behavior of the protons is an important feature for future HERA operation. Specific diagnostic tools must be developed for this reason. In this case a standard wall current monitor is used to detect a beam signal from the incoherent motion of the protons due to both coasting beam and synchrotron oscillations during luminosity operation. This will be helpful to understand the process of coasting beam production in HERA. The coherent rotation harmonics from the bunched beam are strongly suppressed to enable amplification of the Schottky signal. The signal processing will be described and measurements at HERA will be presented.

Table 1: Longitudinal Parameters for Protons in HERA

Beam Energy	$cp = 920\,GeV$
Revolution Frequency	$f_0 = 47.3\,kHz$
Harmonic Number	$h = 4400(1100)$
RF Frequency	$f = 208(52)\,MHz$
RF Voltage	$V_c = 580(100)\,kV$
Momentum Compaction	$\eta = 1.3 \times 10^{-3}$
Synchrotron Frequency	$\nu_s = 37\,Hz$
Bunch Length FWHM	$\tau = 1.2 \ldots 1.8\,ns (10\,h)$
Longitudinal Emittance	$\epsilon = 0.6 \ldots 0.85\,eVs$
Number of Protons/Bunch	$N_b = 7 \times 10^{10}$
Number of Bunches	$n_b = 180(220)$

1 INTRODUCTION

Two rf systems are used to capture and accelerate the proton beam in HERA. Both systems apply fast feedback for stable beam operation. Table 1 lists the longitudinal parameters at high energy. The longitudinal emittance growth during the luminosity run is mainly due to intrabeam scattering. At the same time the acceptance around the bucket becomes populated with coasting beam causing background disturbances for the experiments. The process behind this is not understood so far. In HERA 180 proton bunches are circulating at a distance of $(220 \times f_0)^{-1} = 96\,ns$. Every eleventh bucket is empty and a $1\mu s$ gap for a dump kicker is empty too. Therefore even with equal bunch charges the spectrum measured using a wide-band pick-up has strong coherent revolution harmonics which can obscure the small Schottky signal arising from incoherent particle motion both inside the bunch and from the coasting beam. To achieve the resolution for Schottky signal detection one needs first a pick-up with sufficient sensitivity for an acceptable S/N ratio. But additionally it is important to suppress the revolution harmonics which decreases the dynamic range.

2 DETECTOR CONCEPT

The Schottky signal from bunched and unbunched beams in a circular machine has a periodic time structure. Therefore it is convenient to concentrate on the frequency domain for signal analysis. The full spectral information is inside a band surrounding every harmonic of the revolution frequency. For unbunched beams the power spectral density decrease with the harmonic n until they are overlapping and the Schottky current depends on the square root of the total number of particles N [1]:

$$\Delta f(n) = n f_0 \eta \tfrac{\Delta p}{p} \quad , \quad I_{RMS} = 2e f_0 \sqrt{\tfrac{N}{2}} \, ,$$

where $\Delta p/p$ is the beams' momentum spread.
Bunched beams have symmetric sidebands of the particle synchrotron frequencies [2] [3]. In a small frequency band the Schottky current can be approximated by

$$I^{n,k}_{RMS} = 2e f_0 \sqrt{\tfrac{N'}{2}} J_k \left(n\omega_0 \overline{\tau}_a\right) \, , \quad \text{where}$$

N' is the number of protons in the band with $n\omega_0\overline{\tau}_a$ the average phase space oscillation amplitude and J_k is the Bessel function of the first kind. The detector signal power depends on the square of the pick-up sensitivity S; i.e. $P_s \sim (I_{RMS} \times S)^2$. Therefore high frequency cavity pick-ups are mostly chosen although the Spectral density of unbunched beams is proportional to $(n\omega_0)^{-1}$. In our case the large amplitude behavior of the bunched beam is of main interest so the pick-up should have not only a high sensitivity but also a linear response to the bunched beam. At a given sensitivity the choice for the measurement frequency $n\omega_0$ has to take the argument of the Bessel function $(n\omega_0\overline{\tau}_a)$ and the spectral density of the coasting beam into account.
60 MHz is a good choice for applying a narrow-band crystal filter and for avoiding strong harmonics from the 10.4 MHz bunch frequency. To prevent ringing of the filter due to the strong peak voltage from the beam, a voltage limiter is used at the input. The filter output is purely sine-wave at 60 MHz with a small phase modulation which contains the signal information. The amplitude is related to the coherent revolution harmonic and can be suppressed for dynamic reasons using a limiting amplifier with low phase distortion. A high resolution FFT can be applied to the signal after down converting to baseband.
Fig. 1 shows a block diagram of the detector.

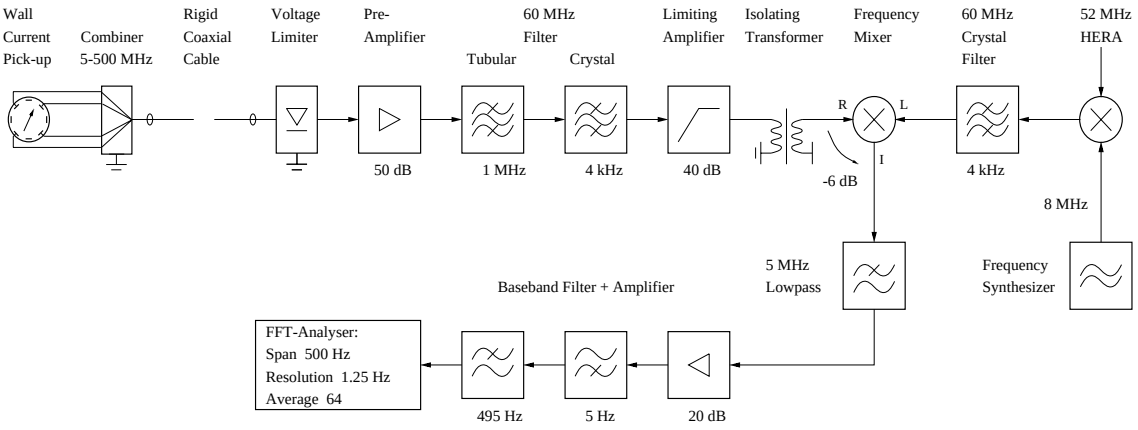

Figure 1: Block diagram of the Schottky Detector.

3 HARDWARE

3.1 Wall Current Monitor

Four dedicated orthogonal striplines from one HERA wideband bunch monitor are combined for a maximum sensitivity of $S = 7\Omega$ around 60 MHz. The output peak voltage into $50\ \Omega$ at the end of 100 m of rigid coaxial cable from a bunch with a 1.6 ns bunch length (FWHM) containing 7×10^{10} protons is about 50 V. For comparison, the signal power from an unbunched beam containing for example 1×10^{10} protons is

$$P_s = \frac{(I_{RMS} \times S)^2}{50\ \Omega} \approx 1 \times 10^{-18}\ W, \qquad I_{RMS} \approx 1\ nA.$$

A $50\ \Omega$ load produces at room temperature the same amount of thermal noise in a frequency band of 270 Hz. Nevertheless, at 60 MHz a particle momentum spread of 1×10^{-4} is concentrated in a band of only 8 Hz which is sufficiently small for good resolution.

3.2 Peak Signal Limiter and Preamplifier

The pick-up signal is fed into a thin-film diode limiter with low phase distortion and fast recovery from saturation (Avantek, Inc.: UTL-1002). This reduces the contribution to the signal from the peak voltage to a level acceptable for input into the two stage low noise preamplifier.

3.3 Bandpass Filter

At this point the detection can concentrate on a single revolution harmonic using analog filtering in two steps. First a tubular bandpass filter is used to reduce unwanted signal power and second a crystal filter with a few kHz bandwidth around $1268 \times f_0$ is used to extract the signal information.

3.4 RF Signal Limiter

This signal information of interest is purely phase modulation of the 60 MHz filter output. Therefore a limiting amplifier can be applied to reduce unwanted contribution from the rotation harmonic. A bipolar three-stage rf limiter with low phase distortion and 40 dB of input power range is used for this task (Avantek, Inc.: UDL-503).

3.5 Down Conversion

To avoid ground loop distortion the detector is isolated up to this stage. The signal level now is high enough to connect to the local ground using an rf transformer. Down conversion to baseband for high resolution FFT is mandatory. A 60 MHz reference derived from the 52 MHz acceleration frequency and 8 MHz from a synthesizer achieve about 0.1 Hz in long term stability. The baseband signal from 5 Hz to 495 Hz centered at 250 Hz is now amplified up to a level convenient for standard signal processing.

3.6 FFT-Analyser

The total detector amplification for the signal power P_s is about 97 dB. A standard FFT-Analyser with 1.25 Hz of resolution detects a noise level of -85 dBV which is equivalent to an input noise figure of 3 dB. Hence the detector resolution is about

$$\frac{P_{s,min}}{\Delta f} \approx 1 \times 10^{-20}\ \frac{W}{Hz}.$$

For data display VEE [1] visual engineering software is used connecting to the FFT-Analyser via an HP-IB [1] interface.

4 MEASUREMENTS

4.1 Coasting Beam Signal

Fig. 2 shows a Schottky signal from a coasting beam just after debunching at 920 GeV/c. The number of protons is about 6×10^{12} and the momentum spread $\Delta p/p$ is 5×10^{-4} within a frequency spread of 40 Hz.

4.2 Bunched Beam Spectra

The spectrum measured just after ramping the beam energy to 920 GeV/c shows many coherent longitudinal modes of

[1] trademark

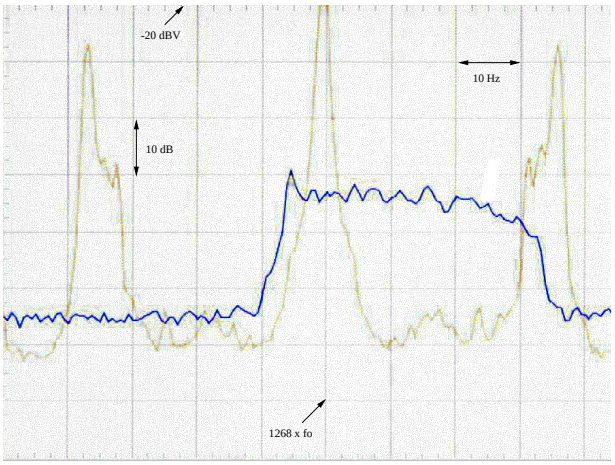

Figure 2: Bunch spectrum with some coherent oscillation in HERA and the coasting beam spectrum at the same output just after switching off both rf systems.

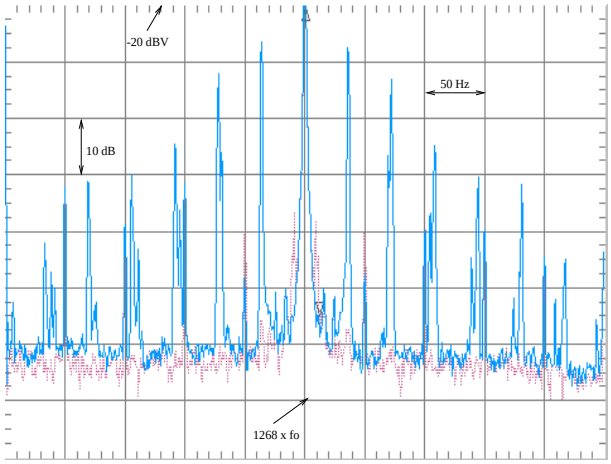

Figure 3: Coherent oscillation modes at the beginning of the high energy run. The 50 Hz lines are artificial due to line disturbance.

oscillation (see Fig. 3). These modes are continuously decaying during the first hour. After several hours the spectrum is more or less relaxed and reveals some structure inside the synchrotron band (see Fig. 4). The sidebands at about 9 Hz are most likely related to some protons inside the outer composite 52 MHz bucket. Probably it is a coherent dipole mode oscillation because of the missing second Bessel component. The oscillation frequency of 9 Hz corresponds to 100 kV from the 52 MHz system in conjunction with 580 kV from 208 MHz. Other conspicuous peaks in the spectrum may result from unknown beam excitation. The synchrotron frequency band of the main 208 MHz bunch at 37 Hz is not particularly pronounced due presumably to the peak signal limiter and the absence of coherent oscillation. Another example For a bunched beam spectrum is shown in Fig. 5. Here the 52 MHz voltage was 140 kV resulting in a slightly higher sideband frequency.

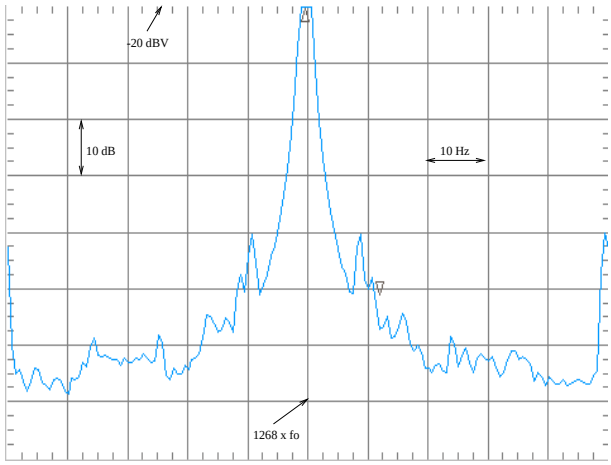

Figure 4: HERA proton spectrum after several hours at 920 GeV. The 52 MHz voltage level is 100 kV composing an island with synchrotron frequencies at about 9 Hz.

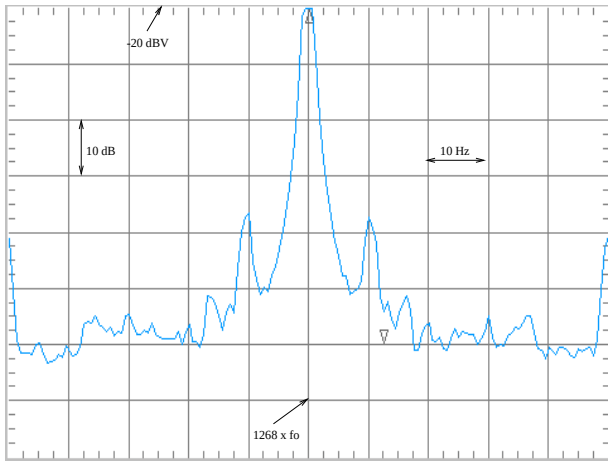

Figure 5: The same condition as in Fig. 4 but the 52 MHz voltage level is 140 kV.

ACKNOWLEDGMENT

The authors would like to thank U. Hurdelbrink and G. Weiberg for their technical support.

REFERENCES

[1] D. Boussard, 'Schottky Noise and Beam Transfer Function Diagnostics', CERN Proc. Accel., 22 Nov 1995, Vol.II

[2] R. H. Seemann, 'Bunched Beam Diagnostics', AIP Conf. Proc. 184 'Physics of Particle Accelerators',199x, Vol.I

[3] S. Krinsky 'Measurements of the Long. Parameters ...', Frontiers of Particle Beams, Observation, Diagnosis and Correction, Proceedings, Anacapri, Isola di Capri, Italy 1988, Lecture Notes in Physics, M.Month, S. Turner (Eds.)

FAIR Requirements for Tune Determination

Peter Forck
Gesellschaft für Schwerionenforschung, Darmstadt, Germany

Demands for the new FAIR facility

FAIR (Facility for Antiproton and Ion Research) will be a very versatile proton and ion accelerator facility. High current proton beams will be accelerated by a new LINAC, composed of CH-structures, injected to the existing SIS18 heavy ion synchrotron used as a booster with a maximum rigidity of 18 Tm and then further accelerated to 29 GeV in the new SIS100 synchrotron having 100 Tm maximum rigidity. The protons will be used for antiproton production. For the ion operation, the existing UNILAC, after some up-grade, will serve as the injector for very high currents of all ion species. The existing SIS18 will serve as a booster. The new SIS100 will accelerate the ions to an sufficient energy for an effective production of radioactive ion beams (RIB) within an in-flight production target and a complex separation spectrometer, the super-conducting fragment separator S-FRS. The RIBs as well as stable ions will be injected in several storage rings for cooling purposes and various experiments. The main advantage of the new facility is the possibility to increase the amount of primary heavy ions by about a factor of 100 with SIS100 (depending on the ion species) as well as an improved transmission of the RIBs up to a factor of 100 by the new S-FRS. Versatile investigations of the RIB species in the storages rings are foreseen, which requires a fast de-bunching scheme and complex stochastic and electron cooling procedures. Deceleration of the RIBs and antiprotons down to 4 MeV/u is an integral part of the foreseen operation at FAIR. The main challenges for the high current operation in SIS100 are described below. More details and meaningful plots are presented in the corresponding talk.

Challenges for high current operation of SIS100

For the RIB production the SIS100 operation scenario is based on storage and acceleration of low charge state ions to prevent for particles losses at several stripper sections prior to SIS18 and between SIS18 and SIS100. For the design ion U^{28+} the injection energy is only 200 MeV/u (as given by the 18 Tm max. rigidity of SIS18). Four batches with two bunches each will build up a complete SIS100 filling. For these parameters several topics are important to estimate the requirements for the closed orbit and tune stabilization of beams for the SIS100 high current ion acceleration:

- **Large tune spread:** Due to the low charge states for the RIB production, the injection energy is only 200 MeV/u in case of U^{28+}. For the design current of $5 \cdot 10^{10}$ ions per bunch, this leads to a large incoherent tune spread of $\Delta Q \approx 0.3$. As given by the maximal ramp rate of the proceeding SIS18, the storage time of the first batch is about 1 s and the beam has to be stabilized during this relatively long duration.
- **Low dynamic aperture:** Super-conducting magnets will be used for the dipoles and quadrupoles at SIS100. These super-ferric magnets are ramped within 300 ms; this fast ramping is required to achieve a large amount of average ion rate delivery to the production target. For the properties of the precursor magnet type constructed at JINR at Dubna and used at Nucletron, the dynamic aperture is calculated with the code MICROMAP. At injection energy, the dynamic aperture is only about $3 \cdot \sigma$, with σ being the standard deviation of the beam size. Taking a realistic space charge tune spread into account as given for the $5 \cdot 10^{10}$ U^{28+}, the dynamic aperture shrinks well below $3 \cdot \sigma$ and the rate of beam loss has to be taking into account in an accurate manner. During the maximum storage for the first batch of about 1 s, the beam has to be stabilized to minimize this beam loss. This concerns the closed orbit as well as the tune to prevent resonance cursing for the beam with large space charge tune spread. Due to the large tune spread an accuracy of about $Q \approx 0.01$ seems to be sufficient for these parameters.
- **Beam loss by electron stripping:** For the low charge state ions, e.g. the design case of U^{28+} electron stripping becomes the dominate beam loss process and special catchers for the dump of the charge changing ions (U^{29+} in the design case) are foreseen in the SIS100. With them a significant increase of the vacuum pressure due to beam induced desorption from the pipe walls should be avoided. Due to the large energy loss at the wall surface by slow heavy ions, this

desorption is the dominant process for a dynamic vacuum pressure increase: The desorbed molecules can than trigger an avalanche effect due to an increase electron stripping rate leading to a vacuum induced instability. But also a significant beam loss due to the crossing of the dynamic aperture leads can lead to this avalanche behavior, even though the loss might better be distributed along the synchrotron circumference. In connection with the low dynamic aperture, beam stabilization is required.

- **Fast acceleration:** At SIS100 a ramp rate of 3 T/s is foreseen, which is relatively fast for super-ferric magnets, resulting in a total ramping time of about 0.5 s. During this time, the closed orbit and the tune has to be stabilized by a fast feedback with an anticipated reaction time of 10 ms only. This fast reaction time is difficult to realize, even though 10 ms correspond to about 1000 turns in the 1100 m long SIS100, a turn-number where also the reaction at LHC is foreseen. Presently, the dynamic effects of the magnets during ramping and the resulting variation for closed orbit and tune is not sufficient well investigated to give a specification of the required beam stabilization accuracy.
- **Bunch gymnastics:** For the transfer from SIS100 to the storage rings, bunch rotation is required, in particular for RIB production to minimize the longitudinal emittance enlargement at the target. Prior to the bunch compression, a controlled de-bunching to one barrier bucket within about 100 ms is foreseen. The diagnostics have to able to cope with the different bandwidth and time requirements during this manipulation.

Challenges for operation of the storage rings

The storage rings will mostly be operated with a low number of RIBs or antiprotons. Therefore, the beam diagnostics is designed to provide the lowest possible detection threshold. Cooling methods are applied, but stochastic cooling works most efficient, if a close orbit feedback counteracts the coherent beam deviation from the ideal orbit. For acceleration a feedback should prevent for beam losses. More challenging is the deceleration of the RIBs and antiprotons foreseen in RESR and NESR with a ramp rate of 1 T/s using normal conducting magnets. Due to the emittance enlargement, which can only be partly counteracted by electron cooling due to the relatively long time constant of the RIB case, a feedback is required with a reaction time of about 10 ms, i.e. comparable parameters as for the SIS100 case. The use of normal conducting magnets might relax the demands on the feedback.

Peculiarities and requirements for tune measurements and feedback at FAIR

Non-relativistic beam are stored prior to the acceleration within the super-ferric SIS100. For the BPM system, the change of the revolution time from 9.1 μs to 4.5 μs for the design case of U^{28+} ions is demanding for the technical realization. Moreover, the long barrier bucket and the short bunch after rotation calls for a large bandwidth of the BPM analogue electronics. The tune measurement and feedback system have to be capable for these varying bunch-length, repetition rate and amplitude. Presently, a possible solution is under first investigation using a direct digitalization of the BPM signals with 125 MSa/s ADC and dedicated digital signal processing, as described by U. Rauch within this session. During the ≈0.5 s long acceleration at SIS100 a possible tune measurement and feedback system should work with a reaction time of ≈10 ms or about 1000 turns, which is quite fast compared to existing systems. Moreover, only a very weak excitation will be allowed due to the small dynamic aperture leading to a challenging technical realization. The tune spread for SIS100 design case U^{28+} is estimated to be $\Delta Q \approx 0.3$ at injection. Most existing tune measurement systems are not designed for such a large value and it is not clear, whether demanding problems occur for these parameters.

For the storage rings, the large dynamic range in terms of amplitude and frequency variation seems to be the most demanding task as the feedback system will mainly be used during acceleration or deceleration of low amount of RIBs or antiprotons.

Acknowledgment

The author likes to thank Jürgen Dietrich (FZJ), Guilliano Franchetti (GSI), Vladimir Kornilov (GSI) and Piotr Kowina (GSI) for valuable discussion and significant contribution to the described considerations.

TUNE, CHROMATICITY, AND COUPLING OBSERVABLES

M. Giovannozzi, CERN, Geneva, Switzerland

Abstract

A review of the three main observables for particle beam dynamics, namely tune, chromaticity and coupling is presented. Their relevance for the analysis of single-particle motion will be discussed together with computational and measurement issues.

INTRODUCTION

The three observables tune, chromaticity, and coupling are the key quantities to characterise the behaviour of charged particles in a circular accelerator. Their measurement is crucial and their control is essential for the performance of a circular machine. In this paper a brief review of their properties as well as their link to the dynamics and the measurement technique is presented. The CERN Large Hadron Collider (LHC) will be used as an example to illustrate how the issues of controlling these quantities have been addressed in a real machine.

TUNE

The tune of a circular particle accelerator represents the value of the betatron oscillation frequency in either the horizontal or the vertical plane. The essence of the dynamics can be extracted by determining whether the tune is a rational (or quasi-rational) value. Indeed in this case the motion is periodic and the beam features a resonant behaviour, which can lead to single-particle instabilities and eventually particle losses. In this context, particle instability is intended as growth of the amplitude of the betatronic motion due to the resonant dynamics.

To avoid resonances, at least low-order ones as rational numbers are dense in the irrationals, is a well-established design principle for particle accelerators. Recently the importance of resonances in the context of space charge effects was re-established and a number of interesting results were obtained (see Refs. [1, 2] for more details).

An essential point in this framework is the capability of measuring with a high accuracy the tune. By applying the very definition it is enough to excite a beam transversely and to record the subsequent betatronic oscillations. This method is affected by two main drawbacks: i) by kicking the beam the emittance is increased due to filamentation induced by many effects (non-linearities, among others). Therefore, a less perturbing approach than to excite the beam is required for the most challenging machines; ii) the data treatment is crucial to derive an accurate estimate of the tune. It is customary to use an FFT analysis to interpret beam position monitor (BPM) data. However, it is widely known that this is not the most efficient way to extract frequency information from measured time series (see, e.g., Ref [3] for an account of the methods developed in the domain of celestial mechanics). In the late nineties efforts were devoted to the transfer of the knowledge of harmonic analysis tools from celestial mechanics to accelerator physics. This resulted in a number of algorithms, analysis of the accuracy as a function of the length of time series, and codes (see Ref. [4-7] for an overview of the main results). The key results can be summarised as follows:

- The plain FFT can be refined providing closed-formulae for determining the tune with a higher accuracy than the FFT [4].
- While the error for the frequency determination for the case of a plain FFT scales as 1/N, with N the length of the time series, the proposed methods have an accuracy that scales as $1/N^a$, with a>1 depending on the use of special filters [4].
- These methods open the possibility of measuring the detuning with amplitude in lepton machines by combining the new methods with moving windows techniques [5] (see Fig. 1 for an example).

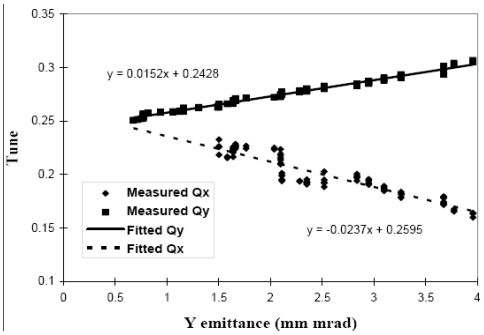

Figure 1: Horizontal and vertical tune as a function of the vertical emittance for the CERN Large Electron Positron (LEP) collider at 20 GeV (from Ref. [5]).

- The presence of electronic noise spoils the performance of the proposed methods, but an accuracy of $1/N^2$ can be achieved in real machines.

What is still an open question is how to apply the proposed methods in the presence of strong signal decoherence. This is the case of proton machines, where the signal amplitude decreases with time, without any real change of the betatronic amplitude of the particles' motion.

CHROMATICITY

The concept of machine chromaticity is essentially linked to the one of tune as it represents the variation of tune as a function of momentum offset, namely

$$Q(\delta) = Q_0 + Q'\delta + \frac{1}{2}Q''\delta^2 + \ldots$$

where δ is the relative momentum offset, Q' the linear chromaticity, Q'' the second order chromaticity and so on (this is the Taylor series of the tune as a function of the

momentum offset). The linear chromaticity induces a coupling between the transverse planes and the longitudinal one. This induces a tune modulation via the synchrotron motion and Q' is proportional to its amplitude. The importance of controlling the chromaticity is two-fold: it allows avoiding hitting resonances by off-momentum particles and it has an impact on the dumping time of collective instabilities.

The standard way of measuring the machine chromaticity is based on its very definition. The beam energy is changed and the corresponding tune measured, thus allowing the reconstruction of the complete function $Q(\delta)$, with an accuracy that depends on the energy span. As an example, the measurements performed in the CERN Proton Synchrotron (PS) machine [8] are shown in Fig. 2. Examples for the CERN Super Proton Synchrotron can be found in Ref. [9].

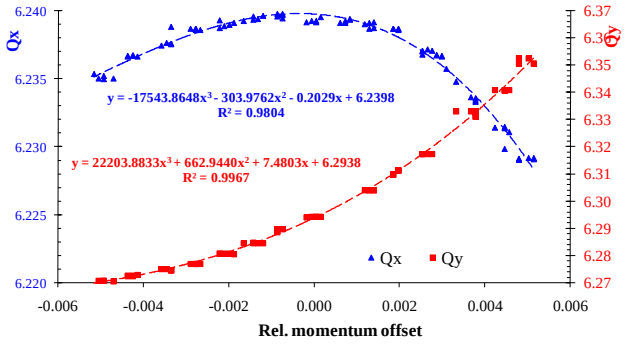

Figure 2: Dependence of the horizontal and vertical tunes on the momentum offset for the PS machine (from Ref. [8]). The fitted curves allow deriving the value of the linear chromaticity and its higher-order generalisations form the measured data.

It is worth stressing that this type of measurements can be used to build an effective model of the accelerator by introducing a number of artificial multipoles, which are used to reproduce the tune as a function of momentum offset.

Alternatively, head-tail frequency shift is another well-established method to measure chromaticity [10, 11]. The main drawback is that it requires a transverse deflection of the beam, thus inducing emittance blow-up. Recently [12], it was proposed an improved method, where the beam is continuously excited with small transverse kicks at the betatron frequency. In case this method proves to work well, it could open up the possibility of implementing a chromaticity feedback.

Tuning the linear chromaticity is possible by means of sextupole magnets, whose contribution is given by

$$Q'_{x,y} = \pm\frac{1}{4\pi}\int_{Ring} ds\, D_x(s) K_3(s)\, \beta_{x,y}(s)$$

where K_3 stands for the normalized, integrated sextupolar gradient and the minus signs is for the vertical plane. It is clearly seen that a sextupole in a dispersion-free region does not have any impact on the linear chromaticity. Furthermore, as it was already stated, there are some constraints on the sign of the chromaticity, as it needs to be negative below transition and positive above, just to avoid negative mass instability.

COUPLING

The linear coupling is the phenomenon for which the two horizontal and vertical planes are no more the eigenplanes of the particle's motion. Such a coupling is generated by longitudinal magnetic fields, e.g., solenoids, or skew quadrupoles. Whenever linear coupling is present, the motion is decoupled in the reference system given by the two eigenplanes, which, however, change their orientation with respect to the horizontal and vertical planes all along the machine circumference. As a consequence, the horizontal and vertical tunes are no more independent and they cannot be set freely.

To evaluate the strength of linear coupling in a machine, it is customary to use the so-called closest tune approach (see Fig.3 for an example).

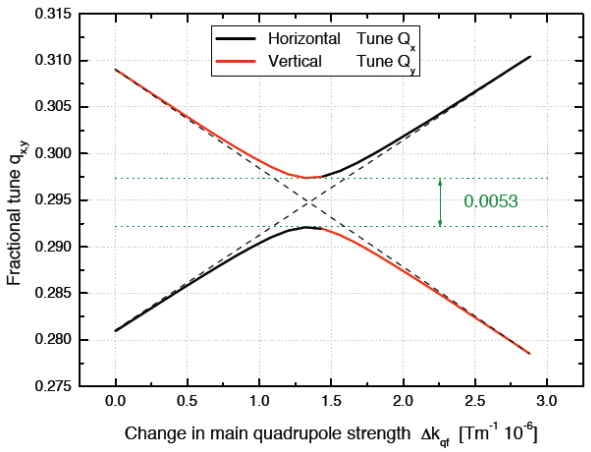

Figure 3: Example of the closest tune approach for the LHC ring in the presence of the experimental solenoid of the CMS detector at injection (from Ref. [13]).

The minimum distance between the tunes is related to the width of the coupling resonance.

Two approaches are possible to compensate the linear coupling, namely a local and a global decoupling. The first consists in reducing to zero the non-diagonal blocks of the transfer matrix at a given location. This means that the particle motion will be decoupled at a given machine section, but elsewhere it will remain fully coupled. The latter is based on the minimization of the difference coupling resonance c_-, whose strength is given by

$$c_{\pm} = \frac{1}{2\pi}\int_{Ring} ds\, \sqrt{\beta_x(s)\,\beta_y(s)}\; e^{i\left[\mu_x(s)\pm\mu_y(s)\right]} K_2(s),$$

by means of the skew quadrupoles located all around the machine circumference. Of course, the correction of the coupling will be global as the resonance strength is a global property of the ring.

THE CASE OF A REAL MACHINE

The simple examples mentioned in the previous sections do not illustrate the complexity of the behaviour of a real machine. The presence of unavoidable magnetic field errors implies that the betatron frequency will be a function of the transverse amplitude. Hence, the tune is now a function of the linear invariants $J_{x,y}$ and the momentum offset δ of the form

$$Q_{x,y} = Q_{x,y}(J_x, J_y, \delta) = \\ = Q_{x,y,0} + \frac{\partial Q_{x,y}}{\partial J_x} J_x + \frac{\partial Q_{x,y}}{\partial J_y} J_y + Q'_{x,y}\, \delta + \dots$$

where the coefficients of the Taylor series for the tune are functions of the magnetic imperfections as well as of the strength of the correctors incorporated in the lattice. Interestingly enough, by using the normal form approach to describe the transverse betatronic motion it is possible to derive the dependence of the various coefficients in the Taylor series of the tune on the multipolar errors according to the following table [14]:

Table 1: Structure of the terms contributing to the Taylor series of the tune as a function of $J_{x,y}$ and δ.

Off-energy order	**Transfer map order (transverse coordinates)** $\left(K_{n+1} = \frac{L}{B\,\rho}\frac{d^n B_y}{d\,x^n}\right)$			
	1	2	3	4
0	K_2	K_3	K_3^2, K_4	$K_3^3, K_3 K_4, K_5$
1	K_2, K_3	K_3, K_3^2, K_4	$K_3^2, K_4, K_3^3, K_3 K_4, K_5$	⋯
2	K_2, K_3, K_3^2, K_4	$K_3, K_3^2, K_4, K_3^3, K_3 K_4, K_5$	⋯	⋯

The structure of the table is clear:

- Only odd orders of the transfer map contribute to the tune function. Furthermore the coefficients of order $2n-1$ in the map contribute to those of the tune development at order $n-1$ in the invariants.
- Each cell in Table 1 inherits the multipoles' dependence from the cell above in the same column and from that above in the right column.
- While quadrupole components affect all cells, higher order multipoles have an impact only from a certain order in the invariants or momentum offset. This implies that, e.g., a chromaticity correction will have an impact on the detuning with amplitude.

In the case of the CERN LHC a number of non-linear correctors are implemented to compensate for the magnetic field errors due to the superconducting magnets [15]. In particular, spool pieces of sextupolar, octupolar and decapolar type are installed next to the main dipoles to provide a local correction of their systematic sextupolar and decapolar components. Furthermore, non-linear corrector magnets are also installed in the low-beta quadrupoles. Indeed, the large value of the beta-function in the low-beta quadrupoles enhances the harmful effects of the field errors, thus requiring a local correction.

Two complications can make machine operation particularly difficult and should be tackled at the level of the machine design, namely:

- Feed down effects and field quality of the correctors might impose an iterative procedure until convergence to the required value of the observable is achieved. For instance, a closed orbit correction might induce a tune variation due to a change in the feed down effects. For the LHC the mitigation measures consisted in imposing tight bounds on the field quality of the magnets so that both effects can be neglected.
- In the case of a superconducting machine, the beginning of the acceleration is a rather delicate phase. In fact, the so-called snap back effect [16], induces a strong variation of the sextupolar component in the dipoles. This generates a non-negligible variation of the main beam dynamics observables and in particular, a huge variation of the linear chromaticity, unless a proper correction is applied during the transient phase.

It is interesting to quote the required accuracy in the resolution of the measurements as a function of the various stages of the LHC operation [17], namely:

Table 2: Required resolution for the measurement of the three observables for the LHC machine.

	Resolution	
	Commissioning	Nominal
Q	3×10^{-3}	0.75×10^{-3}
Q'	2.5	$0.5 - 1.5$
$\lvert c\_\rvert$	3×10^{-3}	0.75×10^{-3}

From these considerations it is clear that the accurate control of the three observables is a challenging task and is crucial for achieving the nominal performance of the LHC.

CONCLUSIONS AND OUTLOOK

Tune, chromaticity, and linear coupling are the key observables for characterising the particle's motion in a circular accelerator. Their control allows curing some specific behaviour, by, e.g., avoiding the harmful effect of resonances, stabilizing collective instabilities and sharing

growth rates. Therefore, continuous measurements for both monitoring and applying the required corrections are of paramount importance for the successful operation of the next generation of circular accelerators. In this sense, the key problem consists in the definition of measurement approaches capable of continuous measurements, without inducing any measurable emittance blow-up.

ACKNOWLEDGEMENTS

The results presented in this paper were worked out by many people in the past years and their contributions are acknowledged here. I would like to express my gratitude to R. Jones for the opportunity of reviewing these topics at the CARE NA3 Workshop. Inspiring and fruitful discussions on the issue of tune computation in real machines with R. Jones, H. Schmickler, R. Steinhagen are also warmly acknowledged.

REFERENCES

[1] G. Franchetti, "Recent development in understanding beam loss in high-intensity synchrotrons", in proceedings of the PAC07 Conference, ed. by C. Petit-Jean-Genaz, IEEE Piscataway - NJ, p. 794, 2007.

[2] G. Franchetti, "Space charge and EC effects", presentation at the Beam07 CARE-HHH Workshop, CERN October 2007.

[3] J. Laskar, "Frequency analysis for multi-dimensional systems. Global dynamics and diffusion", Physica D 67, p. 257, 1993.

[4] R. Bartolini, A. Bazzani, M. Giovannozzi, W. Scandale, E. Todesco, "Tune evaluation in simulations and experiments", Part. Accel. 52, p. 147, 1996.

[5] R. Bartolini, J. Corbett, M. Cornacchia, M. Giovannozzi, C. Pellegrini, W. Scandale, E. Todesco, P. Tran, A. Verdier, "Measurements of the Tune Variations Induced by Non-Linearities in Lepton Machines", in proceeding of the EPAC96 Conference, ed. by J. Poole and C. Petit-Jean-Genaz, Institute of Physics UK London, p. 917, 1996.

[6] R. Bartolini, F. Schmidt, "SUSSIX : A computer code for frequency analysis of non-linear betatron motion" in proceedings of the Workshop on "Nonlinear and Stochastic Beam Dynamics in Accelerators: a Challenge to Theoretical and Computational Physics", ed. by A. Bazzani, J. Ellison, H. Mais, G. Turchetti, DESY 97-161, p. 390, 1997.

[7] J. Laskar, "Frequency map analysis and particle accelerators", in proceedings of the PAC03 Conference, ed. by J. Chew, IEEE Piscataway - NJ, p. 378, 2003.

[8] R. Cappi, M. Giovannozzi, M. Martini, E. M´etral, G. M´etral, R. Steerenberg, A.-S. Müller, "Optics studies for the CERN Proton Synchrotron: linear and nonlinear modelling using beam based measurements", in proceedings of the PAC03 Conference, ed. by J. Chew, IEEE Piscataway - NJ, p. 2913, 2003.

[9] R. Tomás, G. Arduini, R. Calaga, A. Faus-Golfe, G. Rumolo, F. Zimmermann, "Improved Algorithms to determine the Non-Linear Optics Model of the SPS from Non-Linear Chromaticity", Presented at Particle Accelerator Conference, Albuquerque, NM, USA, 2007.

[10] D. Cocq, R. Jones, H. Schmickler, "The Measurement of Chromaticity via a Head-Tail Phase Shift", in proceeding of 8th Beam Instrumentation Workshop, ed. by R. Hettel, S. Smith, J. Masek, AIP Conference Proceedings 451, AIP, NY, p. 629, 1998.

[11] S. Fartoukh, R. Jones, "Determination of Chromaticity by the Measurement of Head-tail Phase Shifts: simulations, results from the SPS and a robustness study for the LHC", LHC-Project-Report 602, 2002.

[12] S. Fartoukh, "A Theory of the Beam Transfer Function (BTF) with Chromaticity Induced Head-Tail Phase Shift", LHC-Project-Report-986, 2007.

[13] H. Burkhardt, "Experimental magnets commissioning", presentation at the LHC Commissioning Working Group, December 2007.

[14] A. Bazzani, G. Servizi, E. Todesco, G. Turchetti, "A normal form approach to the theory of nonlinear betatronic motion", CERN-94-02, 1994.

[15] O. Brüning, P. Collier, Ph. Lebrun, S. Myers, R. Ostojic, J. Poole, P. Proudlock, "LHC design report, Vol. I", CERN-2004-003, 2004.

[16] L. Bottura, T. Pieloni, S. Sanfilippo, G. Ambrosio, P. Bauer, M. Haverkamp, "A scaling law for predicting snap-back in superconducting accelerator magnets", in proceeding of the EPAC04 Conference, ed. by C. Petit-Jean-Genaz, Institute of Physics UK London, p. 1609, 2004.

[17] S. Fartoukh, J.-P. Koutchouk, "On the measurement of the tunes, coupling and detunings with momentum and amplitude in the LHC", LHC-B-ES-0009 rev 1.0, 2004.

Tune Measurement at the Tevatron

C.Y. Tan[1]
Fermi National Accelerator Laboratory, P.O. Box 500, Batavia, IL 60510, USA
(Dated: December 18, 2007)

Betatron tunes in the Tevatron are measured primarily with two instruments: the 21.4 MHz and the 1.7GHz Schottky systems. Two other instruments are currently being worked on as secondary instruments: the 3D-BBQ (direct diode detection baseband tune) system which is a copy of the system to be used at the LHC, and a direct digitization technique which gives very fast bunch by bunch tunes.

1. INTRODUCTION

The Tevatron is a single beam pipe machine which contains both protons and anti-protons for HEP. This poses a challenge for measuring betatron tunes because of the possibility of contamination from the other species. In order to overcome this problem, stripline type structures are usually used because they are directional by construction or for the case of the 21.4 MHz Schottky system, a clever method is used to distinguish between the two. In the Tevatron, tunes are measured primarily with two instruments: the 21.4 MHz and the 1.7 GHz Schottky systems. Two other systems currently in development are the 3D-BBQ (direct diode detection baseband tune) system and a direct digitization technique which gives very fast bunch by bunch tunes.

2. 21.4 MHz Schottky System

The 21.4 MHz Schottky system is the workhorse for measuring betatron tunes. This detector was installed in 1989 and is the oldest of all the tune measuring devices used in the Tevatron. This detector is the default standard for measuring proton tunes despite its limitations because historically it was the only detector available. To distinguish protons from anti-protons, the signals from two resonant structures are electrically combined. See the paper by J. Marriner:

- J. Marriner, "The Tevatron Resonant Schottky Detectors", Fermilab EXP Notes, EXP-193.

Despite this, the proton signals contaminate the anti-proton signals and so in order to see the anti-proton tunes, the anti-protons have to be excited. Furthermore, because of its high *Q*, it is not possible to gate individual bunches at the detector. However, by gating the kick instead, individual anti-proton tunes can be measured. This gated kick method cannot be used for the protons because the unkicked signal is already strong enough to produce a tune spectrum.

Other references to the 21.4 MHz Schottky system are:

- D. Martin, et al, "A Resonant Beam Detector for Tevatron Tune Monitoring", Accelerator Science and Technology Proceedings, vol 3 1486-1488, 1989.

3. 1.7 GHz Schottky System

This detector was installed in 2002. It was a breakthrough detector for the Tevatron because it was designed to be able to see anti-proton tunes without excitation and to measure individual bunch tunes.

1 Email address: cytan@fnal.gov

This detector is a slow wave waveguide structure which has directivity and designed with a low Q ~20 so that individual proton and anti-proton tunes can be gated and measured.

References for the 1.7GHz Schottky system are:

- R. Pasquinelli, "A 1.7 GHz Waveguide Schottky Detector System", Proceedings of the Particle Accelerator Conference 2003, p. 3068-3070.
- A. Jansson, "Effect of Coupling on Tevatron 1.7 GHz Schottky Tunes", Beams Document 1576-v2, http://beamdocs.fnal.gov, 2005. (This reference discusses why the 1.7 GHz Schottky system only sees "set" tunes and not coupled tunes).
- P. Lebrun, "Tevatron Tune Fitters, 1.7 GHz & 21.4 MHz:Sept 04 Status Report", Beams Document 1339-v2, http://beamdocs.fnal.gov, 2004. (This reference discusses how the tunes are fitted and datalogged and thus useful for having a tune history of all the HEP stores.)

4. 3D-BBQ System

This system in the Tevatron is similar to the one that will be installed at the LHC. The novelty of this system lies in the electronics which at its heart is a diode detector. It uses a stripline pickup so that the proton and anti-proton signals can in principle be distinguished. Presently, it is an R&D project funded under US LARP. This system is presently not operational, but is being worked on by a student.

A reference for the 3D-BBQ System is:

- M. Gasior & R. Jones, "High Sensitivity Tune Measurement by Direct Diode Detection", 7th European Workshopon Beam Diagnostics and Instrumentation for Particle Accelerators (DIPAC), 2005.

5. Direct Digitization

This system is called the "Digital Tune Monitor" at Fermilab. It uses direct digitization of the transverse signal from a standard beam position monitor stripline. Unlike the other systems which in principle do not need any beam excitation, this system requires kicks to the beam transversely in order to get the signal above noise floor. The advantage of this system is its speed in getting tunes of individual bunches because it digitizes all the bunches at every turn, compare this with the gated systems which looks at one bunch for many turns and then goes on to the next bunch. Presently, it is an R&D project and is not operational.

A reference for the digital tune monitor is:

- A. Semenov, "Status of the FNAL Digital Tune Monitor", Proceedings of the Particle Accelerator Conference 2007.

6. COMPARISON

A comparison between all the detectors is shown in the table below. A summary of all the detectors are in the talk associated with this report:

- http://adweb.desy.de/mdi/CARE/chamonix/tune.pdf

Detector	Injection	Ramp	Flattop Squeeze	Bunch by Bunch	Coupled Tunes	Accuracy
21.4 Mhz	Y	Y	Y	N	Y	1.00E-004
1.7 Ghz	Y	?**	?**	Y	N	1e-3 to 1e-4
3D-BBQ	Y	Y	Y*	Y	Y	1.00E-004
Tune Monitor	?	?	?	Y	Y	1.00E-004

*For 3D-BBQ tunes at collisions S/N gets really poor

**For 1.7GHz, tunes tend to either disappear or look coherent when going up the ramp and squeeze. The accuracy of 1e-3 is for single bunch mode and 1e-4 is for average mode.

The digital tune monitor has not been demonstrated to work up the ramp and squeeze.

TUNE MEASUREMENT AT COSY-JÜLICH WITH NOISE EXCITATION

J. Dietrich, Forschungszentrum Jülich GmbH, Germany

A real time method for betatron tune measurements at COSY-Jülich was developed and tested from the early 1997. A bandlimited broadband noise source was used for beam excitation, the transversal beam position oscillation was bunch-synchronous sampled and digitized with a high resolution ADC. The Fourier transform of the acquired data represents immediately the betatron tune. After the first promising experiments an automatic tune meter was constructed. The tune meter is used as routine diagnostic tool since end 1998 [1-5].
Via the stripline unit, coherent betatron oscillations in horizontal and vertical direction can be raised by means of broadband transversal excitation. The cumulative effect of subsequent excitations on the circulating beam results in a coherent oscillation at resonance frequencies only. Other components of the excitation are neutralized and therefore have virtually no effect on the beam. A white noise source generates the exciting signal. A bandpass filter with fixed cutoff frequencies (BW = 100 kHz to 5 MHz) limits the excitation bandwidth. The frequency range of the noise always covers at least one betatron sideband at the fundamental frequency over the whole ramp without frequency feedback. The excitation can be enabled/disabled by means of a fast GaAs switch that is controlled by either remote commands or a timer unit. The programmable excitation level changes in real-time. A beam position monitor (or Schottky-pickup) picks up the beam response on the excitation. Low noise gain controlled amplifiers determine the level of the sum and difference signals. The bunch-synchronous pulse required for the sampling is derived from the sum signal of the same BPM (or Schottky-pickup). A phase locked loop with narrowband loop filter generates the clock pulse with low tracking jitter over the whole range between injection and flat top. With proper signal processing, the clock generator tracks also the synchrotron oscillation. For investigations of the synchrotron oscillation, a signal proportional to the synchrotron oscillation can also be derived from the tracking circuitry of the clock generator. A high resolution ADC digitizes the difference signal. The timers of the measurement trigger and of the excitation gate are synchronized. Fig.1 shows the block diagram of the FFT tune meter.

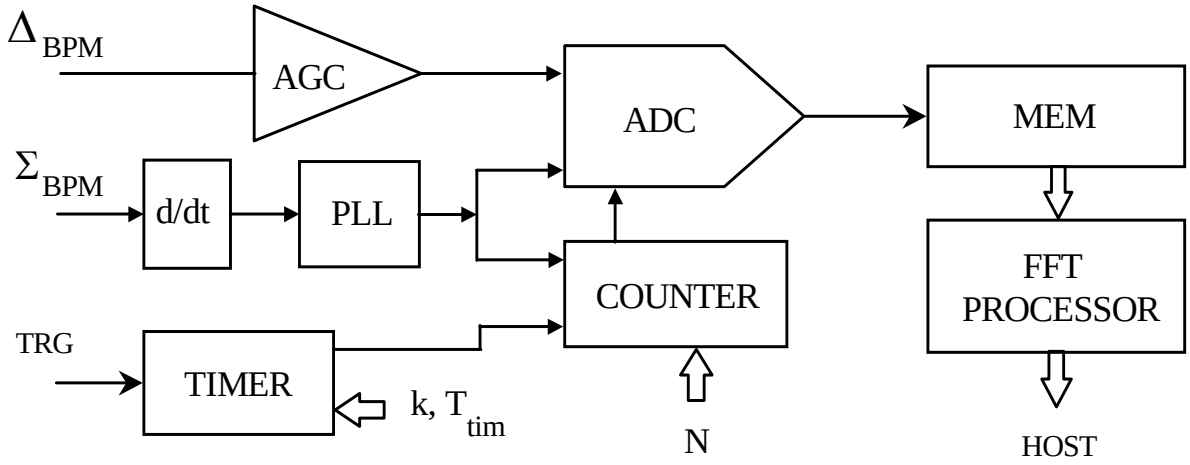

Figure 1: Block diagram of the FFT tune meter.

The betatron oscillation appears as an amplitude modulation on the beam position signal evoking double sidebands around each harmonic of the revolution frequency and also around DC in the spectrum of the position signal of the bunched beam. The peak value of the BPM difference signal is proportional to the beam position and can be sampled by means of a fast sample and hold circuitry and digitized with a high resolution ADC. The positive edges of the bunch-synchronous clock start the sampling at the bunch peaks, i.e. at the highest betatron amplitude. The gain controlled amplifiers allow an optimum utilisation of the 14 bit ADC. The peak value of subsequent bunches carrying the betatron oscillation are recorded. The Fourier transform of this array gives the fractional betatron tune q. This method combines the functions of a synchronous demodulator and a frequency normalizer. Due to the bunch-synchronous sampling, the frequency components of the synchrotron oscillation are suppressed. The sampled data therefore contain mainly the betatron sidebands transposed into the range

between DC and $f_0/2$ (f_0 = revolution frequency). The lowest normalized frequency is zero (DC component), the highest usable one is $f_0/2$ and the corresponding range of q or (1-q) falls between 0 and 0.5. Whether the measured value represents q or (1-q) depends on the machine lattice. Subsequently acquired spectra with the same time intervals are displayed as a waterfall diagram (Fig.2.) showing the tune as a function of time. On the left edge of the screen the values of the detected tune peaks are also numerically displayed.

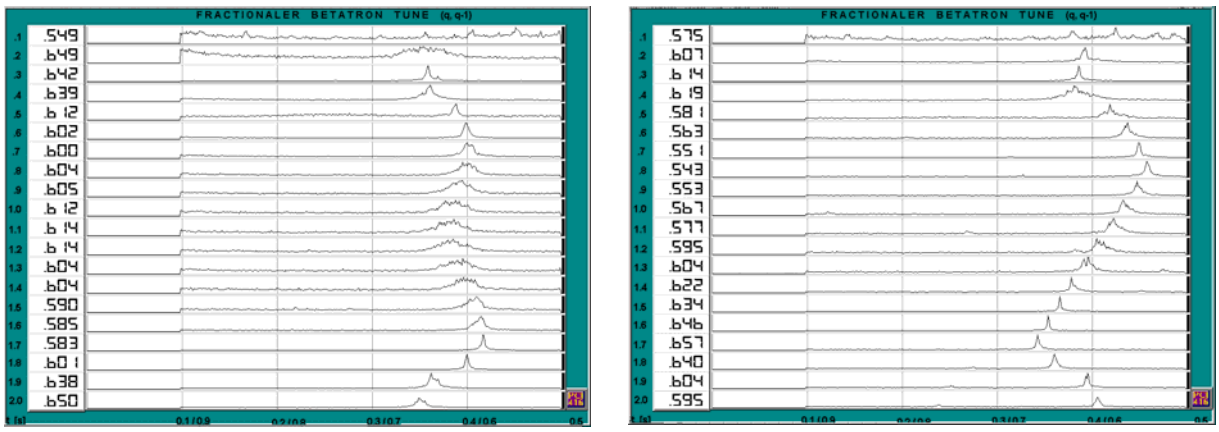

Figure 2: Display of a tune measurement in the ramp consisting of averaged FFT spectra (left horizontal, right vertical fractional tune. Beam parameters: 2.1 GeV/c, $2 \cdot 10^{10}$, time interval 100 ms).

The beam rigidity is low in the lower energy range, therefore very weak excitation is adequate for a distinct betatron response. The excitation strength in the ramp has to be increased. Hence the excitation level is programmable as a function of time. It is held as low as possible for an optimum signal to noise ratio with minimum particle losses. For this reason the excitation is switched on only for the duration of the data acquisition by means of a fast GaAs switch. The data are taken in blocks of N datawords each and stored sequentially in memory. To start the process the COSY timing system triggers an internal timing logic which in turn generates k timing pulses with constant time interval for k tune values. The number k of timing pulses and their interval must be properly chosen to cover the tune measurement time overlapping the total acceleration ramp time as desired. In one data acquisition cycle, k×N samples corresponding to k tune values are sequentially acquired. These data blocks are transformed by FFT resulting in frequency spectra with N/2 data points. As the duration of the acquisition depends on N, its value must be properly chosen, because it also determines the frequency resolution of the FFT-spectra (equal to 1/NT with $1/T = f_S = f_0$). Although the duration changes in the acceleration ramp, the resolution of the tune (1/N) remains constant. The larger the quantity of the samples is in the array used for evaluation, the higher the frequency resolution will be and consequently also the accuracy of the tune measurement. The average acquisition time (N×T) for a tune resolution of 5×10^{-3} is less than 2 ms. The transformation of a record needs 35 ms in the used configuration, thus real time tune measurements can be carried out with a frequency up to 25 Hz. With fast FFT processors or with stored records and off-line processing, equivalent rates above 500 Hz can be achieved. To improve the noise floor, the spectra can be averaged. A graphic and numeric display shows the tune as a function of time.

REFERENCES

[1] Dietrich, J. et al., "Transverse Measurements with Kicker Excitation at COSY-Jülich", EPAC'96, Barcelona, 1996

[2] Bojowald, J. et al., "Stripline Unit," Jül-2590, 1992 and Bojowald, J. et al.,"Longitudinal and Transverse Beam Excitations and Tune Measurements," Jül -2879, 1993

[3] Biri J. et al., "Beam Position Monitor Electronics at the Cooler Synchrotron COSY-Jülich," IEEE Trans. Nucl. Sci.,1994

[4] Bojowald, J. et al., "Dynamical Tune Measurements at COSY-Julich, DIPAC97, Frascati

[5] Dietrich, J. et al., "Broadband FFT method for Tune Measurements in the Acceleration Ramp at COSY Jülich", BIW'98, Stanford, 1998

Investigations on BaseBand Tune Measurements using Direct Digitized BPM Signals

U.Rauch, P.Forck, P.Kowina, P.Moritz
GSI, Darmstadt, Germany

Abstract

In the present work the tune evaluation based on direct digitized beam position data is discussed. During first measurements performed at heavy ion synchrotron SIS-18 at GSI this method showed that tune can be determined with a resolution better than 10^{-3}. It has been shown that this method is applicable when position data from BPM is available, also for machines with strongly varying beam parameters.

Introduction

The Q value of a circular accelerator is the number of betatron oscillations per revolution in either horizontal or vertical plane [1]. As it is a periodic oscillation of the beam its fractional part q, which is the ratio of the betatron frequency to the revolution frequency, can be calculated by measuring the beam position at a certain location over several (e.g. 2000) turns. The exact determination of this tune value is crucial for a stable operation as the working point of horizontal and vertical tune needs to be stable within $\Delta Q = 0.01$ (for parameters at SIS-18) in order to avoid resonances of the beam.

The GSI heavy ion synchrotron is normally running with three to six equally distributed bunches. The bunching factor, which is the bunch length multiplied by revolution frequency, is about 0.6 at injection (see Fig. 1). Also due to the injection at non-relativistic velocity $\beta = 15,5\%$ the acceleration frequency ramps from 0.8 to 5MHz. This rather high bunching factor and the range of RF leads to the conclusion, that tune measurement systems using one harmonic betatron side-band or currently established systems (see [4]) may not give satisfying signal intensities for measuring tune along a whole ramp. As in addition the position value out of the SIS-BPMs is anyway to be calculated due to the SIS-18 upgrade program for the future

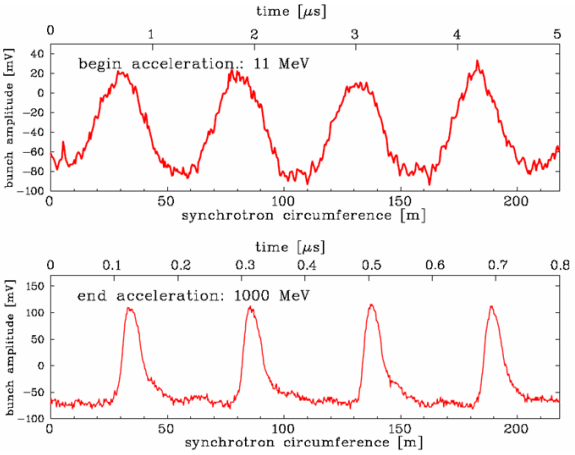

Fig. 1: Pickup amplifier signal of bunched beam at GSI SIS-18. The machine is running on fourth harmonic producing four bunches, thus the whole circumference is displayed on horizontal axis. Note the high bunch width at the beginning of acceleration [8]

accelerator project FAIR (see [3]) it is a possible way to use the existing digital online turn-by-turn position data in order to determine the tune directly in baseband.

Position Calculation

The proper calculation of beam position out of the digitized data is the fundament of this measuring method, therefore it is described first.

The task of the signal processing algorithm is to extract a single value for vertical and horizontal position for each bunch. For this purpose the bunch signal data is integrated over a certain window containing a single bunch. See Fig. 2 for signal shape and calculated window.

The single plate signals from the four plates of a shoebox type pick-up (PU) is fed to a high impedance amplifier and digitized by a

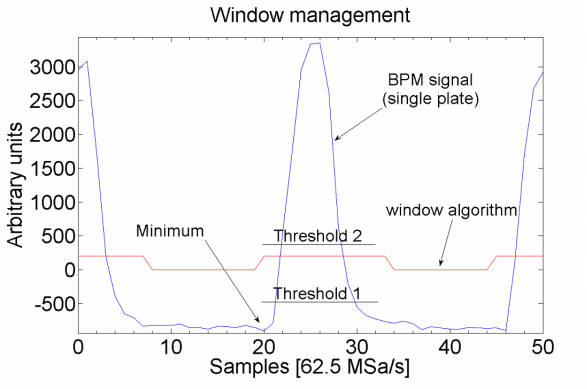

Fig. 2: Typical single plate signal from shoebox type BPM with the corresponding results from the windowing algorithm

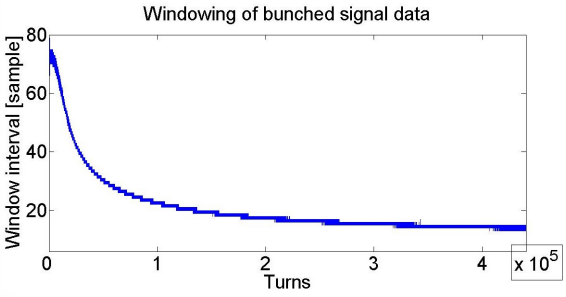

Fig. 3: Window intervals during a ramp cycle of about 430000 turns at ramp rate of 1.2 T/s.

fast 125MSa/s 14-bit ADC suited on a "Libera Hadron" manufactured by Instrumentation Technologies (I-Tech). An online signal processing can be done by a furthermore installed FPGA, but up to now the raw signal data is transferred via LAN to the PC in order to adapt and improve the signal processing algorithm.

First the algorithm determines the minimum value "m" between two consecutive bunches (see Fig. 2) which is negative due to the AC coupling of the analog signal path. Out of m for each bunch two values are calculated dynamically which are used as two thresholds Th1 $<$ Th2 very similar compared to a double threshold discriminator. The window is opened when the signal is crossing sequentially Th1 and Th2 and is closed when the thresholds are crossed in the opposite order. The arbitrary factors for the threshold values were set to produce stable and comparable windows for real beam data using also different ion types and for a whole acceleration ramp. Actually $\frac{3}{4} \cdot m$ is taken as first (Th1) and $-\frac{1}{2} \cdot m$ as second threshold (Th2), and the time $t(Th)$ is taken, when the signal rises (or falls) above (below) the threshold. Thus the negativity of the baseline due to the baseline shift is used for obtaining the threshold values.

This kind of algorithm has proven to be stable over all types of ramps measured so far, this is i.e. over more than 10^6 bunches and different ion types, varying magnet ramp rate and varied ion flux. No tracking error due to the windowing has been observed. As it has been verified that no bunch is lost during a whole ramp (see Fig. 3) one can focus on one bunch by simply counting the bunches digitally.

The thereby received bunch-wise integral of a single PU plate gives a first approach to beam position, but the signal is pulled to a lower signal level due to the AC coupling. In order to allow numerical integration of full data the baseline is compensated to zero level, the so called Base Line Restoring (BLR).

Base Line Restoring

For the BLR data out of three copies of the dataset is added point by point. This is done complete using the digitized data only [2], therefore an algorithm has to be formed which is able to represent this compensation, but one has to keep in mind, that the signal processing has to be quick in order to process data online. One dataset is delayed by half a RF period and one by a whole RF period (see Fig.4). The original signal is used inverted as well as the one being delayed by a whole RF period and by adding those signals the result is $y(t) = (-x(t) - x(t-f))/2 + x(t-f/2)$. As only the data within a window is of interest other data is set to zero (Fig. 5). Due to the high bunch width at low frequencies the spacing between two bunches is too short for this kind of correction. As this would lead to a signal correction where the signal is not corrected by inverted baseline but by inverted bunch signal, the algorithm would run erroneous by 2% [2]. This systematical error is corrected nevertheless as the difference-over-sum-value is taken for the position. The current acceleration frequency f (in samples) is obtained using the bunch spacing out of the windowed dataset. The obtained restored signal can be seen in Fig. 5.

For the tune calculation the single bunch position is taken (Fig. 7) but an example for beam position integrated over 1000 turns (roughly a 1 kHz filtering) is however given in Fig. 6.

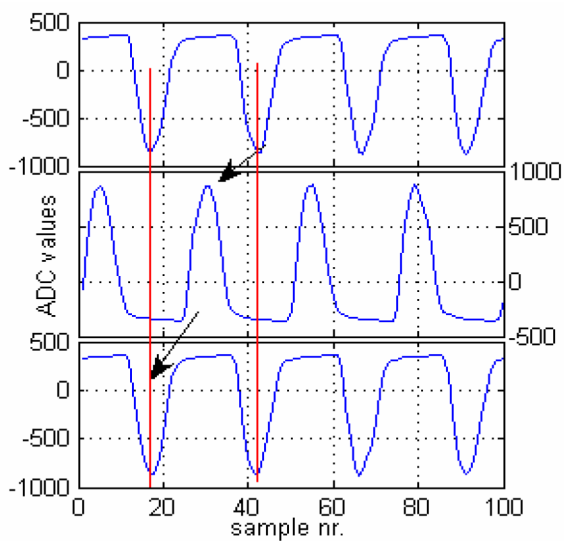

Fig. 4: Top: inverted original signal, middle: original signal delayed by half RF period, bottom: inverted original signal delayed by one RF period. Black arrows mark one particular bunch. [2]

Tune measurement

Simply by transforming position data, which is one position information per bunch, into its corresponding frequencies one obtaines a frequency range from 0-0.5·f_{rf}, which is 0-2·f_{rev} at fourth harmonic acceleration. As we are interested in single bunch position on one side and especially interested for tune which lies in the frequency range of 0-0.5·f_{rev}, the single bunch position (see Fig. 7) is taken for the fourier transformation. Thus the proper betatron frequency at base-band is instantly and explicitely obtained normalized to the revolution frequency.

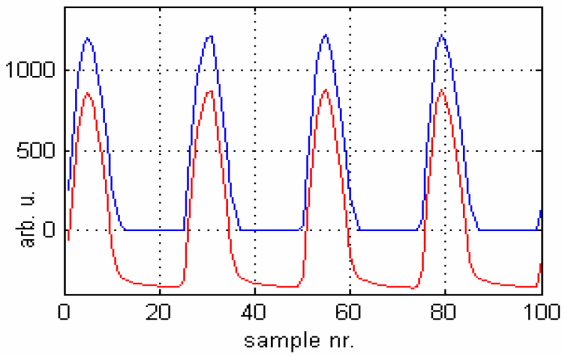

Fig. 5: Red: original signal, blue: signal corrected by blr. [2]

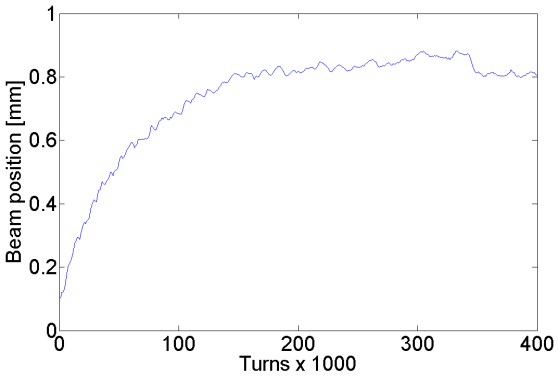

Fig. 6: Beam position integrated over 1000 turns of U^{73+}−beam; 10^9 particles, energy range 11MeV/u to 250MeV/u

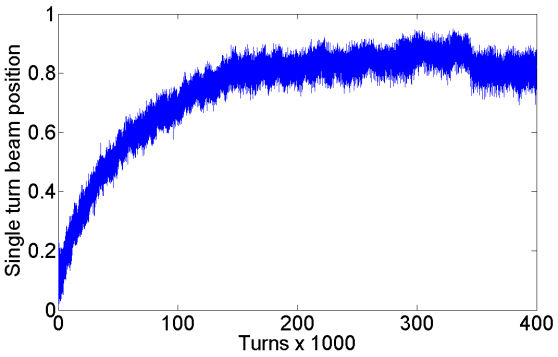

Fig. 7: Single bunch position, same ramp as Fig. 6

An accelerator ramp is cut into slides of FFTs which cover each 2048 turns, what is about one image per ms.

Since the beam is stable enough one cannot see the existing tune without excitation when the tune track of a whole ramp is required. Therefore a Direct Digital Synthesizer (DDS) [6] with digital Pseudo Random Noise (PRN) phase modulation, similar to the device originally developed for Radio Frequency- Knock Out (RF-KO) extraction [7], was used for transverse excitation of the beam (see Fig. 8). While tracking the accelerator rf, the synthesizer generates a spread spectrum signal with adjustable width centered around the betatron frequency, see Fig. 9. The carrier frequency thus lies at $f_c = f_{\mathrm{rf}} \cdot \frac{q}{h}$ with q as tune and h the harmonic number. The noise bandwidth was chosen adequately to the expected tune spread which allows for the reduction of needed amplifier power.

An example for the track of the tune on an acceleration ramp is given in Fig. 10. It dis-

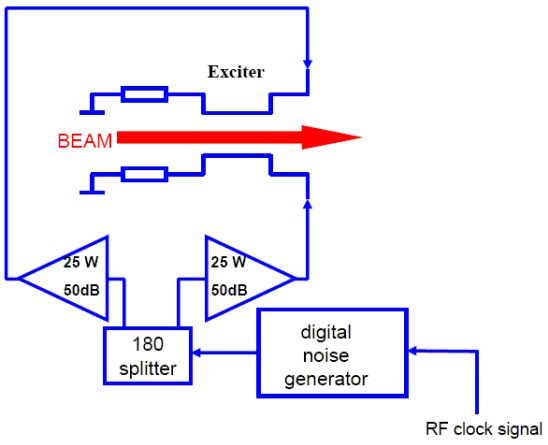

Fig. 8: Connection principle of Digital Random Noise Generator at a BTF exciter

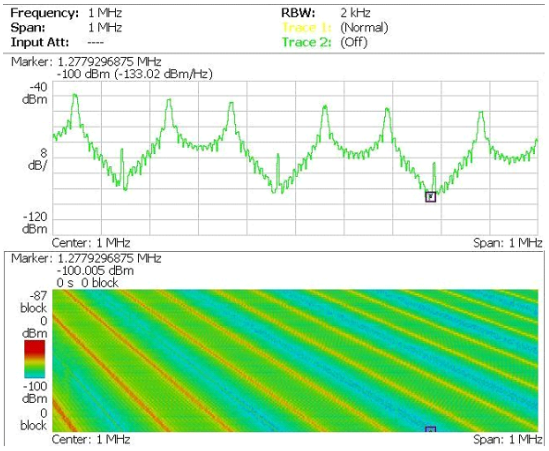

Fig. 9: Noise on ramp

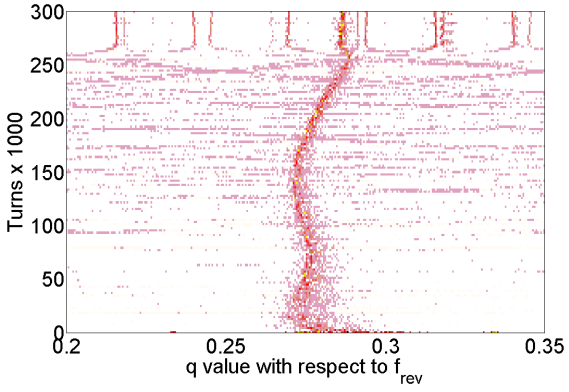

Fig. 10: Tune track of vertical tune with very small excitation (1.5W of excitation power on a BTF exciter) with no significant beam disturbance; Details see text

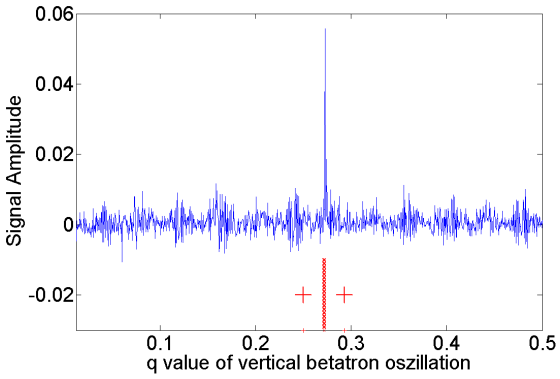

Fig. 11: Tune spectrum of vertical tune out of tune track of Fig.10, noise subtracted, second weighted moment and its σgiven

plays a whole acceleration cycle of about $5 \cdot 10^8$ Uranium-73 ions from injection at 11.4MeV/u to end energy of 250MeV/u after approx. 270.000 turns. Thereafter the magnetic flattop is hold for another 30.000 turns and the beam is extracted.

Fig. 11 shows a single slide of Fig. 10 at half way up the ramp. Clearly the tune can be seen and several background frequencies as well as noise could be subtracted by subtracting the averaged spectrum of non-excited beams.

Increasing the amplitude of noise excitation leads to growth of the integrated tune frequency. In order to have a good comparison every amplitude was taken at the same time on ramp (also same time as was taken for Fig. 11) and every spectrum was integrated over the same frequency range around the tune peak. The resulting increase in integral size can be seen in Fig. 12.

Due to the resulting shape of the tune track (see Fig.10) the sigma value of the distribution (see Fig. 11 lower part) can not be taken in order to estimate the resolution of the herein proposed method of measuring tune. The method resolution is much better than Δq, what was aimed. The variation of the center of distribution is taken instead. In Fig. 13 it can be seen, that the variation even over differently excited beams is below 10^{-3}Q (Q = 4.273 $\pm$0.001), which is the aimed goal of this work.

Conclusion

The tune has been measured during ramping for different ion types and different ramp rates. With the presented algorithm for the integration window all bunches are detected safely and thus tune can be calculated out of position data.

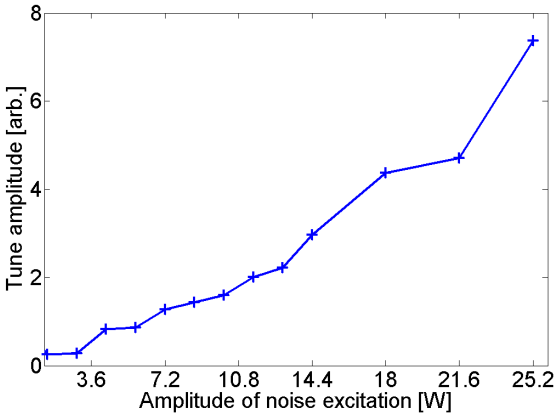

Fig. 12: Increase of tune signal with increasing noise excitation amplitude. A somewhat linear increase can be seen. Notice that q is clearly visible at 1.5W already (see Figs. 10 and 11)

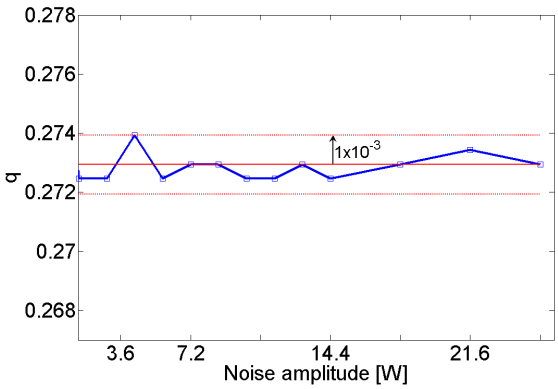

Fig. 13: Variation of center of the tune frequency over several measurements

The resolved worst-case resolution of the tune frequency equals according to Nyquist theorem to the inverse of the number of acquired turns, which is $5 \cdot 10^{-4}$q, the aimed resolution. By using more precise integration methods a higher resolution is reachable. As the position algorithm proofs to be stable and as the determination of tune is working properly it will soon be brought online in order to make tune visible on ramp without significant disturbance of the beam.

Acknowledgements

We gratefully acknowledge M.Gasior and R.Steinhagen (CERN) for fruitful discussion and ongoing help on the construction of the BBQ setup for GSI-SIS.

References

[1] e.g. K.Wille: The physics of particle accelerators. An introduction, Oxford University Press, 2001

[2] A.Galatis, P.Kowina, K.Lang, A.Peters: Digital techniques in BPM measurements at GSI-SIS; Proceedings of EPAC 2006

[3] A.Galatis, K.Lang, P.Forck, A.Peters: First tests with the SIS18 digital BPM system

[4] M.Gasior: Base-band tune (BBQ) measurement system, Proceedings of beam instrumentation workshop, Chamonix 2007

[5] M.Gasior: , R.Jones: The principle and first results of Betatron Tune Measurements by Direct Diode Detection. LHC-Project-Report 853, CERN CH-1211 Geneva 23 Switzerland

[6] K.Blasche et al: SIS Status Report, GSI Darmstadt, 2000

[7] P.Moritz: RF-KO-Extraktion S07BO1E, Rev. 2.9.7, GSI Darmstadt, 2005

[8] P.Forck: Lecture Notes on Beam Instrumentation and Diagnostics, JUAS 2007

BASE-BAND TUNE (BBQ) MEASUREMENT SYSTEM

M. Gasior, CERN, Geneva, Switzerland

Abstract

The fractional part of the betatron tune for a circular accelerator can be measured by observing beam oscillations on a position pick-up. In frequency domain the betatron frequency is seen as sidebands on either side of the revolution harmonics. Usually beam signal pulses from the pick-up are very short with respect to the revolution period, resulting in a broadband spectrum. Classical tune measurement systems filter out just one of the betatron sidebands. As a consequence, most of the betatron energy is lost and only a very small fraction remains for further processing. This paper describes a new method, referred to as Direct Diode Detection (3D). It is based on the idea of time stretching beam pulses from the pick-up in order to increase the betatron frequency content in the baseband. The 3D method is employed in Base-Band Tune (BBQ) Measurement Systems built for the CERN SPS, PS, PSB and LEIR machines, as well as for the BNL RHIC. Results from all these machines [1, 2, 3, 4] show that this method can increase the betatron signal level by orders of magnitude as compared to classical systems, making it possible to observe tunes with no explicit excitation. Frequency resolution in the order of 10^{-5} and amplitude sensitivity in the order of 10 nm has been achieved with this very simple hardware.

3D PRINCIPLE AND THE HARDWARE

The crucial part of a 3D-based tune measurement system is the peak detector. Two such detectors connected to opposing electrodes of a beam position pick-up (PU) (see Fig. 1) yield the amplitude modulation envelope of the beam signals. Such signals, depicted in Fig. 2, are superimposed on a DC voltage related to the bunch amplitude (revolution frequency content). The signal difference, shown in Fig. 3 for single bunch in the machine, contains almost the whole bunch modulation amplitude, with a DC component related to the beam offset from the centre of the pick-up. Since the DC content can be easily suppressed by series capacitors, most of the corresponding revolution frequency (f_r) background can be removed by the peak detectors before the first amplifying stage. In Fig. 4 the f_r attenuation characteristic is shown assuming single bunch in the machine, which is the most difficult case to deal with. For a detector time constant $\tau = R_f C_f$, which is larger than the machine revolution period $T=1/f_r$, the suppression of the revolution line goes as $4\tau/T$ [1]. This makes it possible to obtain f_r attenuation in the order of 50 dB for $\tau \approx 100$, which is easily achievable in practice.

The 3D circuit in Fig. 1 can be also understood as two sample-and-hold blocks, sampling bunch signals close to their maxima at the bunch repetition rate, downmixing the wideband bunch spectrum into the baseband.

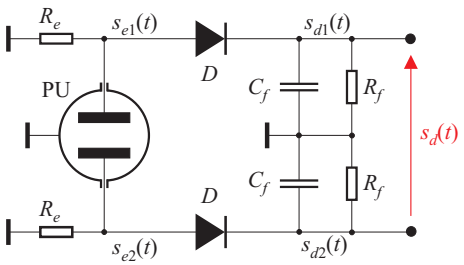

Figure 1: Direct Diode Detection principle.

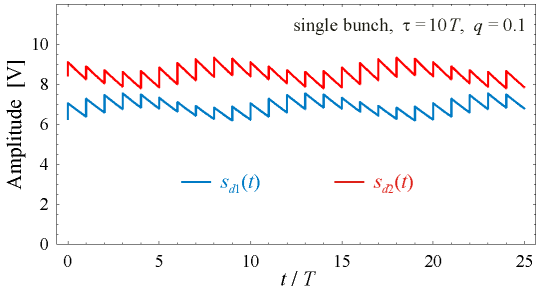

Figure 2: An example of peak detector voltages.

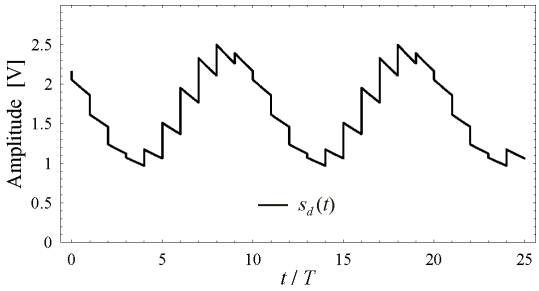

Figure 3: Difference of the signals in Fig. 2.

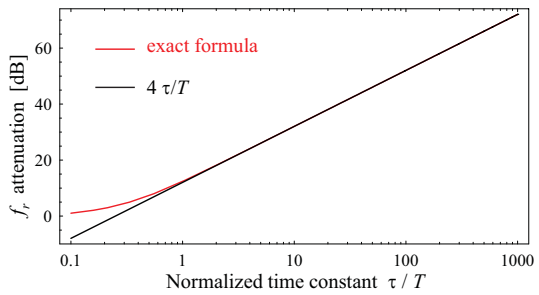

Figure 4: 3D circuitry revolution frequency attenuation.

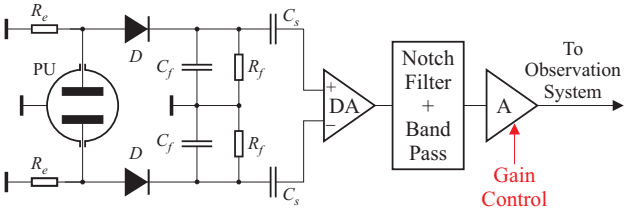

Figure 5: Block diagram of a 3D-BBQ system.

A block diagram of a 3D Base-Band tune (BBQ) measurement system is depicted in Fig. 5. The peak detector voltages with the DC content removed by the series capacitors are subtracted by the differential amplifier (DA), further increasing the suppression of f_r for beams close to the PU centre and improving the interference immunity. Filters attenuate f_r by another large factor, in the order of 100 dB [1]. The high cut-off frequency of the band pass filter is $0.5f_r$, as for all possible tune values one betatron sideband is always present in the band $(0, f_r/2)$. The typical low cut-off is $0.1f_r$, which means that the observation system only has to process frequencies between 0.1 and $0.5f_r$. For large machines, therefore, the 3D-BBQ output signal can be digitised with a 24-bit audio ADC at the revolution frequency, requiring relatively little processing power to yield a signal spectrum through an FFT, or to build a tune tracker based on a digital phase-locked loop (PLL) [2].

Notice that a 3D-BBQ system is 'low frequency' only after the detectors, due to the 'time stretching' of the short beam pulses. Before the detectors the processed bandwidth can easily be as high as a few GHz. In the detection process the spectral content from this wide bandwidth is converted to the baseband, resulting in a very high sensitivity.

3D-BBQ systems according to the block diagram of Fig. 5 have been installed on four CERN machines, namely SPS, PS, PSB and LEIR, as well as on BNL RHIC. All systems were based on very similar hardware.

A detailed comparison of the 3D and classical tune measurement methods are given in [1], together with a quantitative estimate of the signal to noise improvement given by the 3D method operated on a machine with a single bunch. This factor is in the order of 30 dB for the PS, 40 dB for RHIC, 50 dB for the SPS, and 60 dB for the LHC.

RESULTS

Most of the installed systems were sensitive enough to observe betatron oscillations with no explicit beam excitation. Such oscillations, with amplitudes in the μm range, were seen to be almost always present in the beam. The only exception is the PS, where a very short pick-up yielded too small signals to give clear tune paths without explicit oscillations.

Examples of such measurements made with the SPS BBQ system and no intentional beam excitation are shown in Fig. 6 and 7. Figure 6 shows the horizontal tune path for the lowest intensity SPS beam of $\approx 5 \cdot 10^9$ protons in a single bunch at 26 GeV, during a programmed tune change of $\approx 5 \cdot 10^{-3}$. Figure 7 shows the SPS horizontal tune variations induced by the jaws of an LHC collimator prototype as it was cycled between a fully opened position and a gap of 1.96 mm. This measurement was performed with a single bunch at 270 GeV and formed part of a series used to evaluate impedance-induced tune changes introduced by LHC collimators [5]. Tune variations as small as a few Hz could be resolved in this

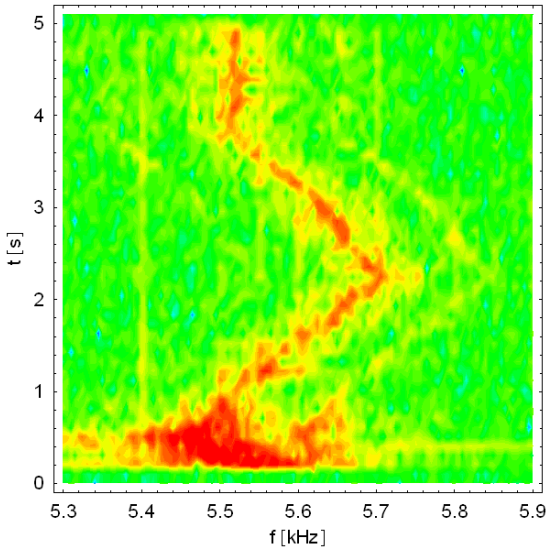

Figure 6: SPS, single bunch LHC pilot beam ($\approx 5 \cdot 10^9$ p^+).

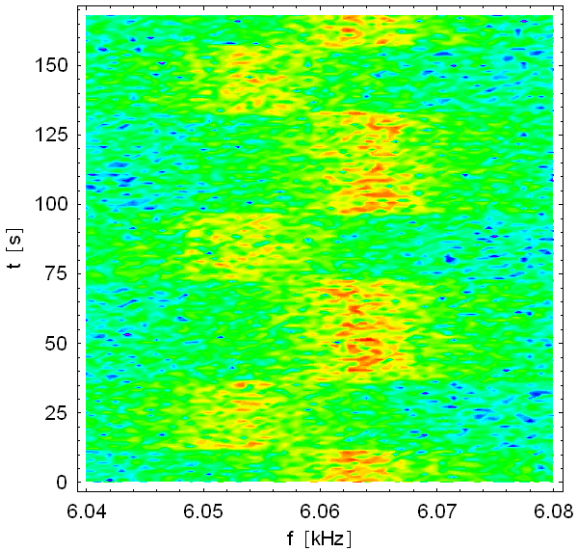

Figure 7: SPS, single bunch LHC beam ($\approx 10^{11}$ p^+).

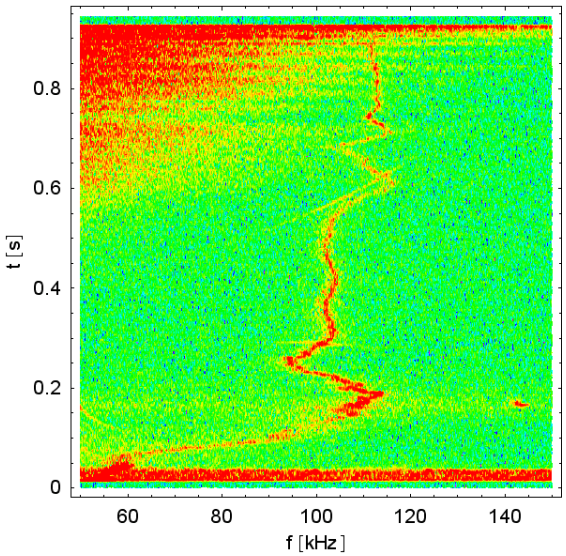

Figure 8: PS, AD beam (4 bunches, $\approx 4 \cdot 10^{12}$ p^+/b).

way, with the tune resolution in the order of 10^{-5}. These SPS measurements were acquired using a low cost 24-bit PC sound card followed by off-line spectral analysis.

Figure 8 shows the horizontal tune evolution measured by the PS BBQ system with no explicit excitation for a beam destined for the Antiproton Decelerator (AD), and accelerated from 1.4 to 26 GeV. The noise-like components appearing from the middle of the record onwards result from the RF beam gymnastics performed for this type of PS beam.

Figure 9 shows a vertical plane time record from the RHIC 3D-BBQ system, with the corresponding frequency spectra shown in Figure 10. The largest amplitude signals correspond to beam oscillations caused by high voltage sweeps, related to the operation of an Ionization Profile Monitor (IPM). Each excitation consists of a burst of a hundred pulses, applied every 100th revolution. If either of the tunes happen to be a multiple of $f_r/100$, then these kicks resonantly excite the beam, as seen in the spectra for frequencies around 17.1 kHz ($0.22 f_r$, close to the horizontal tune) and 17.9 kHz ($0.23 f_r$, vicinity of the vertical tune).

Mains harmonics are clearly visible around the betatron tune paths throughout the RHIC acceleration cycle. These lines increase considerably once the main ramping power supplies are turned on around 26 s from the beginning of the record. The corresponding increase in the time domain signal can be seen in Figure 9. The presence of mains harmonics in the beam spectrum is reported in detail in [3] and is thought to be caused by magnetic field ripple in the main RHIC dipoles. Similar phenomenon was observed with the 3D-BBQs on the SPS, PS and Tevatron.

A comparison at RHIC between spectra from calibrated, million turn BPM data and that of the 3D-BBQ data has quantified the noise floor of the RHIC BBQ prototype at less than 10 nm. This is an order of magnitude better than most existing tune measurement systems.

CONCLUSIONS

This paper has described the principle of tune measurement using Direct Diode Detection. It has been shown to be highly sensitive while using simple, cheap and robust hardware. BBQ systems based on the 3D method were built for four CERN machines, namely the SPS, PS, PSB and LEIR, as well as for the BNL RHIC. They have given very good results and are in the process of further optimization. A dedicated BBQ system is being installed on the LHC, also as part of a PLL tune tracking system, for the measurement of tune, chromaticity and coupling [5], with the ultimate aim of providing reliable tune and coupling feedback.

The 3D method is still under development and its full potential has probably not yet been fully realised. Extensive studies will therefore continue on this technique.

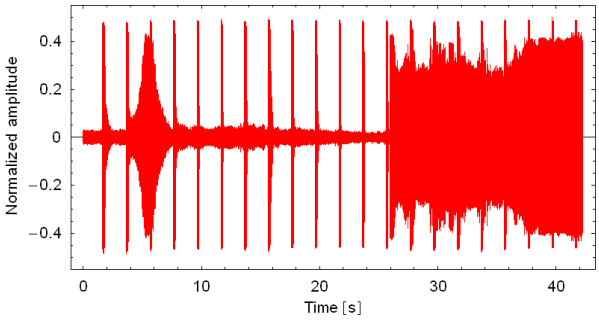

Figure 9: RHIC, a 3D-BBQ signal sound card record.

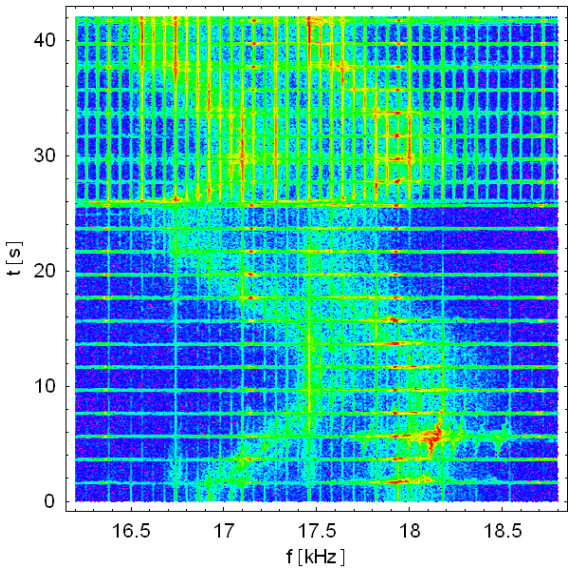

Figure 10: RHIC, spectra of the signal in Fig. 9.

ACKNOWLEDGMENTS

We would like to thank P. Cameron and J. Belleman for their help throughout the whole development.

REFERENCES

[1] M. Gasior, R. Jones, "The Principle and First Results of Betatron Tune Measurement by Direct Diode Detection", CERN-LHC-Project-Report-8XX.

[2] P. Cameron et al., "Advances Towards the Measurement and Control of LHC Tune, Chromaticity, and Coupling", these proceedings.

[3] P. Cameron, M. Gasior, R. Jones, C.-Y. Tan, "The Effects and Possible Origins of Mains Ripple in the Vicinity of the Betatron Spectrum", this proceedings.

[4] C.-Y. Tan, "Novel Tune Diagnostics for the Tevatron", PAC 2005.

[5] H. Burkhardt et al., "Measurements of the LHC Collimator Impedance with Beam in the SPS", PAC 2005.

[6] P. Cameron, M. Gasior, R. Jones, Y. Luo , "Towards a Robust Phase Locked Loop Tune Feedback System - The Continuous Measurement of Global Betatron Coupling Using a Phase Locked Loop Tune Measurement System", these proceedings.

THE MEASUREMENT OF CHROMATICITY BY HEAD-TAIL PHASE SHIFT ANALYSIS

R. Jones CERN, Geneva, Switzerland

5th Workshop in the framework of CARE-N3-HHH-ABI
"Schottky Diagnostics and Real Time Tune and Chromaticity Control"

11th – 13th December 2007, Chamonix, France

1 INTRODUCTION

The determination of chromaticity by following the evolution of head-tail phase shifts after a transverse dipole excitation is a technique which does not rely on an accurate knowledge of the fractional part of the betatron tune and, for a machine operating well above transition, is virtually independent of beam energy.

Early experiments in the SPS (CERN) [1,2], and at HERA-p (DESY) [3] have shown the feasibility of the technique for high-energy proton beams, while more recent experiments [4] at the Tevatron (Fermilab) have highlighted how the same data can be used to measure other machine parameters such as the resistive wall impedance and second order chromaticity.

Extensive theoretical work has also been carried out to validate the robustness of this method for chromaticity measurement in the LHC [5].

2 THE HEAD-TAIL PRINCIPLE

Assuming longitudinal stability, a single particle will rotate in longitudinal phase-space at a frequency equal to the synchrotron frequency. During this longitudinal motion the particle also undergoes transverse motion, which can be described by the change in the betatron phase, θ(t), along the synchrotron orbit. If the whole bunch is kicked transversely, then the resulting transverse oscillations for a given longitudinal position within the bunch can be shown to be given by [1]

$$y(n) = A\cos[2\pi n Q_0 + \omega_\xi \hat{\tau}(\cos(2\pi n Q_S) - 1)] \qquad \textbf{(1)}$$

where n is the number of turns since the kick, Q_0 is the betatron tune, Q_S is the synchrotron tune, $\hat{\tau}$ is the longitudinal position with respect to the centre of the bunch, and ω_ξ is the chromatic frequency and is given by

$$\omega_\xi = Q'\omega_0 \frac{1}{\eta} \qquad \textbf{(2)}$$

Here Q' is the chromaticity, ω_0 is the revolution frequency and $\eta = 1/\gamma^2 - 1/\gamma_{tr}^2$. If we now consider the evolution of two longitudinal positions within a single bunch separated in time by $\Delta\tau$, then from Eq. 1 it follows that the phase difference in the transverse oscillation of these two positions is given by

$$\Delta\Psi(n) = -\omega_\xi \Delta\tau(\cos(2\pi n Q_S) - 1) \qquad \textbf{(3)}$$

This phase difference is a maximum when $nQ_S = ½$, i.e. after half a synchrotron period, giving

$$\Delta\Psi_{MAX} = -2\ \omega_\xi\ \Delta\tau \qquad \textbf{(4)}$$

The chromaticity can therefore be written as

$$Q' = \frac{-\eta\ \Delta\psi(n)}{\omega_0 \Delta\tau(\cos(2\pi n Q_s) - 1)}$$

$$Q' = \frac{\eta\ \Delta\psi_{MAX}}{2\omega_0\ \Delta\tau} \qquad \textbf{(5)}$$

3 THE SPS HEAD-TAIL MONITOR

A schematic layout of the SPS Head-Tail monitor set-up is shown in Fig. 1. A straight stripline coupler followed by a 180° hybrid is used to provide the sum and difference signals for a given measurement plane. These signals are fed into a fast-sampling (>2GS/s), high analogue bandwidth (>2GHz) digital oscilloscope. A VME front-end acquisition crate then retrieves the data via a GPIB or Ethernet link. All the oscilloscope and acquisition parameters are accessible from the SPS control room through a dedicated graphical user interface.

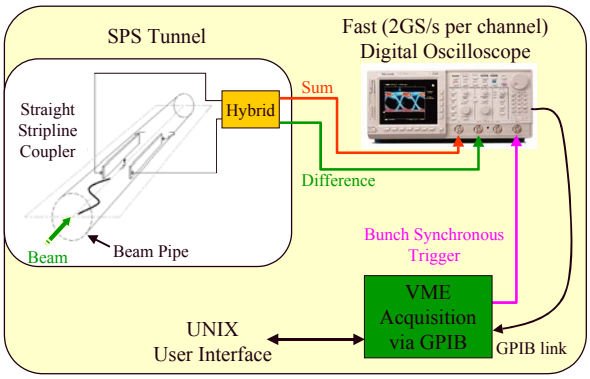

Figure 1. Layout of the SPS Head-Tail Monitor

The oscilloscope is triggered by bunch synchronous timing. Combining this with the "Fast-Frame" capabilities of the oscilloscope allows one bunch (25-50ns worth of data) to be captured over many SPS turns (up to 2000). In this way it is possible to track the evolution of the signal from a single, specific bunch. Even though the bunch synchronous timing has an rms jitter of only 100ps, the sum signal still has to be acquired to enable the difference signal to be accurately re-aligned for each turn. In this way, the timing jitter is reduced to well below the sampling frequency.

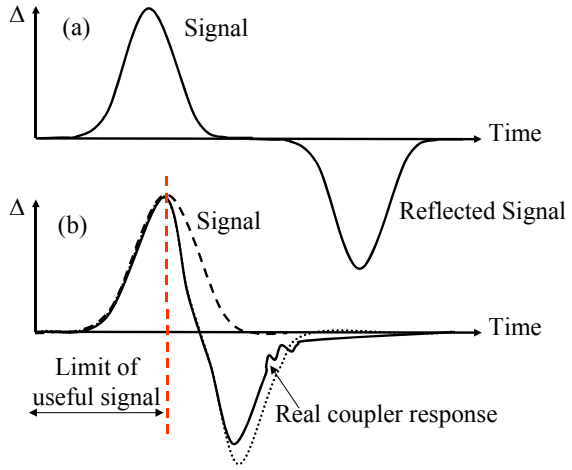

Figure 2. Typical coupler response.
a) total bunch length < 2 × coupler length.
b) total bunch length > 2 × coupler length.

Fig. 2 shows some typical signals obtained from the coupler. If the total bunch length is less than twice the coupler stripline length, Fig 2(a), then the signal from the bunch and its reflection from the opposite end of the stripline are well separated in time. If, however, the bunch is longer than twice the stripline length then the signal and reflection are no longer separated, Fig. 2(b), and the useful part of the signal is limited. This latter case was true for the early SPS set-up, where the typical bunch length (4σ) was ~4ns and twice the coupler length corresponded to 2.5ns. Hence measurements on the tail of the bunch were not possible. However the current system uses a 60cm stripline coupler, allowing bunches of 4ns to be fully resolved.

Figure 3 shows the result of an SPS head-tail chromaticity measurement. The top two plots show the transverse movement of the head and tail of a single bunch respectively after the beam has been kicked. The lower left plot shows the evolution of the phase of the head and tail and the phase difference. It can be seen that the signals are re-phased after one synchrotron period, with the phase difference a maximum after ½ a synchrotron period. The final plot (lower right) shows the calculated chromaticity (using equation 5) for all turns where the phase difference is well defined.

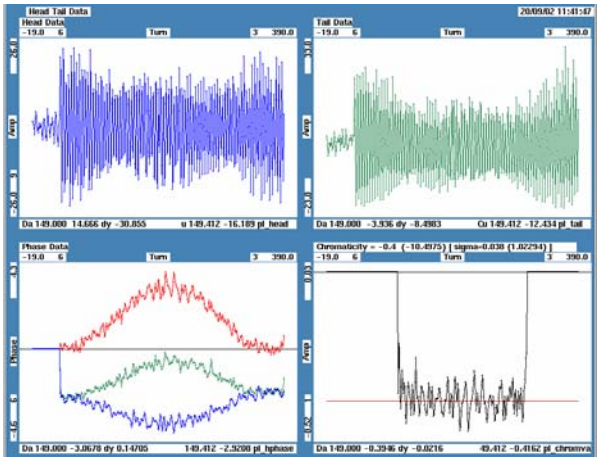

Figure 3. Head-tail monitor acquisition.

THE EFFECT OF ACCELERATION

Asymmetric Head-Tail Measurements on Accelerating Buckets

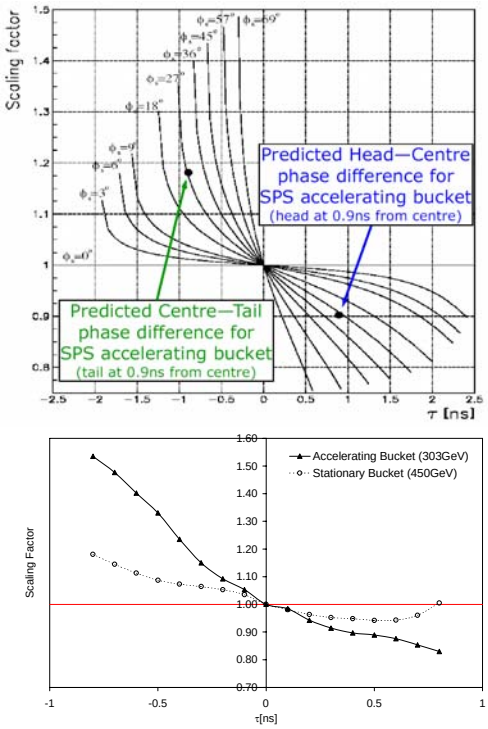

Figure 4. (a) Scaling factor S(τ) as defined in Eq. 1 for a 200 MHz RF system and different values of the synchronous phase. (b) Results from the SPS for an accelerating and stationary bucket.

During acceleration, the deformation of the bunch alters the way in which the head and tail change phase. Calculations using a simple two particle model have

shown that the phase change at the head of the bunch is reduced, while that at the tail is increased. This can be expressed in terms of a scaling factor with respect to the expected maximum phase difference ($\Delta\psi_{max,lin}$) obtained between any two slices in the bunch for a stationary bucket.

$$\Delta\psi_{\max}(\hat{\tau}) = S(\hat{\tau})\,\Delta\psi_{\max,lin}(\hat{\tau}) \qquad \textbf{(6)}$$

Fig. 4(a) shows the result of this for various synchronous phases of the RF when phase difference is calculated asymmetrically between the head and centre or centre and tail. It is clear from these results that an asymmetric measurement on an accelerating bucket can lead to large errors in the calculated chromaticity.

The results of the simulations were compared to measurements taken at the SPS (Fig. 4(b)). In the case of the stationary bucket it can be seen that there is only a slight effect on the value of chromaticity even when the head or tail reach the extreme edges of the distribution, where the effects of non-linear synchrotron motion become important (which was not taken into account in the simulations). However, for the accelerating bucket there is a marked difference between measurements taken at the head of the bunch and those taken at the tail. A comparison with the simulations of Fig. 4(a) show a good agreement in the general trend of the scaling factor, with the measured factor being somewhat larger than that predicted.

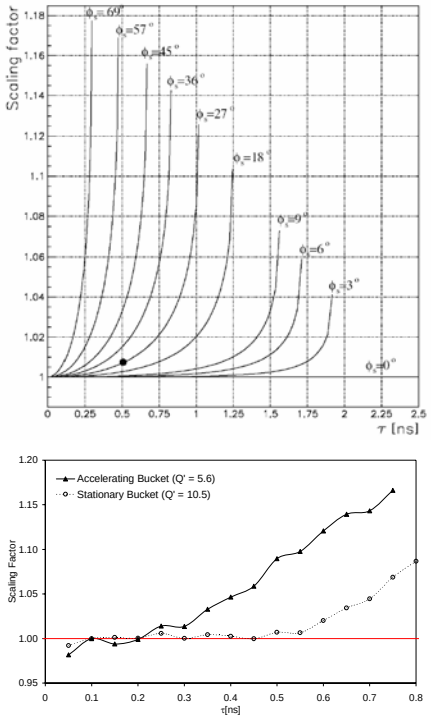

Figure 5. Scaling factor $S_{sym}(\tau)$ as defined in Eq. 2 for a 200 MHz RF system and different values of the synchronous phase.

Symmetric Head-Tail Measurements on Accelerating Buckets

If one now considers symmetric head-tail measurements, i.e. calculating the phase difference between two positions located symmetrically about the bunch centre, then one obtains the results shown in Fig.5(a). Here the scaling factor $S_{sym}(\tau)$ is defined as:

$$S_{sym}(\tau) = [S(\tau) + S(-\tau)]/2 \qquad \textbf{(7)}$$

with $S(\tau)$ being the scaling factor defined in Eq 6. It can be seen that the error resulting from such symmetric measurements is very small for head/tail positions relatively close to the bunch centre.

The experimental results obtained from the SPS for a stationary and accelerating bucket are shown in Fig 5(b). For the stationary bucket there is no significant error up to head/tail positions of 0.6ns. After this the error increases, probably due to the residual imperfections and noise in the acquisition system. The general trend for the accelerating bucket is also in agreement with that obtained by calculation. However, for a reason which is not clearly understood, the overall scaling factor is found to be significantly larger than that predicted by the simulations.

THE EFFECT OF IMPEDANCE AND SECOND ORDER CHROMATICITY

The same head-tail technique has been applied at the Tevatron where it became the main instrument for measuring chromaticity during the Tevatron ramp. Traditional tune measurement during RF modulation is not feasible in all cases as the change in RF required to resolve the chromaticity often results in losses, and as the RF frequency modulation is too slow to resolve chromaticity during snapback where there is a rapid change in the tune.

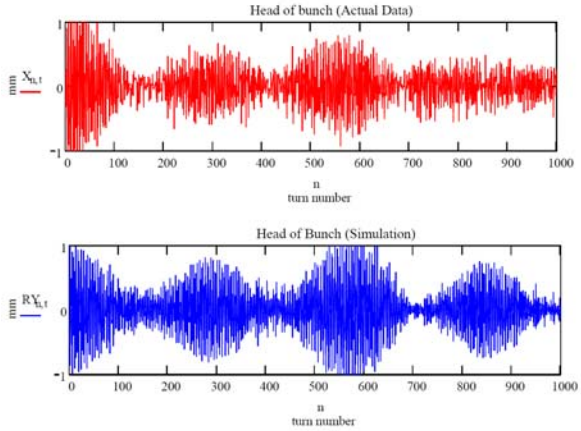

Figure 6. Comparison of actual head oscillation data (top plot) with a simulation including resistive wall impedance (bottom plot).

In addition to chromaticity measurement, the Fermilab scientists have used the head-tail data to provide an

insight into the more complicated beam dynamics of their machine. In particular, using head-tail oscillation data, it was possible to use simulations to fit for the resistive wall impedance of the Tevatron. The wake field generated by this impedance influences the head-tail behaviour and is visible as a modulation on the oscillation amplitude. Fig. 6 shows a comparison of actual head oscillation data after a kick with that of a simulation including the effects of a resistive wall wake field. It can be seen that by fitting the impedance a very good match is obtained between actual and simulated data.

The remaining discrepancies have been explained by introducing second order chromaticity into the simulations on top of the resistive wall wake field. Results from such a simulation are shown in Fig. 7, where the actual oscillation data (red) is compared to fit results from simulations using only the resistive wall wakefield (blue) and those containing both resistive wall and second order chromaticity (green). There is a clear improvement in the results when second order chromaticity is included, so allowing a good estimate of Q'' to be obtained.

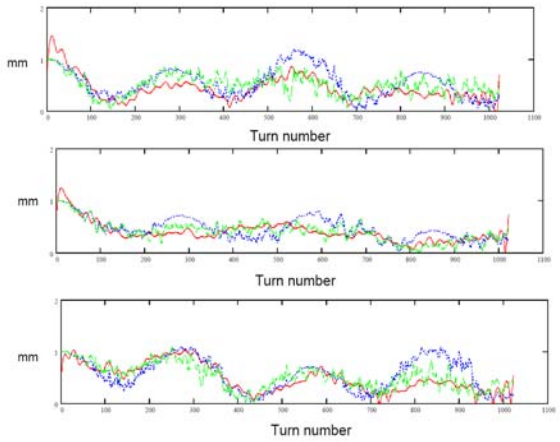

Figure 7. Red line: envelope of turn-by-turn data of Head (top), Center (middle) and Tail (bottom) after a 1 mm kick. Blue line: simulation results with resistive wall impedance. Green line: simulation results with resistive wall impedance and 2nd order chromaticity.

CONCLUSIONS AND OUTLOOK FOR THE LHC

On the experimental side, both the method and acquired data is now well understood. The main limitation of this technique is still that it requires significant transverse kicks, leading to emittance blow-up. This will currently limit its use in the LHC to non-operational beams. New experimental set-ups are under investigation to improve the sensitivity of the acquisition and allow the measurement to be made with much smaller excitation amplitudes.

In agreement with the simulations, it has been experimentally verified that the method is applicable both for stationary and accelerating buckets with the constraint that the measurement is performed close to and symmetrically about the bunch centre. In addition, dedicated calculations have been performed for the LHC to take into account other possible causes of perturbation. Simulations of the effects of second and third order chromaticity show that even for the most pessimistic case the error introduced is less than 0.2 units of chromaticity. A 20% off momentum beta-beating and linear coupling (if arc-by-arc compensated as foreseen in the LHC) have also been shown to give very little perturbation to the measurement. Finally, an extrapolation of SPS data taken at 26 GeV seems to indicate that, at nominal current, the accuracy of the head-tail chromaticity technique should practically not be affected by the transverse impedance of the LHC ring.

The experience from the Tevatron has shown that such a system can be used during normal operation for setting-up the machine. In addition, further analysis of the Tevatron data and its comparison to simulations has allowed estimations of both the resistive wall impedance and second order chromaticity to be obtained.

ACKNOWLEDGEMENTS

I would like to warmly acknowledge Stephane Fartoukh (CERN) for his large contribution to the theoretical understanding of the SPS data, and Vahid Ranjbar (formerly of Fermilab, now with the Tech-X Corporation) for permission to discuss his Tevatron data.

REFERENCES

[1] D. Cocq, O. R. Jones, H. Schmickler, "The Measurement of Chromaticity via a Head-Tail Phase Shift" presented at BIW'98, Stanford, CA, USA, May 1998.

[2] R. Jones, H. Schmickler, "The measurement of Q' and Q'' in the CERN-SPS by head-tail phase shift analysis" (CERN-SL-2001-020-BI), presented at PAC2001, Chicago, IL, USA, June 2001.

[3] A. Boudsko, O. R. Jones, H. Schmickler, M. Wendt, F. Willeke, "Chromaticity Measurements at Hera-p using the Head-Tail Technique with Chirp Excitation", presented at DIPAC'99), Chester, UK, May 1999.

[4] V. H. Ranjbar, P. M. Ivanov, "Chromaticity and Wake Field Effect on the Transverse Motion of Longitudinal Bunch Slices in the Tevatron", to be published in Phys. Rev. Spec. Top. Accel. Beams (2008).

[5] S. Fartoukh, R. Jones, "Determination of Chromaticity by the Measurement of Head-Tail Phase Shifts: simulations, results from the SPS and a robustness study for the LHC" (CERN-LHC Project Report 602).

Continuous Head-Tail Chromaticity Measurement

C.Y. Tan[1]
Fermi National Accelerator Laboratory, P.O. Box 500, Batavia, IL 60510, USA
(Dated: December 18, 2007)

The continuous head-tail chromaticity measurement technique measures chromaticity from the constant phase difference which arises when continuous transverse kicks are applied on the beam. Although the phase difference has been demonstrated clearly from our experiments, the measurements do not agree with the theory.

1. INTRODUCTION

The head-tail chromaticity measurement technique has been explored at Fermilab to see if it is a good way for measuring chromaticity. The attractiveness of this method arises from its compatibility with the tune tracker PLL which already continuously kicks the beam transversely. Therefore, no extra modulations are required to measure the chromaticity of the beam. We (and others) have derived a simple formula which relates chromaticity to head-tail phase, however, the measurements which have been made at the Tevatron show that the correlation between chromaticity and head-tail phase is non-linear and do not agree with the simple theory. Our hypothesis is that the transverse impedance of the machine introduces non-linear terms which our theory do not take into account.

2. THEORY

The head-tail chromaticity theory has been derived by both C.Y. Tan and V. Ranjbar, and S. Fartoukh in the following references:

- C.Y. Tan and V. Ranjbar, Tech. Rep., Fermilab (2007), Fermilab Technical Memo TM-2376.
- S. Fartoukh, Tech. Rep., CERN (2007), CERN-LHC-PROJ.REP.-986.

From the above, the fomula which relates the chromaticity to the head-tail phase is

$$\Delta\psi(\xi,\tau_B)=+\frac{2\xi\omega_0\tau_B}{\eta} \tag{1}$$

where $\Delta\psi$ is the phase difference between the head at τ_B and the tail at $-\tau_B$, ξ is the chromaticity, ω_0 is the angular revolution frequency and η is the slip factor.

Unfortunately, from measurements that was done in the Tevatron, the data does not agree with the above formula. See Figure 1. There are clearly a non-linear terms which are not taken into account by the theory. We suspect that the nonlinearity comes from transverse impedance. See Figure 2.

1 Email address: cytan@fnal.gov

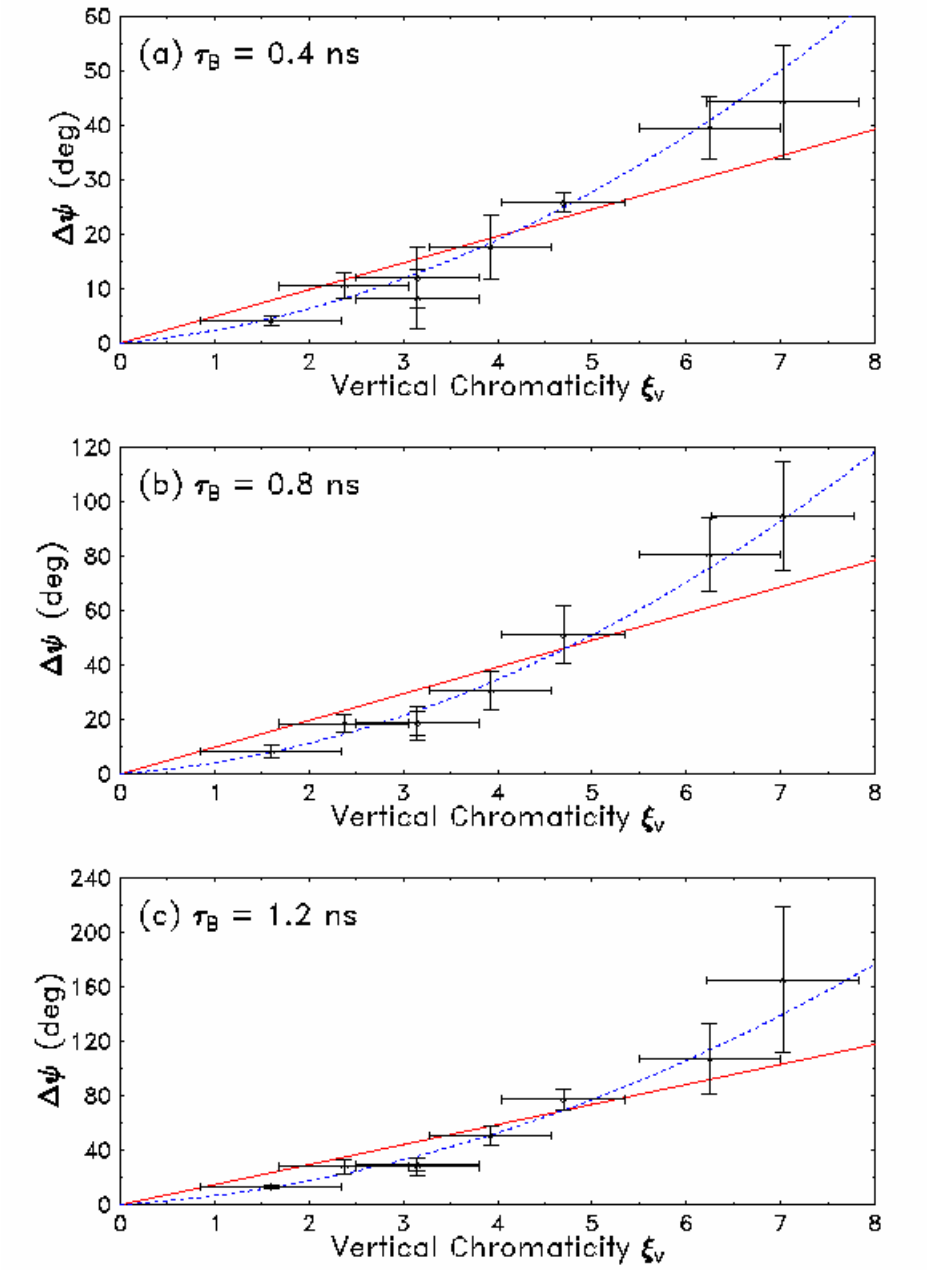

Figure 1.:These plots show the data analysed for τ_B = 0.4 ns, 0.8 ns and 1.2 ns. The red line is calculated from Eq. (1) and the blue dotted line is a quadratic fit of the data.

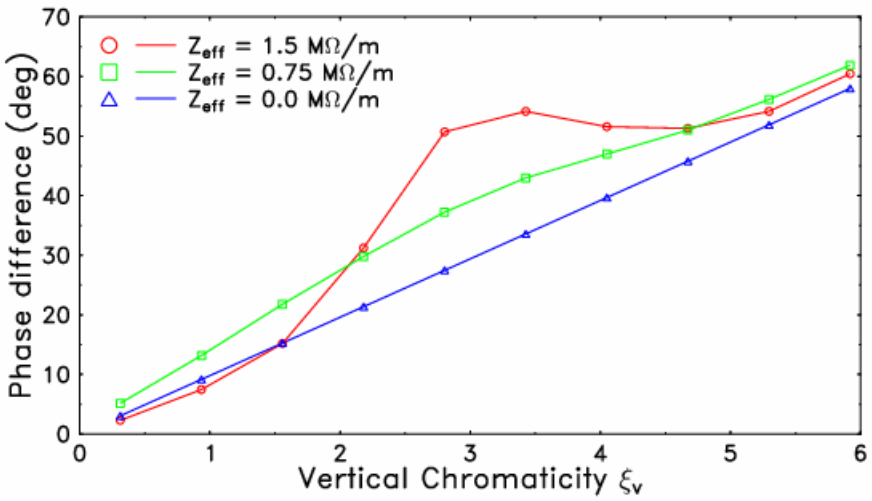

Figure 2.*:* The effect of the resistive wall wake field on the measured phase difference between the head slice (+0.4 ns from bucket center) and the tail slice (−0.4 ns from bucket centre) for a *single* kick is shown here. 1.5 MΩ/m at 100 MHz is a realistic value for the Tevatron.

3. CONCLUSION

Although it has been definitively demonstrated that the phase difference between the head and the tail of the bunch is dependent on the chromaticity, the current theory is insufficient to match it to the data. More work needs to be done to obtain an analytic solution which takes into account the transverse impedance to see if the formula is of any practical use.

The Tevatron PLL System for Q Measurement

C.Y. Tan[1]
Fermi National Accelerator Laboratory, P.O. Box 500, Batavia, IL 60510, USA
(Dated: December 18, 2007)

The Tevatron phase locked loop (PLL) system has been operational since 13 Sep 2005 and has been turned on for all HEP stores since. This system has proved to be invaluable in keeping a record of the tunes up the ramp and through the squeeze for all the stores so that comparisons can be made when things go wrong.The design of the system is very simple so that very little human intervention is needed. The system is also very robust and only requires tune ups of approximately once every few months.

1. INTRODUCTION

The Tevatron phase locked loop (PLL) system has been operational since 13 Sep 2005 and has been taking data of the Tevatron betatron tunes up the ramp and squeeze for all HEP stores since then. The data that has been taken has proved invaluable in post mortem analysis for stores which do not make it to HEP. This system has been designed with simplicity in mind and so very little human intervention has been needed for it to work. Furthermore the system has been very robust and requires tune ups of approximately once every few months.

2. THEORY

The idea behind the PLL system is extremely simple. Suppose the transverse frequency response of the beam is that of a simple harmonic oscillator (SHO), then it is well known that at resonance, the phase of the SHO w.r.t. the kick is exactly -90° out of phase. See Figure 1(a). If we add +90° to the phase response, then the resonance is at phase null. See Figure 1(b). Therefore, it is obvious how the resonance is found: if the beam is kicked at a frequency below the resonance frequency, the phase is positive and if the frequency of the kick is above resonance, the phase is negative. Therefore, the phase null is easily found by iterating the kick frequency until the phase null is found.

The above algorithm is easily implemented as a PLL. See Figure 2. Notice that the Tevatron PLL is not a PID loop, but it is essential that the integrator (1/s) term be in loop for the PLL to track tune ramps. There are only two input parameters to the loop which are the overall gain and the overall phase offset.

The theory of the Tevatron PLL is fully described in two papers:

- C.Y. Tan, “The Tevatron tune tracker pll -- theory, implementation and measurements”, Fermilab Technical Memo, TM-2275.
- C.Y. Tan, “Tune tracking with a PLL in the Tevatron”, Nucl.Instrum.Meth.A557:615-620, 2006.

1 Email address: *cytan@fnal.gov*

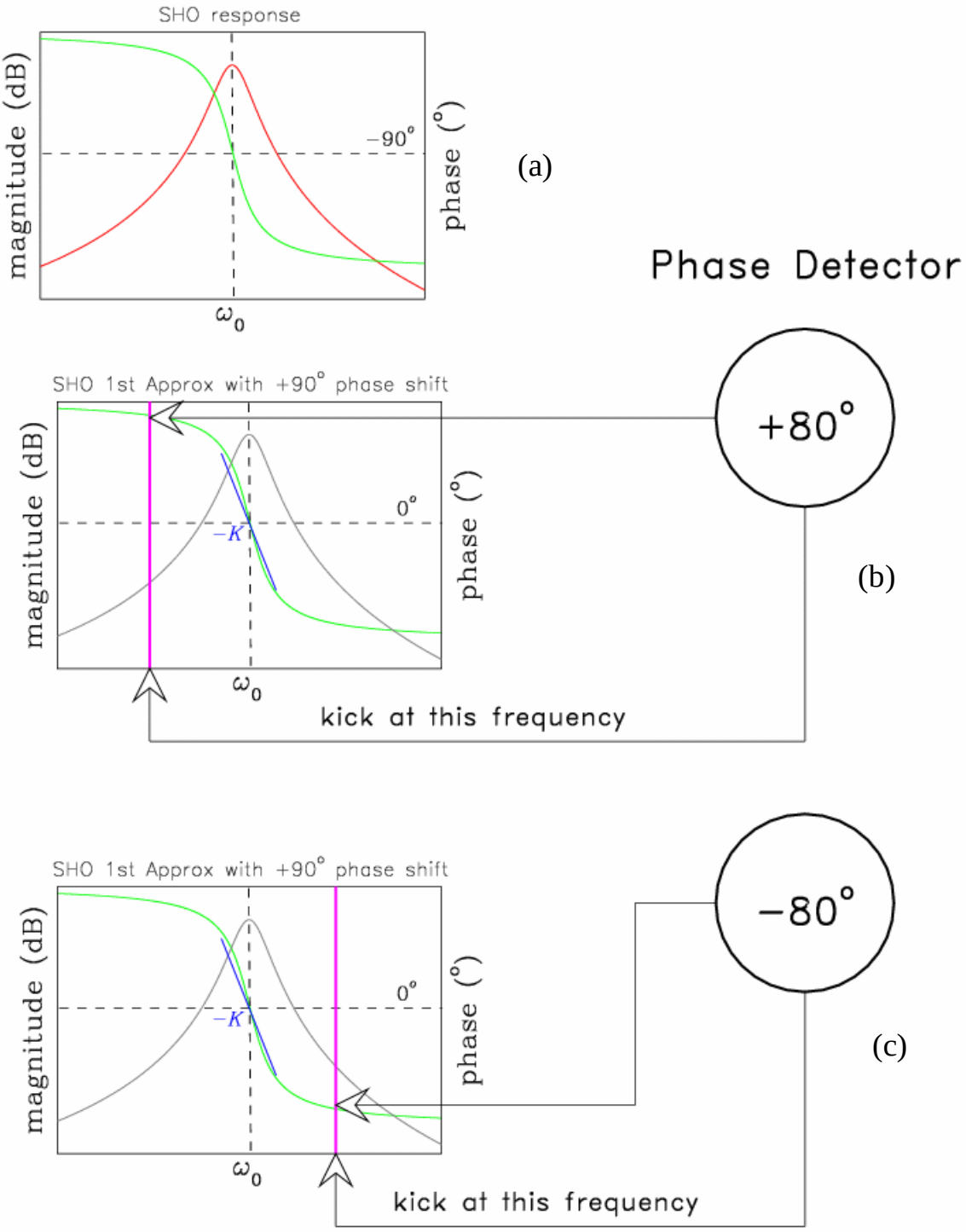

Figure 1.: (a) The frequency response of a SHO is well known. At resonance, the phase of the SHO is exactly 90° out of phase w.r.t. kick. (b) For simplicity, 90° is added to the phase response, so that if the kick frequency is too low, the phase is positive and (c) if the kick frequency is too high, the phase is negative. The kick frequency can thus be iterated towards zero phase which corresponds to the resonant frequency of the SHO.

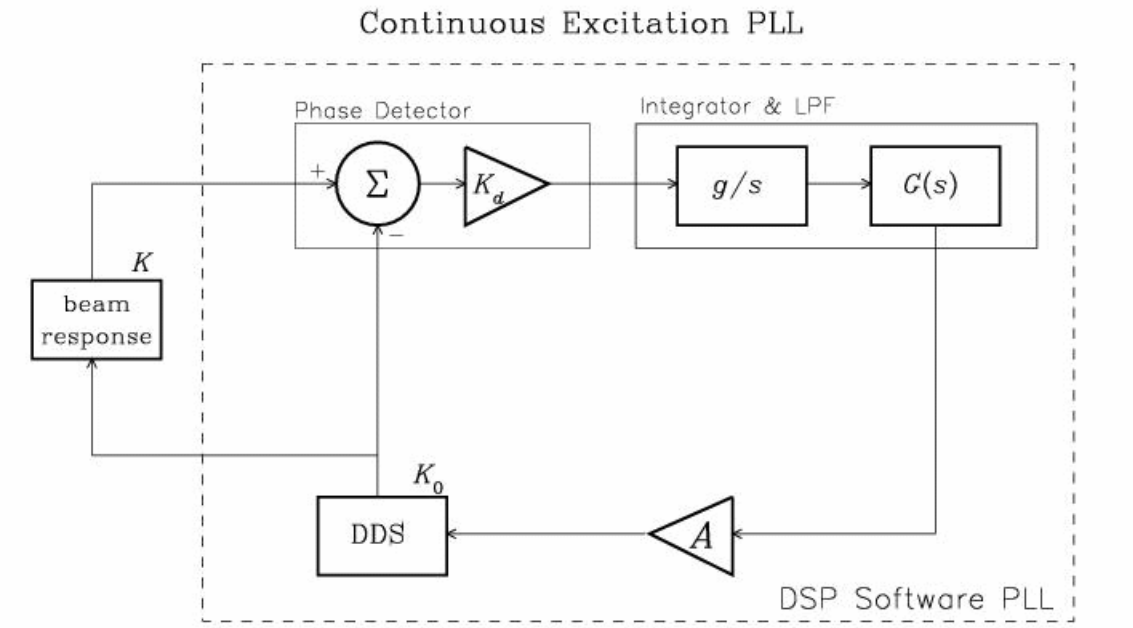

Figure 2.: This is the block diagram of the PLL. The integrator 1/*s* is essential for the loop to work. *G*(*s*) is the low pass filter which can be calculated from the measured beam frequency response. The direct digital synthesiser (DDS) is the digital form of a voltage controlled oscillator (VCO).

3. OTHER OBSERVATIONS

The Tevatron PLL has proved to be very useful in post mortem analysis especially when a store fails because of some change that is not anticipated. For example, there was a failed store when the tunes landed on a 12th order resonance because of a smaller beam-beam tune shift from 44% less pbars than the previous store . See Figure 3.

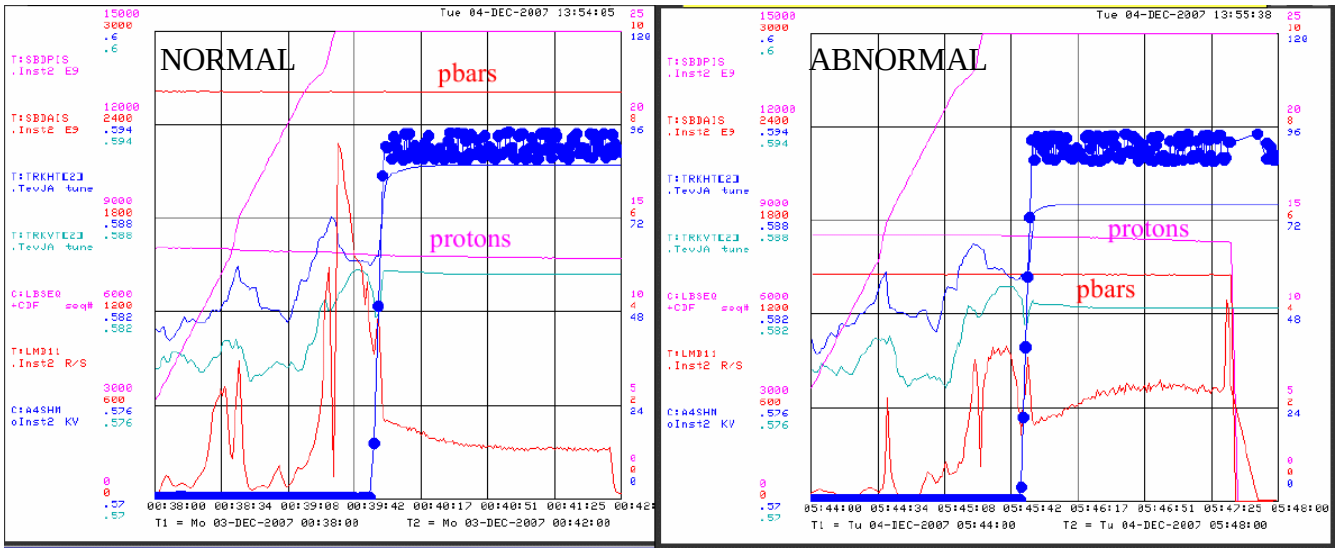

Figure 3.: Two consecutive stores are shown here. The normal store had 44% more pbars than the abnormal store. The final tunes at collisions (blue and cyan curves) clearly do not land at the same place for the abnormal store and in fact was on the 12th order resonance. This produced much higher losses (red curve) than usual which caused the store to abort.

4. CONCLUSION

The Tevatron PLL has functioned very well in the last 2 years and should work until 2009 when the Tevatron is scheduled to shutdown.

Tune Measurement with Chirped Excitation in the Hera Proton Ring

CERN Tune/PLL Workshop
June 10,11 2002
S. Herb, DESY

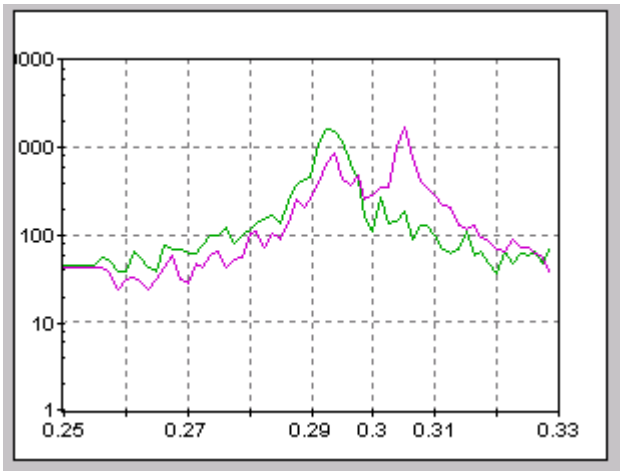

HERA P Ring Parameter Sheet 2002

Parameter	Injection	Luminosity
Circumference (m)	6336	6336
Rev. Freq (Hz)	47,303	47,316
Energy (GeV)	40	920
B Field (T)	0.226	5.2
RF (MHz)	52/208	52/208
Bunch Spacing (MHz)	10.4	10.4
Bunch Length (m, fwhm)	0.36	0.18
dp/p (rms)	.0004	.0001
# Bunches	~ 180	~180
Total Current (A)	~ 0.100	~0.100
Synch Freq (Hz)	~ 40	~ 40
Integer β Tunes	31/31	31/31
Fractional β Tunes	0.293/0.297*	0.293/0.297*
(Hz)	~13,900	~13,900
Natural Chrom.	-60 / -60	-60 / -60
Persistent Current Chrom.	≈ +-40 ??	≈ 0 / 0

HERA P Ring Beam Parameter Control Summary

Problem: **Limited Reproducibility** (day to day and week to week)

Reference Magnet System [2 SC Dipoles in series with Ring]

- NMR Probes [Measure Injection Field]
- Dipole Integration Coil [Measure Field Change during Ramp]
- Rotating Sextupole Coil [Measure Sext field during Injection, Ramp]

Injection Field Control (Compensate Persist. Current decay)

- Reference NMR changes drive Horizontal Correction Coils in Arcs
- Reference Sext drives Sextupole Strings in Arcs

Injection Procedures (Bring to nominal conditions)

Operators have knobs for:
Qx, Qy (drive quad strings in arcs)
Sx, Sy (drive sext strings in arcs)
Sk_a,Sk_b (drive 2 skew quads in West straight)

Inject 10 Bunch Test Shot(s) and
- Measure P offset from Longitudinal Inj Oscillation and correct
- Measure Tunes from Inj Oscillations, stored beam, and correct
- Adjust coupling by 'nearest approach' of Tunes
- Adjust Chromaticity by Peak Width , and/or RF stepping

Inject 180 Bunch Train for Ramp

Ramp Field Control

- SC Dipole Circuit Driven by Pulse Generator
- Reference Dipole Integrator coil drives ramp of 'other' magnets
- Reference Sext drives Δs adding to linear current ramp of Sexts
- Tables drive non-linear corrections to Quad Strings
- Tables drive non-linear corrections to Sext Strings
- Operators drive Qx,Qy via knobs and Sx,Sy, Sk_a,Sk_b as necessary

[new tables periodically produced from smoothed knob data]

Hera P Tune System

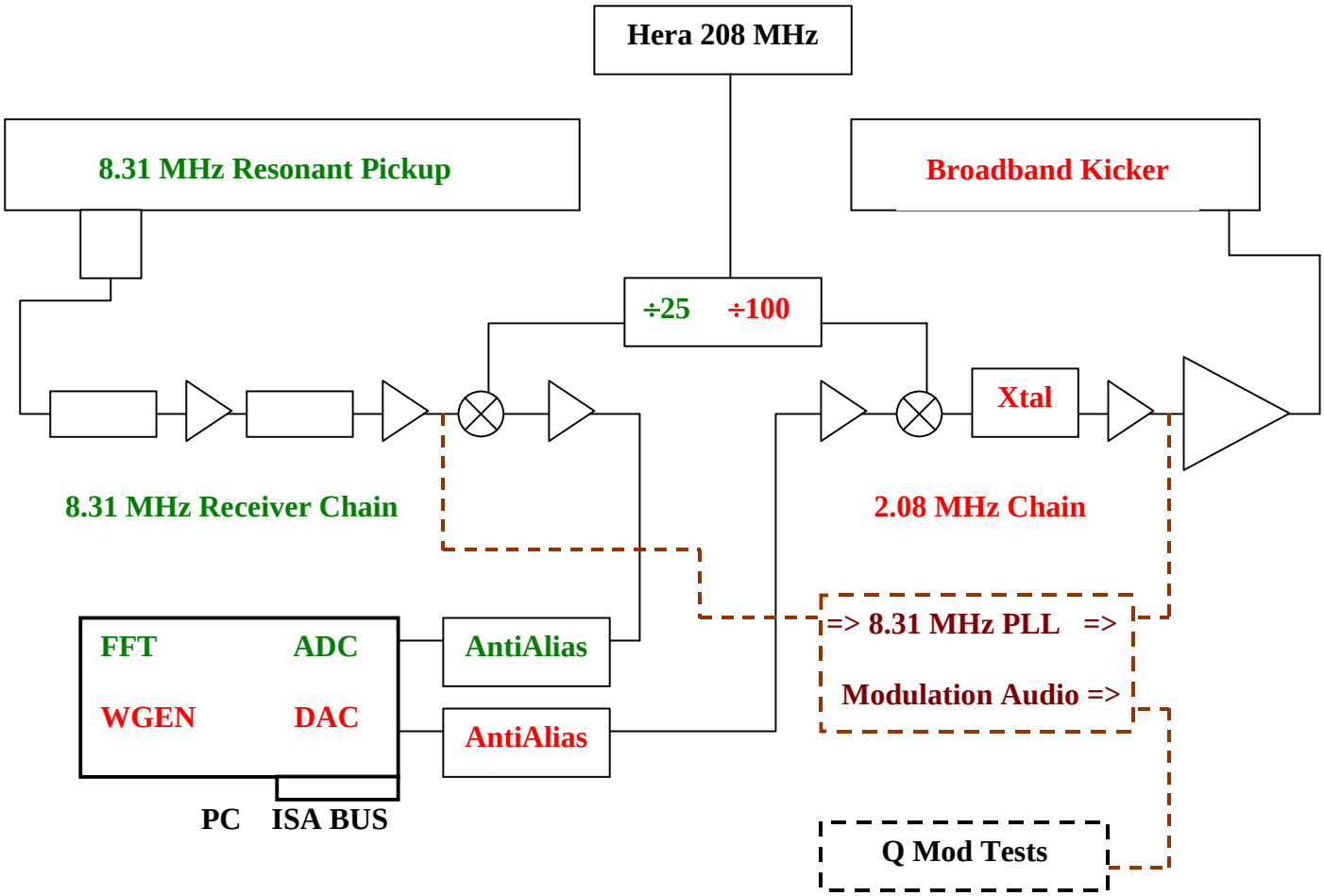

Comments

- Concept from SPS “Schottky” System (Boussard, Linnecar, Scandale)

- Signal from ALL bunches in Hera but a SINGLE multibunch mode

- Kicker drives ALL bunches in that SAME multibunch mode

- Monitor Sensitivity ~ 5Ω /mm, Input Sensitivity ~ 3 nV/Hz^{½}
  [For 100 ma, 100 Hz band, S/N~10 for 6 nm *in multibunch mode*]

- Standard Operation uses ‘Chirped’ Excitation during Injection, Ramp Frequency 10 => 20 kHz with Trapezoidal Window, during FFT

fft range 0-30 kHz , 2048 pts, acquisition time 34 msec
fft rate 8 Hz , avg 4 => 2 Hz at console

Simple PLL Module

(L. Becker, DESY, ~1992)

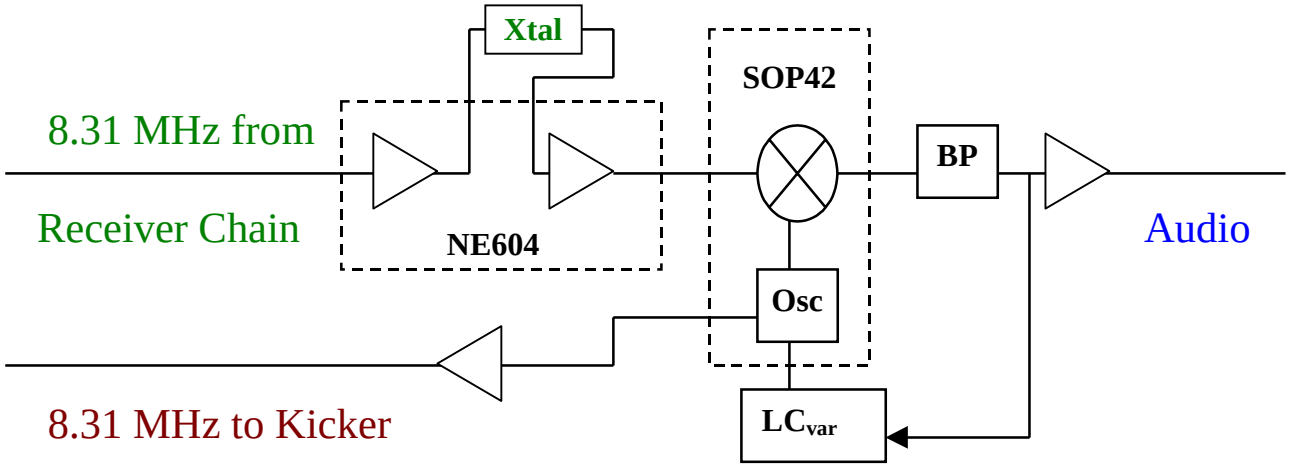

[Used for measuring tune modulation, O. Bruening, 1994 (?)]

Some Comments on Hera Resonant Monitor + Chirped Excitation System

- During early operation of Hera P, the linear chirp was found to be a very simple general purpose excitation, and we have hardly experimented with anything else (very little new development work in past 6 years!)

- What does the excitation look like? Does linear chirp ~~deexcite,~~ as well as excite the bunch oscillations, or are they left ringing after passing through resonance? *[observations suggest something in between]*

- Sensitivity means that kicker can be used without much worry about emittance growth (when machine is reasonably tuned up)

- Sensitivity means that system is useful for diagnosing problems responsible for slow beam emittance growth

- Width and coupling observable (but not always easy to interpret)

- Lots of information for good operators, but **hard to automate!** (peak shapes very different in various machine conditions, coupling & chromaticity correction require 'dithering' tests)

- Tune spectra sensitive to many aspects of machine performance (messenger blamed for bad news?)

Possible Modifications?

- Better fitting of available data [*Wavelets?]*

- More sophisticated signal processing? Now throwing away time/phase information.

- Single Impulse Kick as alternative? (eg 8.3 MHz for 2-3 turns) Would this permit simple coupling measurement via mixed time/frequency domain analysis?

- Use 8.3 MHz system together with Klute digital PLL for tune control? We have not tried to think about how this interacts with coupling and chromaticity in the Hera P.

The real issue is **RELIABLE CONTROL** during the ramp!

With the Hera P Ring, it seems not realistic to require that automatic tune control need work only on a machine which is already in a ‘very well tuned’ condition. The system must also be able to cope with a ‘moderately well tuned’ machine, and must have ‘sane’ responses to states in which clean tune information is not available.

Introduction to Beam-based Feedback Design

Ralph J. Steinhagen (CERN, Geneva, Switzerland)

Abstract

Tight beam parameter stability requirements have been most pronounced for light sources and lepton colliders but are now becoming increasingly important for present and future hadron accelerator operation, not only for performance but also for reasons of machine protection, as recent improvements have led to significantly increased stored beam energies.

In the latest generation machines, performance depends critically on the stability of the beam. In order to counteract disturbances due to magnetic imperfections, misalignments, ground motion, temperature changes and other dynamic effects, fully automated control of the key beam parameters – orbit, tune, coupling, chromaticity and energy – becomes an increasingly important aspect of accelerator operation.

This contribution presents an overview of the design of beam-based feedback systems, their architecture, performance limitations and the design choices involved.

INTRODUCTION

With respect to beam-based feedback systems, the wide range of accelerators can be roughly grouped into synchrotron light sources, lepton colliders, and hadron colliders that are distinct in their requirements of number and type of feedbacks deployed.

The requirements on beam stability in synchrotron light sources are determined by the quality and properties of the photon beam seen by experiments. Depending on the time scale of the experiment's data integration and perturbation frequency, movements of the beam centroid may either "smear out" the effective emittance, which has a deteriorating effect on the photon beam quality, or lead to an increase of measurement noise. Due to synchrotron radiation, the beam emittance is usually much smaller in the vertical plane. To preserve and minimise the effective emittance, nearly all light sources deploy fast orbit and energy feedbacks. These feedbacks minimise transverse beam movements, minimise spurious dispersion by centring the beam in the quadrupoles and maintain a stable vertical orbit inside the sextupoles that would otherwise give rise to emittance coupling. A summary and overview of beam stability requirements and stabilisation in synchrotron light source can be found in [1–4].

Beam stability requirements in lepton and present hadron colliders are driven by luminosity optimisation inside the experimental insertions. They favour, similar to light sources, small emittance and stable beam overlap at the interaction point ([5–7]). In addition to orbit feedbacks, tune feedbacks are also often deployed ([8, 9]) to stabilise the beam during acceleration and to avoid resonances that may cause increased particle loss.

Recent improvements in hadron colliders lead to significantly larger stored beam energies that require an excellent control of particle losses inside a superconducting machine. In the case of the LHC, the energy stored in the beam is sufficient to quench all magnets and cause serious damage [10]. Thus, most requirements on key beam parameters in superconducting hadron colliders strongly depend on the capability to control particle losses inside the accelerator. The Cleaning System has the tightest constraints on the orbit and requires a stability better than $25\,\mu\mathrm{m}$ during nominal operation at the location of the collimators [11, 12]. Other requirements range from 0.5-0.2 mm r.m.s. for global stabilisation down to $10\,\mu\mathrm{m}$ for physics analysis improvements in the TOTEM experiment [13].

In contrast to lepton machines that require tune stability in the order of $\delta Q \approx 10^{-2} \ldots 10^{-3}$ to avoid up to 4th order resonances, synchrotron radiation damping is negligible in hadron colliders. In order to provide sufficient beam life-time, resonances of up to the 12th order have to be avoided [14]. The corresponding tune stability δQ is thus required to be better than 0.001 at the LHC. The chromaticity has to be controlled within $Q' \approx 2 \pm 1$, while the uncorrected chromaticity changes are expected to exceed 100 units within a few hundred seconds after the start of the ramp [14].

PARAMETER STABILITY

The wide range of perturbation sources that may affect orbit, tune, coupling, chromaticity and energy can be grouped into:

1. Environmental sources, driven by temperature and pressure changes, ground motion, tides and noise induced by human activity that are mostly propagated through quadrupoles and their girders onto the beam,

2. Machine-inherent sources, such as the decay and snap-back of magnet multipoles, cooling liquid flow, vibration of pumps and ventilation, eddy currents and changes of machine optics (final focus),

3. Machine element failures, which are mainly important for large machines such as the LHC where the single circuit failure out of more than 1300 corrector circuits is non-negligible during regular operation.

Their time scale ranges usually from short term (milliseconds to hours), over medium term (hours to days) up to

long-term (days to month). Beam-based feedbacks can contribute and improve beam parameter stability for perturbations on slow to medium time scales but are ultimately limited by thermal drifts, noise and systematics of corrector circuits and beam instrumentation [15]. The sensitivity to thermal drifts in 3^{rd} generation light sources lead to a rigorous stabilisation of not only the orbit but also the temperature of the experimental hall, tunnel, cooling water, and vacuum chamber to a level of about $\pm 0.1\,^{\circ}\mathrm{C}$ [16]. The quest for temperature stabilisation leads also to 'top-up' operation that maintains a constant beam current and thus constant heat load inside the tunnel [1, 2].

FEEDBACK VS. FEED-FORWARD

The classic control theory distinguishes two paradigms that may be used to drive and stabilise a given process:

Feed-Forward

In this scheme the process control depends only on the desired parameter reference and requires usually a precise knowledge on the process and driving disturbance transfer function. While this scheme is often sufficient, it also has an intrinsic weaknesses for processes where either the transfer function has given uncertainties, unknown or less precisely known disturbance sources that may lead to a systematic error $\Delta\epsilon = 1 - \epsilon$ in between the reference and actual beam process variable as illustrated in Figure 1. For a

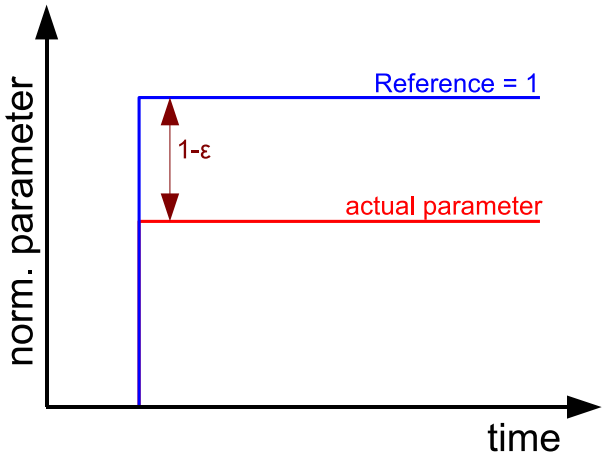

Figure 1: Feed-forward signal to a step response reference change: the actual value of process variable and residual error $1 - \epsilon$ is indicated.

steady-state scenario, the residual error between actual and desired beam process parameter stays constant and may be outside the required accuracy margins. Still, this type of control is suitable for processes such as for example the transfer function between main dipole magnets, RF voltage and resulting particle momentum as these are usually known on the 0.1% level. Also, in third-generation light sources, the effect of changing insertion elements (undulators) is usually anticipated and at least partially corrected by feed-forward systems and only the residual perturbation reduced by beam-based feedbacks.

Feedback

In case the knowledge on the process model error is limited (due to, for example, multiple dependencies or most often random disturbance sources) but a measurement of the actual value of the beam process variable exists, one may choose to use this measurement to stabilise the process by comparing the measured value with an external reference. In this case the difference $\Delta\epsilon = 1 - \epsilon$ drives a controller that iteratively optimises the actuator signal by minimising $\Delta\epsilon$ till the actual beam process variable matches the desired reference value as shown in Figure 2. The ad-

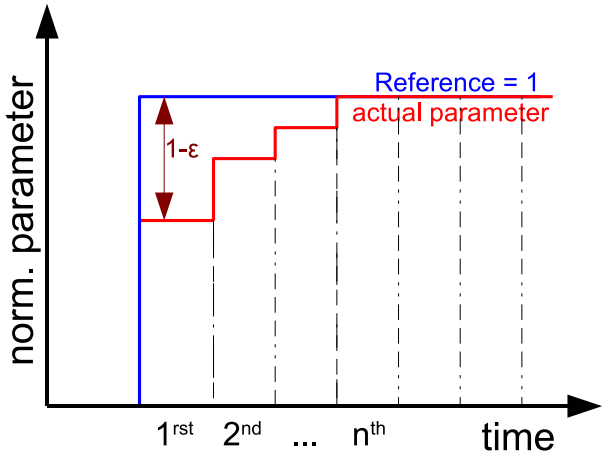

Figure 2: Feedback signal to a step response reference change: the minimisation of the residual error $1 - \epsilon$ as a function of iteration number is visible.

vantage of feedbacks is that they require, in comparison to feed-forward systems, only a rough process model while reducing the residual error through continuous measure-and-correct iterations. For a steady-state scenario, the final parameter stability is ultimately limited by the noise and systematic error of the underlying beam parameter measurement. Since the robustness and stability of the beam instruments directly translates through this into the robustness and stability of the feedback loop, a good understanding of the underlying instrument, measurement and diagnostic principle is of paramount importance while designing beam-based feedback systems. In many cases, the systematic measurement error and noise is usually much smaller than the uncertainties on machine alignment and magnet circuit transfer function, and thus feedbacks are usually the favoured solution to stabilise the beam.

The accelerator controls domain often distinguishes two types of feedback: those acting within a given accelerator cycle (e.g. injection, acceleration, store, dump) and cycle-to-cycle feedbacks where the disturbance measurements of the previous cycle are used to drive the actual state. The latter is sometimes incorrectly referred to as "fill-to-fill feed-forward" though – in the strictest sense – they usually also

rely on beam-based measurements. While both cases are similar and differ mainly on the time-scale in between measurements and corrections, the latter offers less strict requirements in terms of read-out speed and bandwidth of the involved beam instrumentation's acquisition system and often initially favoured to a continuous read-out. The basic measurement and control principles are the same.

Traditionally, operators and physicists tend to hesitate using fully-automated feedback systems, as these often evade their direct supervision, due to the often fast timescales of the feedback controller measurements and application of corrections. From the beam diagnostics point of view, in case the given instrument is to be used in beam-based feedbacks, instrumentation experts seem to have thus the tendency to first optimise the performance of the beam instrument – often including significant filtering to reduce the measurement noise – before the initial attempt to close the feedback loop. While this habit is usually suitable for systems that are used only for verification, this approach has certain disadvantages when used in feedback e.g. through introducing additional often unnecessary sampling delays. Most modern feedback controllers are digital and implement usually at least one low-pass filter to perform the above described minimisation of $\Delta\epsilon$. Thus, combining the filtering of beam instruments and closed-loop responses of the controller can often greatly improve the feedback response by minimising the total loop delay.

FEEDBACK CONTROL DESIGN

In the case of low-order beam parameters – orbit, tune, coupling, chromaticity and energy – the effect of individual corrector circuits is, for most accelerators, sufficiently linear and can be cast into matrices. In the case of the orbit, for example, one can write

$$\Delta\underline{z}(t) = \mathbf{R} \cdot \underline{\delta}(t) \tag{1}$$

with $\Delta\underline{z} = (z_1, \ldots, z_m)^T$ holding the readings of m beam position monitors (BPMs) and $\underline{\delta} = (\delta_1, \ldots, \delta_n)^T$ holding the strengths of n dipole corrector circuits (CODs) and the matrix elements R_{ij} describing the response of the i-th BPM to the j-th COD circuit. Similar parameter relations can be derived for the other parameters.

The external perturbations, corrector circuit strengths $\underline{\delta}(t)$ and thus the beam parameters themselves are usually a function of time. Many feedback designs on beam parameters decouple the control into what is further referred to as *space* and *time domain* which makes the choice of parameter correction strategy and the controller adjustment of the temporal behaviour of the corrector circuits more flexible, particularly in the presence of element failures that require quick adjustments of the feedback controller and response matrices.

Space Domain

The parameter control in space domain establishes corrector circuit strengths $\underline{\delta}_{ss} = \lim_{t\to\infty}(\delta_1(t), \ldots, \delta_n(t))^T$ that for steady-state perturbations minimises the residual r of

$$r = \left\|\underline{z}_{ref} - \underline{z}_{actual}\right\|_2 = \|\mathbf{R} \cdot \underline{\delta}_{ss}\|_2 < \epsilon \tag{2}$$

with $\mathbf{R}$ the beam response matrix, $\underline{z}_{ref}$ the reference and $\underline{z}_{actual}$ the measured parameter. The two-norm (or r.m.s.) of the parameter vector is defined as $\|\underline{x}\|_2 = \frac{1}{N}\sqrt{\sum_{i=0}^{N} x_i^2}$ with x_i being the individual vector entry and N the total number of entries.

The control in space domain essentially consists of the inversion of the beam response matrices. Singular-Value-Decomposition (SVD) is one of the most popular and widely used inversion algorithms ([1–3]) and a generalisation of the Jacobi matrix eigenvalue decomposition to the general case of non-square matrices [17, 18]. As shown in [17] and visualised in Figure 3, any matrix $\mathbf{R} \in \mathbb{R}^{m\times n}$ with $m \geq n$ can be decomposed into

$$\mathbf{R} = \mathbf{U} \cdot \lambda \cdot \mathbf{V}^T \tag{3}$$

with $\mathbf{U} \in \mathbb{R}^{m\times n}$ being a dense unitary matrix, $\lambda = diag(\lambda_1, \ldots, \lambda_n)$ a diagonal matrix holding the eigenvalues of $\mathbf{R}$, and $\mathbf{V} \in \mathbb{R}^{n\times n}$ an orthogonal matrix containing the eigenvectors of $\mathbf{R}$ in its columns.

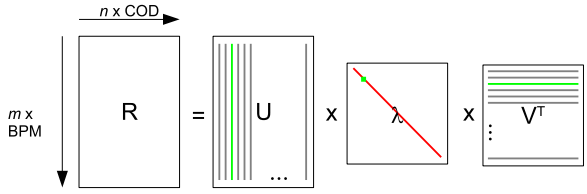

Figure 3: Schematic of the Singular Value Decomposition (SVD): An arbitrary real matrix $\mathbf{R}$ with dimension $m \times n$ can be decomposed into a rectangular matrix $\mathbf{U} \in \mathbb{R}^{m\times n}$, diagonal eigenvalue matrix $\lambda = diag(\lambda_1, \ldots, \lambda_n) \in \mathbb{R}^{n\times n}$ and transpose eigenvector matrix $\mathbf{V}^T \in \mathbb{R}^{n\times n}$.

Depending on the device layout and lattice parameters, equation 1 may contain singularities that can, using SVD, be identified by eigenvalues close or equal to zero. The SVD can be used to compute a so-called *pseudo-inverse* response matrix $\tilde{\mathbf{R}}^{-1}$ that relates the required steady-state circuit strengths $\underline{\delta}_{ss}$ to the measured orbit error $\Delta\underline{z}$:

$$\underline{\delta}_{ss} = \mathbf{V} \cdot \tilde{\lambda}^{-1} \cdot \mathbf{U}^T \cdot \Delta\underline{z} = \tilde{\mathbf{R}}^{-1} \cdot \Delta\underline{z} \tag{4}$$

Possible singularities are removed by setting the inverse of singular eigenvalues to zero. As a special case, for beam parameter which can be decomposed into two independent variables (Q'_x/Q'_y, Q'_x/Q'_y and $\Re(c^-)/\Im(c^-)$), all but two eigenvalues vanish. The ratio between the largest λ_{max} and smallest eigenvalue λ_{min} is a measure of the matrix's *condition number*

$$C_R \approx \left|\mathbf{R}^{-1}\underline{z} \cdot (\mathbf{R}\underline{\delta})^{-1}\right| \tag{5}$$

$$C_R \approx \left|\frac{\lambda_{max}}{\lambda_{min}}\right| \tag{6}$$

For example, the eigenvalue spectrum of the decomposition of LHC injection and collision orbit covers about six orders of magnitude. One can show that the '2' logarithm of the condition number

$$n_{bits} \approx log_2(C_R) \tag{7}$$

can be used to estimate the number of digits n_{bits} that are lost during the inversion of the matrix. Thus, for the LHC, roughly 20 significant bits are lost during decomposition, which indicates the necessity to perform the computations and transformations at least in *double* (64 bit) floating point precision.

The number of eigenvalues used for the inversion defines the trade-off between precision and robustness of the correction: A higher number of eigenvalues provides a better convergence but at the same time tends to be more prone to spurious parameter readings and noise. Figure 4(a) and 4(b) illustrate this using the LHC orbit feedback correction as an example.

In case the true accelerator response differs from the one used during the design of the parameter control, the correction error gradient $\underline{\delta}_s s$ may point off the true minimum, as illustrated in Figure 5. It is visible that independent of the

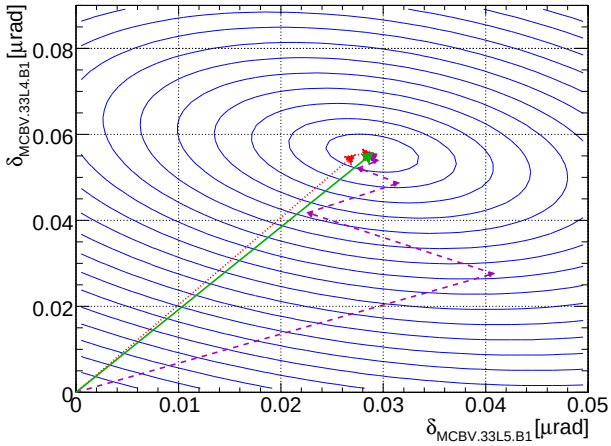

Figure 5: SVD residual contour: The perfect correction (solid green), the correction with optics error (dotted red) and COD calibration errors (dashed violet) are indicated. The contour lines correspond to constant values of the residual orbit error r. The correction is based on a regular FODO lattice (LHC arc) and shows the projection of two selected COD settings.

type of error, the corrections converge to the same steady-state setting. However, depending on the errors the convergence speed can vary between one (perfect) and about seven iterations (20% COD calibration errors).

In most digital approximations, analogue systems are sampled at least 10 times higher than the analogue bandwidth. Since the deteriorating effect due to beam response matrix uncertainties can be mitigated through a higher sampling frequency, it is usually favourable to sample much higher than a factor of 10. In case of synchrotron light sources, typical sampling to bandwidth ratios are about 40 or more [1–3].

Time Domain

A simple loop block diagram consisting of a single-input-single-output (SISO) process $G(s)$ and controller $D(s)$ is shown in Figure 6. The stability and sensitivity

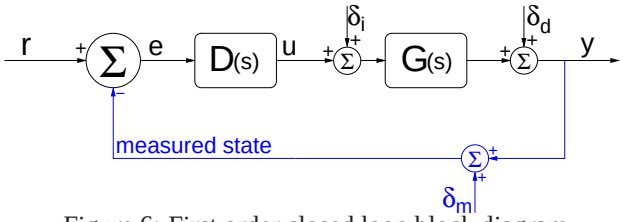

Figure 6: First order closed loop block diagram

to perturbations and noise is defined by the following functions

$$T(s) := \frac{y}{r} = \frac{D(s)G(s)}{1 + D(s)G(s)} \tag{8}$$

$$S_d(s) := \frac{y}{\delta_d} = \frac{1}{1 + D(s)G(s)} \tag{9}$$

$$S_i(s) := \frac{y}{\delta_i} = \frac{G(s)}{1 + D(s)G(s)} \tag{10}$$

$$S_u(s) := \frac{u}{\delta_d} = \frac{D(s)}{1 + D(s)G(s)} \tag{11}$$

where $T(s)$ is the complementary (nominal) transfer function, $S_d(s)$ the *nominal sensitivity* defining the loop disturbance rejection, $S_i(s)$ the *input-disturbance sensitivity* and $S_u(s)$ the *control sensitivity*. The state variable is indicated in Figure 6. The sensitivity to measurement noise is equal to the nominal transfer function T_0.

Linear-System Design

Classic feedback designs rely on the discussion of denominator zeros in equation 8 and 9 while keeping constraints such as required bandwidth, minimisation of overshoot, limits on the maximum possible excitation signal and robustness with respect to model and measurement errors. For ideal processes, this yields adequate controller designs but often falls short of providing a simple comprehensive method for estimating and modifying the loop sensitivity (robustness) in the presence of process uncertainties, non-linearities and noise.

This paper focuses on Youla's affine parameterisation method for optimal controllers, based on the analytic process inversion, first introduced in [19]. For an open-loop stable process $G(s)$, the nominal closed-loop transfer function is stable if and only if $Q(s)$ is an arbitrary stable proper transfer function and $D(s)$ parameterised as:

$$D(s) = \frac{Q(s)}{1 - Q(s)G(s)} \tag{12}$$

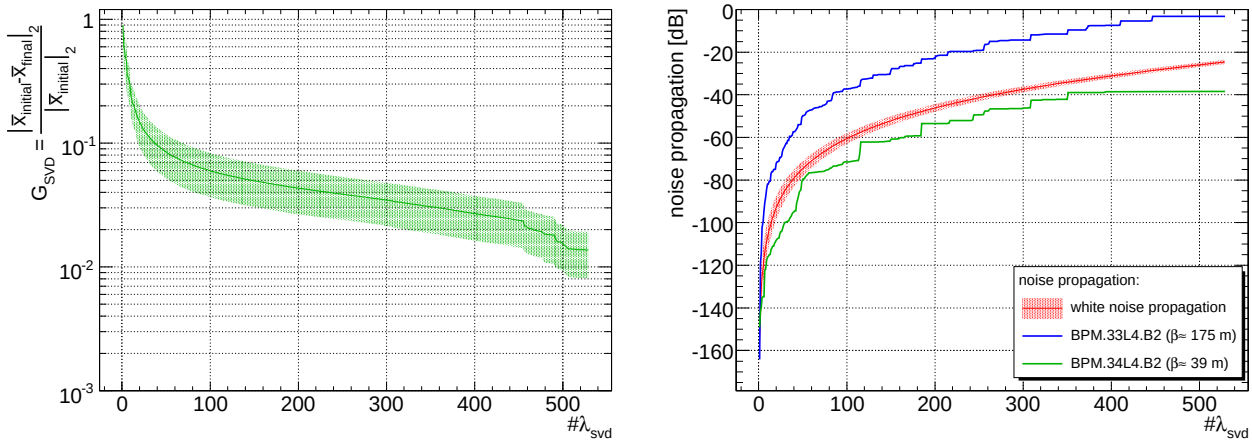

(a) LHC orbit feedback attenuation

(b) LHC BPM noise propagation

Figure 4: Attenuation (left) and BPM noise propagation onto the orbit (right) of the SVD based vertical LHC orbit correction during injection as a function of the cut parameter $\#\lambda_{SVD}$. The correction is performed for both beams using all available monitors and based on a seed of 100 different orbits per COD iteration. The orbit correction attenuation decreases and the noise propagation increases with the number of chosen eigenvalues.

The stability of the closed loop system follows immediately out of the above definition if inserted into equations 8 to 11. The sensitivity functions in the $Q(s)$ form are given as:

$$T(s) = Q(s)G(s) \quad (13)$$
$$S_d(s) = 1 - Q(s)G(s) \quad (14)$$
$$S_i(s) = (1 - Q(s)G(s))G(s) \quad (15)$$
$$S_u(s) = Q(s) \quad (16)$$

Assuming $G(s)$ is stable, the only requirement for closed loop stability is for $Q(s)$ to be stable. The strength of this method is the explicit controller design with respect to required closed loop performance, as visible in equation 13, and required stability (equations 14 to 16). Equations 13 and 14 are complementary and illustrate the intrinsic limiting trade-off of feedbacks that either have a good disturbance rejection or are robust with respect to noise. The ultimate limit is hence defined rather by bandwidth and noise performance of the corrector circuits and beam measurements than by the feedback loop design itself. Systematic and thorough analysis of involved beam instrumentation and corrector circuits are thus essential for achieving best beam parameter stabilisation.

The design formalism can be demonstrated using a simple first order system $G_0(s) = \frac{K_0}{\tau \cdot s+1}$ with open-loop gain K_0 and time constant τ. A common controller design ansatz is to write $Q(s)$ as

$$Q(s) = F_Q(s) \cdot G_0^i(s) \quad (17)$$

with $F_Q(s)$ a trade-off function and $G_0^i(s)$ the pseudo-inverse of the process. Since G_0 does not contain any unstable zeros, the pseudo-inverse equals the inverse and is given by $G_0^i(s) := [G_0(s)]^{-1} = \frac{\tau \cdot s+1}{K_0}$. $Q(s)$. In order for $D(s)$ to be biproper, $F_Q(s)$ must have a degree of one and can be written as:

$$F_Q(s) = \frac{1}{\alpha s + 1} \quad (18)$$

Inserting equation 17 into Youla's controller parameterisation equation 12 yields the following controller

$$D(s) = \frac{\tau}{K_0 \alpha} + \frac{1}{K_0 \alpha s} = K_p + K_i \cdot \frac{1}{s} \quad (19)$$

which shows a simple PI controller structure with proportional gains K_p and integral gain K_i. Inserting equation 17 into equation 13 yields:

$$T_0(s) = F_Q(s) \quad (20)$$

It is visible that the closed loop response is essentially determined by the choice of trade-off function $F_Q(s)$ and that the closed loop bandwidth is proportional to the parameter $1/\alpha$. This can be used to tune the closed loop between: high disturbance rejection but high sensitivity to measurement noise (small α) and low noise sensitivity but low disturbance rejection (large α) depending on the operational scenario. The maximum possible closed loop bandwidth is limited by the excitation, as described by equation 16. In the case of power converters, for example, the excitation is limited by the maximum available voltage.

Non-Linear System Design

The same method can be extended to open-loop unstable and multi-input-multi-output (MIMO) systems [19]. Real life beam-based feedbacks usually contain delays λ (due to e.g. data transmission, data processing etc.) and non-linearities $G_{NL}(s)$, most of them related to either saturation and/or rate limits of the corrector circuits' power supplies. The latter introduces a systematic delay if the converter is requested to perform sinusoidal oscillations with amplitude I_a beyond the given frequency f_{max}, which depends on the current rate limit $|\Delta I/\Delta t|_{max}$:

$$f_{max} = \frac{1}{2\pi I_a} \left| \frac{\Delta I}{\Delta t} \right|_{max} \tag{21}$$

Above this frequency the current rate reaches the maximum slew rate, gets clipped and the converter starts to produce a distorted approximative saw-tooth while introducing an additional delay $\Delta\tau$ as illustrated in Figure 7. The full rate-

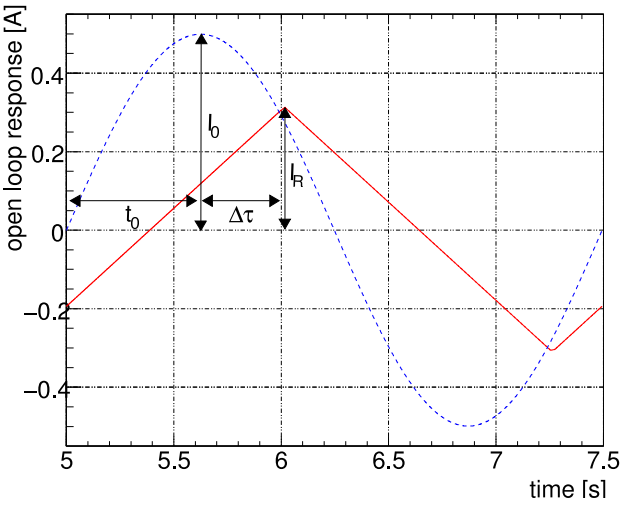

Figure 7: Rate limiter response. The additional delay due to the rate limiter is visible.

limited response $M(f)$, including control T_c and sampling delay T_s, can be written as

$$M(f) = |M(f)| \cdot e^{i\cdot\varphi(f)} \tag{22}$$

$$|M(f)| = \begin{cases} 1 & \text{if } f \le f_{max} \\ \frac{1}{2\pi I_a} \left|\frac{\Delta I}{\Delta t}\right|_{max} \cdot \frac{1}{f} & \text{if } f > f_{max} \end{cases} \tag{23}$$

$$\varphi(f) = \pi f \cdot (T_s + T_c) + \arccos(|M(f)|) \tag{24}$$

with I_a the requested current, f the requested frequency, $\left|\frac{\Delta I}{\Delta t}\right|_{max}$ the maximum current ramp limit and f_{max} the transition frequency, given in equation 21, which is the limit between the linear and non-linear regime. The open-loop frequency response for various requested excitation amplitudes I_a is exemplarily shown for the LHC dipole corrector circuit ($|\Delta I/\Delta t|_{max} = 0.5\,\mathrm{A/s}$) in Figure 8. The feedback controller design could in principle be carried out in the linear domain for small signals and/or slow oscillation frequency which respects the above limits. However,

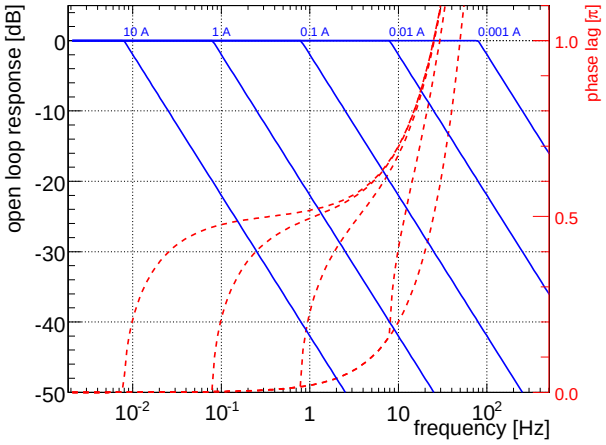

Figure 8: Open loop response of the $\pm 60A$ converter that powers the MCBH and MCBV magnets. The non-linear magnitude and phase lag are plotted for various reference currents. A current change of 0.01 A corresponds to an average orbit r.m.s. change of about $15\,\mu$m at 7 TeV. The reduced bandwidth and increased phase advance for increasing amplitudes I_a is visible.

using such a design would also significantly reduce the performance and possible operational range of the corrector circuits and resulting feedback loop performance and may even lead to overshoot and instabilities in case the above linear regime limits are not respected as illustrated in Figure 9. In order to fully exploit the converters' and feedback's capabilities one can extend the linear control law by additional predictor branches that introduce additional controller inhibiter signals accounting and compensating for the non-linearities once reaching this regime. Using the same ansatz as for the linear system, the delayed rate-limited process can be written, for example as:

$$G(s) = G_0(s) \cdot e^{-\lambda s} G_{NL}(s) \tag{25}$$

Using the same pseudo-inverse $G_0^i(s)$ as for the above example and inserting equation 17 into equation 12 yields a controller parameterisation $D_{NL}(s)$ including a classic Smith-Predictor and Anti-Windup paths, discussed in more detail in [20, 22]. An more elaborate feedback control design example is shown for the LHC orbit feedback in Figure 10. The classic linear loop with controller $D(s)$, delayed process $e^{-\lambda s}G(s)$, the Smith-Predictor and Anti-Windup branches are visible. Using this scheme the controller can be designed as for a regular linear system, while the predictor branches ensure that the system is kept stable even in the presence of non-linearities. Since these branches are extensions of the regular linear controller, they can be easily disabled during testing or commissioning of the feedback loop, if required. Details of this scheme can be found in [21].

Inserting equation 17 including the delay and non-linearities into equation 13 yields the following closed loop

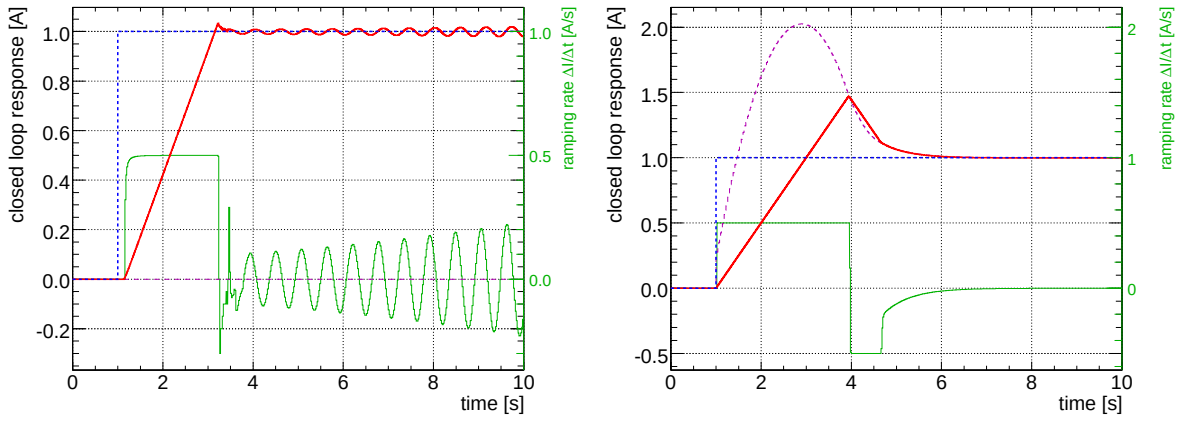

(a) without Smith-Predictor (b) without Anti-Windup scheme

Figure 9: Closed loop feedback response to a reference step function without Smith-Predictor (left) and without Anti-Windup scheme (right). The reference function (blue), the current response (red), current change rate (green) and differential controller signal (violet) are plotted. The transient oscillations and overshoot are visible.

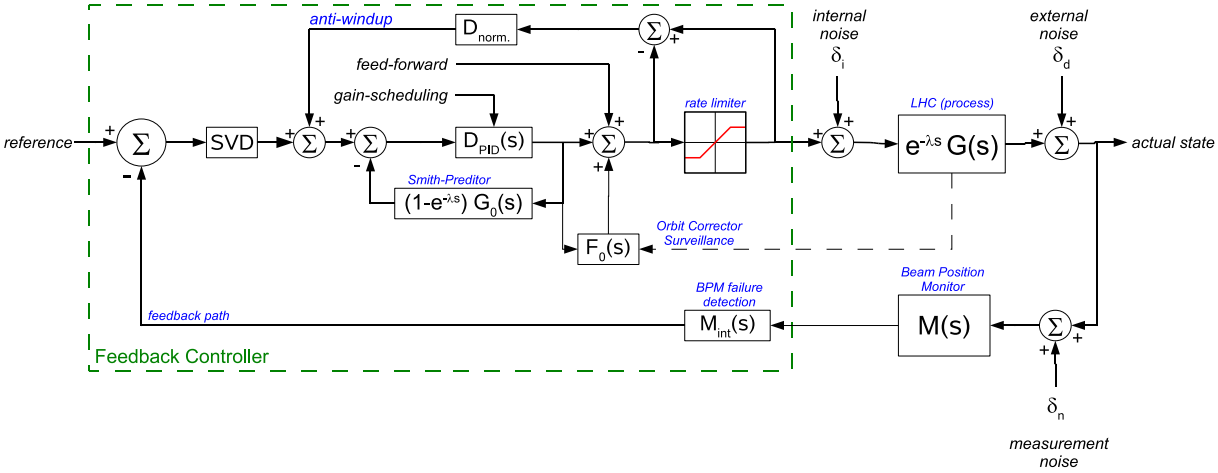

Figure 10: Full LHC orbit feedback block diagram. $G(s)$ abbreviated $G(s) = G_0(s) \cdot G_{NL}(s)$ for better readability. The Smith-Predictor and Anti-Windup branch are indicated.

transfer function:

$$T(s) = F_Q(s) \cdot e^{-\lambda s} G_{NL}(s) \tag{26}$$

It is visible that for $\lambda = 0$ and frequencies below f_{max} the non-linearities have a vanishing contribution to the closed loop transfer function. Similar to the linear case discussed above, the closed loop is essentially defined by the function $F_Q(s)$ that within limits can be chosen arbitrarily based on the required disturbance rejection and robustness during possibly different operational scenarios (gain-scheduling). The simulated closed loop response for above system including the Smith-Predictor and Anti-Windup scheme is shown in Figure 11. Further information and a review on Youla's parameterisation can be found in [22, 23].

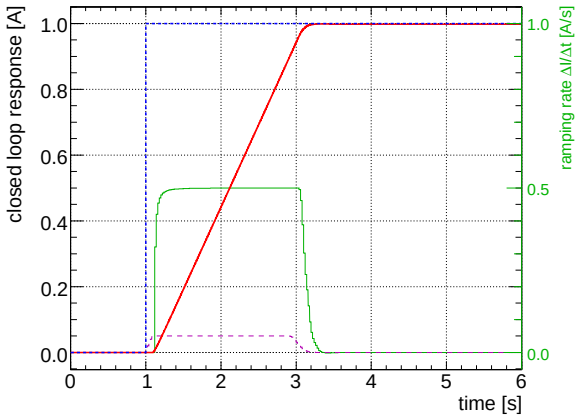

Figure 11: Closed loop feedback response to a reference step function including Smith-Predictor and Anti-windup scheme.

DEPENDABILITIES AND CROSS-TALK

In many accelerators, beam-based feedbacks are usually established and designed one by one, and often, little effort is put into the study of cross-dependency and decoupling of these loops. However, for robust and reliable control it is necessary to address possible cross-constraints, cross-talk and coupling between several simultaneous and possible nested loops, already in the design stage.

A typical cross-dependency is intrinsic to stability requirements on orbit and tune: though tight constraints on orbit excursion to micrometre level are beneficial to minimise feed-down effects and beam life-time, it also imposes constraints on other feedbacks such as tune and chromaticity, the measurements of which rely on transverse excitations and momentum modulation. In the case of the LHC, the tight constraints lead to the development of a robust diode-based tune measurement technique that is capable of detecting nanometre scale beam oscillations ([24]) and that enables a tune and coupling phase-locked-loop (PLL) that can operate with transverse excitation levels below $1\,\mu\mathrm{m}$ [25, 26].

Another possible cross-dependency is given by coupling due to the beam response itself. As described in [27], a robust and reliable tune PLL requires also the measurement and control of global coupling. Classic tune PLL designs ([8,9]) often model the PLL as a first order process defined by the phase detector's filter time constant and open loop gain K_0 that depends on the angle of the phase slope at the location of the tune resonance. In the presence of varying chromaticity, the open loop gains K_0 and thus the optimal controller parameter are functions of chromaticity itself. Using linear control design only, this cross-dependence implies either a controller design that is optimal for large chromaticities, which becomes sensitive to noise and unstable for low values of chromaticity, or a controller design that is optimal for small chromaticities but lags behind the real tune for large values of chromaticity [25, 28].

A more complex example for inter-loop coupling can be illustrated by the LHC, which requires a simultaneous control of orbit, tune, coupling, chromaticity and energy. The foreseen nested control scheme for chromaticity, tune and coupling is shown in Figure 12. The tune PLL is the innermost loop measuring the global tunes and coupling parameters. The loop is first nested within the loop that measures and controls the chromaticity and is then surrounded by the feedback loop controlling the global tunes and coupling. The decoupling is obtained by choosing gradually reduced bandwidths for the tune PLL ($f_{bw} \approx 8\,\mathrm{Hz}$), chromaticity ($f_{bw} \approx 1\,\mathrm{Hz}$) and tune feedback ($f_{bw} < 1\,\mathrm{Hz}$). This nesting hierarchy is required in particular to eliminate the cross-talk between tune and chromaticity feedback, as the tune feedback would otherwise minimise the momentum-driven modulation as well as tune modulation and thus compromise the chromaticity measurement.

In addition, cross-talk is introduced between the chromaticity and orbit/energy feedback through the dispersion orbit driven by the momentum modulation required by the chromaticity feedback. In order to minimise this cross-dependence, the foreseen LHC orbit feedback filters and separates the dispersion orbit from the measured closed orbit prior to performing any orbit correction.

CONCLUSIONS

Beam-based feedbacks can contribute and improve beam parameter stability for perturbations on slow to medium time scales but are ultimately limited by thermal drifts, noise and systematics of involved devices on long time scales from days to months. Systematic and thorough analysis of involved beam instrumentation and corrector circuits are thus essential for achieving best beam parameter stabilisation.

The use of imperfect design beam response does not necessarily affect the precision of the correction but may lead to a reduction of effective feedback bandwidth. This effect can be mitigated by higher sampling frequencies which are usually 40 times higher than the desired feedback bandwidth.

Youla's affine parameterisation provides a simple yet powerful design tool for optimal adaptive non-linear control. Its strength is the explicit controller representation that enables an un-obscured feedback design with respect to closed loop robustness (noise insensitivity) and steering precision. It can further be used to design controllers with adaptive gains that are scheduled depending on the requirements of the applicable operational scenario.

It is advisable to address the incorporation of cross-constraints and coupling of multiple simultaneous nested loops early in the design stage as well as to design feedbacks as an ensemble.

REFERENCES

[1] PSI, Proceeding of "3rd International Workshop on Beam Orbit stabilization", 2004, http://iwbs2004.web.psi.ch/

[2] M. Böge, "Achieving Sub-micron Stability in Light Sources", EPAC'04, Lucerme, Switzerland, 2004

[3] G Decker, "Beam Stability in Synchrotron Light Sources", DIPAC'05, Lyon, France, 2005

[4] R. Hettel, "Beam Stability Issues at Light Sources", 25th ICFA Adv. Beam Dyn. WS., Shanghai, 2002

[5] M. Masuzawa et al. "IP orbital feedback for collision tuning at KEKB", EPAC'00, p. 1211, 2000

[6] J. Wenninger, "Slow BPM Based LEP Orbit Feebdack Control", private communication

[7] L. Hendrickson et al., "Slow Orbit Feedback System for PEP-II", EPAC'00, Vienna, Austria, 2000.

[8] O. Berrig et al., "The Q-Loop: A Function Driven Feedback System for the Betatron Tunes During the LEP Energy Ramp",CERN SL-98-039, 1998

[9] A.Fisher et al., "Tune Feedback in PEP-II",SLAC-PUB-10230, 2003

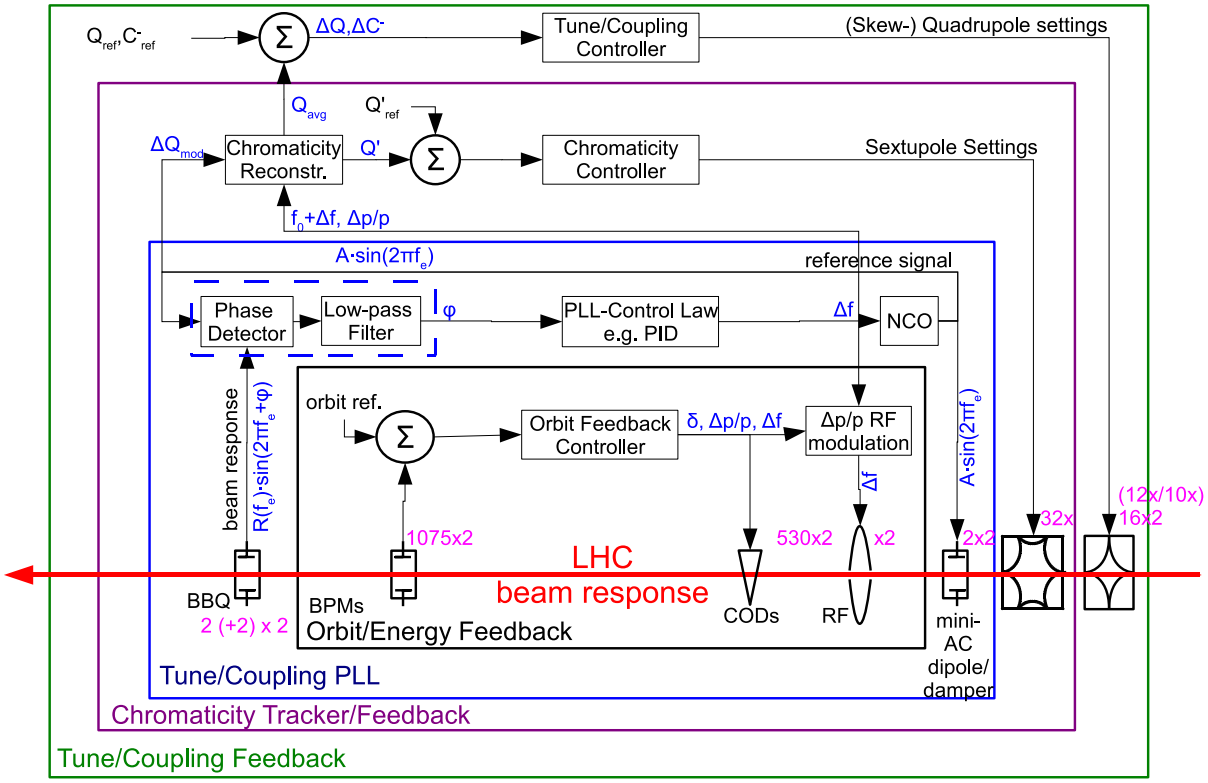

Figure 12: Nested loop scheme required for a coherent control of tune, coupling and chromaticity. The numbers in magenta indicate the total number of beam instruments and corrector circuits connected to the individual feedback loop.

[10] "Damage levels - Comparison of Experiment and simulation", Chamonix XIV and PAC'05, Knoxville/TN, 2005

[11] R. Assmann, "Collimation and Cleaning: Could this limit the LHC Performance?", CERN, Chamonix XII, 2003

[12] S. Redaelli, "LHC aperture and commissioning of the Collimation System", CERN, Chamonix XIV, 2005

[13] TOTEM collaboration, "Technical Design Report", CERN-LHCC-2004-002, p. 21 ff., 2004

[14] S. Fartoukh, O. Brüning, "Field Quality Specification for the LHC Main Dipole Magnets", LHC Project Report 501

[15] R. Assmann et al., "Non-Linearities in the Response of Beam Position Monitors", AIP 546, Boston, MA, 2000, pp. 267-274, CERN-SL-2000-055-BI

[16] T. Schilcher, "Commissioning and Operation of the SLS Fast Orbit Feedback", EPAC'04, Lucerne/Switzerland, 2004

[17] G. Golub and C. Reinsch, "Handbook for automatic computation II, Linear Algebra", Springer, NY, 1971

[18] K.G.J. Jacobi, "Über ein leichtes Verfahren, die in der Theorie der Säcularstörungen [..]", Crelle's Journal, 1846, 30 p. 51-94, 97-144

[19] D. C. Youla et al., "Modern Wiener-Hopf Design of Optimal Controllers", IEEE Trans. on Automatic Control,1976, Vol. 21-1,pp. 3-13 & 319-338

[20] O. Smith, "Feedback Control Systems", McGraw-Hill, 1958

[21] R. J. Steinhagen, "LHC Beam Stability and Feedback Control - Orbit and Energy", CERN-AB-2007-049, 2007

[22] Goodwin, Graebe, Salgado, "Control System Design", Prentice Hall, 2000

[23] B. Anderson, "From Youla-Kucera to Identification, Adaptive and Non-linear Control", Automatica, 1998, Vol. 34, No. 12, pp. 1485-1506

[24] M. Gasior, R. Jones, "The principle and first results of betatron tune measurement by direct diode detection", CERN-LHC-Project-Report-853

[25] R. J. Steinhagen, "First Results of the PLL Tune Tracking in the SPS", Tune Feedback Final Design Review, BNL, $www.agsrhichome.bnl.gov/LARP/061024\_TF\_FDR$

[26] R. J. Steinhagen et al., "The LHC Phase-Locked-Loop for Continuous Tune Measurement - Prototype tests at the CERN-SPS", PAC'07, 2007

[27] R. Jones et al., "Towards a Robust Phase Locked Loop Tune Feedback System", DIPAC'05, Lyon, France, 2005

[28] R. J. Steinhagen et al., "Influence of Varying Chromaticity on Robustness of the LHC Tune PLL and its Application for Continuous Chromaticity Measurement.", PAC'07, 2007

Requirements for Tune, Coupling, and Chromaticity Feedbacks for Light Sources

M.Dehler,
Paul Scherrer Institut, CH-5232 Villigen PSI, Switzerland
e-mail: Micha.Dehler@psi.ch

Abstract

In terms of machine stability, synchrotron light sources generally are relatively tolerant to fluctuations in tune, coupling and chromaticity. The main requirements are coming from the user side, where a tight control over coupling and beam tilt is important, especially in the view of the tendency towards small gap insertion devices. Perturbation sources are user configurable insertion devices and other beam lines, which create fluctuations in the beam optics, which need to be corrected locally. The document describes a measurement strategies and discusses new challenges requiring dynamic stabilization systems.

INTRODUCTION

Synchrotron radiation damping plays a big role in the particle dynamics of synchrotron light sources, the sensitivity to fluctuations in the beam optics is quite different compared to those of e.g. hadron colliders.

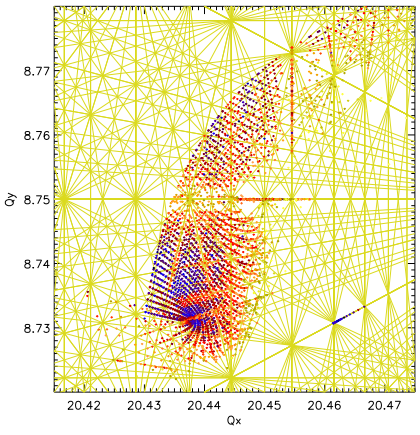

Figure 1: Tune diagram at the swiss light source, the clustering of the points indicate tune resonances (plot court. A. Streun/PSI)

As the example of a tune diagram in figure 1 shows, high order magnet resonances in the optic play a much smaller role leaving more leeway for tune variations. The specific setting of the chromaticity, which influences parameters like energy acceptance, beam life time and the beam size in dispersive sections is normally of even less importance (with exceptions as shown later).

The key parameter of a synchrotron light source is the brilliance, the photon flux density, which is optimized by minimizing the vertical emittance. To be able to employ high field insertion devices used to generate hard x-ray synchrotron radiation, low gap vacuum chambers with vertical apertures of few millimeters are needed, requiring a tight control of vertical beam size and halo to avoid beam losses. As a consequence, there is a strong interest in creating and maintaining a minimum coupling.

In that context, coupling actually stands for two different concepts. One is the global coupling in the horizontal and vertical beam motion, which is typically measured by shifting horizontal and vertical tunes to similar values. The coupling leads to perturbed states, whose amplitude is defined by the global coupling parameter. By contrast, we can have local coupling or beam tilt, which is simply the rotation of the eigenvector denoting the oscillation planes away from the horizontal and vertical axis, something, which is highly interesting in the context of low gap apertures. In principle, one can have non zero local coupling without any global coupling and vice versa.

SOURCES OF BEAM OPTICS FLUCTUATIONS

Orbit jitters in the focusing magnets are one of the dominant sources of optics variations. For these perturbations, the most effective cure is not a feedback on tune but a well functioning orbit feedback. Similar is the effect of varying beam current and the fill pattern leading to a fluctuating heat load on the ring chamber, something which is best handled by top up injection and a fill pattern feedback.

A special case are accelerators using energy ramping. First we have hysteresis in the magnets as well as heat up of the magnet core due to eddy current losses. As the magnets come back to thermal equilibrium, field strength and distribution drifts. These effects are repetitive and predictable, so using a feed forward system is the appropriate remedy.

Where as the perturbation described above are relatively minor for the operation, the big impact is coming from high field, small gap insertion devices as wiggler, super conducting undulators and in vacuum devices. These are typically adjustable by the user, so that a static correction of the nonlinear optics introduced by these devices is not possible. These user adjustments are performed in standard operation, so these action need to be transparent for the global ring optics as well as for other insertion devices and users.

Figure 2 shows a measurement of the tune fluctuations at DIAMOND. Short term, the tunes vary in the order of $10-4$, from run to run this figure goes up to 0.03. Coupling is drifting from the nominal value of 1% up to 2.2%, which

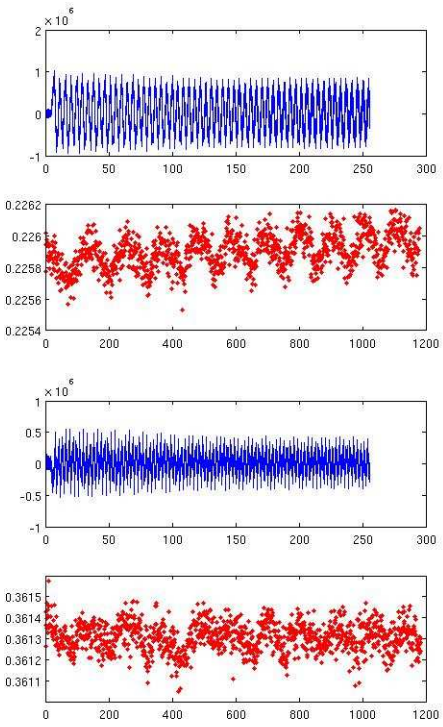

Figure 2: Fluctuations of the horizontal (upper graphs) and vertical tunes (lower graphs) at DIAMOND light source.

is probably due to orbit drift in the sextupoles[1].

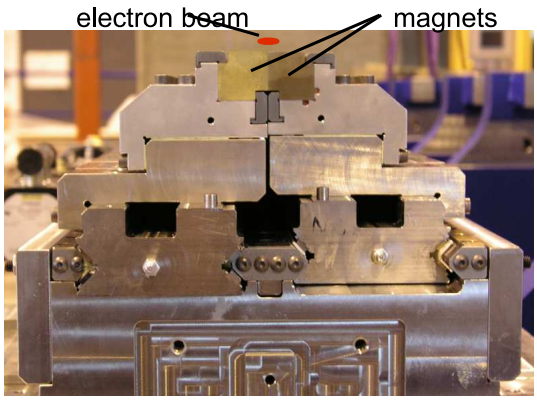

Figure 3: Lower half of an Apple II undulator

As a typical example, figure 3 shows the lower half of an Apple II undulator. The device consists of 4 arrays of permanent magnets, of which two diagonally opposed can be shifted longitudinally. Additionally, the vertical gap can be adjusted. As figure 4 demonstrates, the longitudinal shifts affect the polarization of the generated synchrotron light, allowing all horizontal, vertical and elliptical polarizations. The gap mainly determines the photon energy (apart from also influencing the polarization). The setup is extremely flexible for the users, but is also prone to generate lots of side effects for the beam optics.

A second example concerns the fast polarization switch

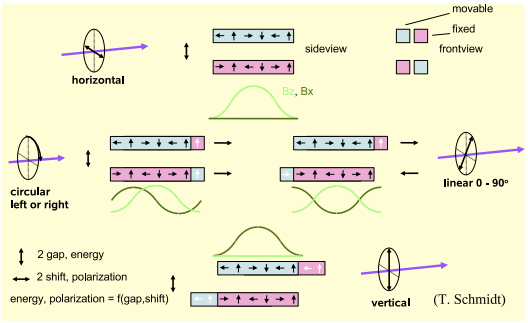

Figure 4: Adjusting photon energy and polarization in an Apple II undulator

of the synchrotron light at a bending magnet beam line[2]. The effect exploited here is, that whereas the synchrotron radiation generated in a bending magnet is polarized horizontally in the plane of deflection, it becomes circular polarized as we move above or below this plane (at the penalty of a decreased photon flux). This a performed at the SLS beam line using a vertical bump generating a beam angle of up to 300 μrad.

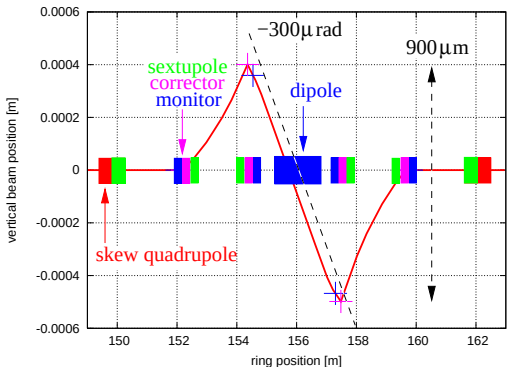

Figure 5: Layout of the vertical asymmetrical “polarization” bump consisting of four successive correctors (bars) for the dipole (thick blue bar) SLS beamline PolLux.

Figure 5 shows the layout of the section containing the beam line. Trajectory perturbation caused by the polarization bump are taken care of by the global orbit feedback, but we have sextupoles within the bump leading to a deterioration in coupling. So dedicated skew quadrupoles were inserted to compensate locally for the effects on the coupling.

Figure 6 shows the quality of the correction. Combined with the global orbit feedback, switching rate for the polarization of up to 10 Hz are expected without affecting other beam lines.

MEASUREMENTS

The inherent noise in electron beams is extremely small, so the most common type of tune measurement uses a driven excitation of the beam either by a frequency sweep

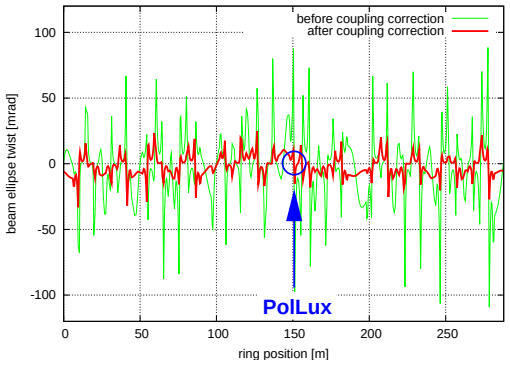

Figure 6: Simulated twist of the electron beam ellipse along beam trajectory for a -300 μrad steering for the PolLux beamline before and after betatron coupling correction.

as at DIAMOND [3] or colored noise as at SOLEIL [4]. A variant is used at the SLS, where residual beam motion during the injection in top up mode is analyzed - the measurement happens only, when there is injection resulting in update rates in the order of a minute.

Another interesting option is available for many bunch by bunch feedbacks as at ELETTRA[5]. Here one has the option of specifying filter characteristics for individual bunches. Setting a negative feedback filter for one of the bunches will cause it to oscillate at the tune frequency. Since this "witness" bunch represents only a tiny fraction of the overall beam current, the measurement will not perturb the user. The difficulty of this approach lies in getting the witness bunch to start the oscillatory motion – sometime the beam noise is too small in starting the instability – and to avoid losing the witness bunch due to too high gains.

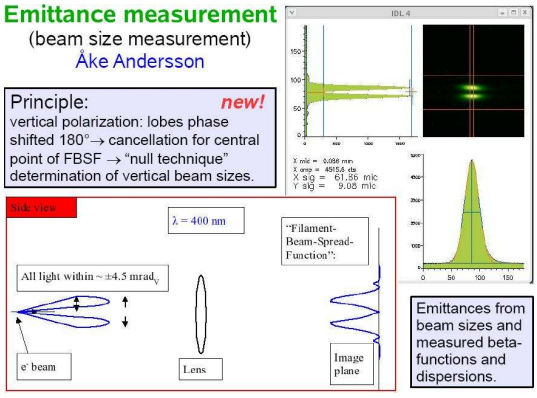

Figure 7: Measurement of vertical beam size/emittance/coupling using the minimum of the double lobes of synchrotron radiation

Coupling is typically obtained by measuring the synchrotron light through a pin hole, where one does a Gaussian fit on the image of the pin hole and deduces the beam size by deconvoluting the effect of the width of the pin hole. Horizontal and vertical beam sizes correspond to the emittances and the ratio gives the coupling. This approach becomes quite challenging, as one goes to extremely small beam sizes and emittances.

An interesting alternative of an synchrotron light measurement[6] is shown in figure 7. The measurement makes use of the fact, that the side lobes of synchrotron light in the vertical plane are 180 degrees out of phase, canceling out each other in the central plane. For synchrotron light in the visible range, this leads to a kind of a transmission function (or filament beam spread function) with two main lobes at a rather big angle of ± 4.5 mrad. A non zero vertical beam size smears out the response, the zero between the main lobes gets filled up.

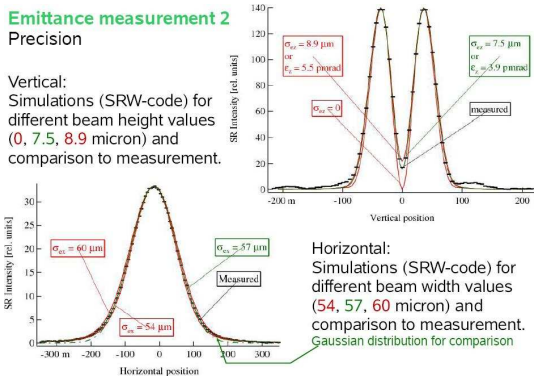

Figure 8: Beam size/emittance/coupling measurement: comparison between simulated and measured data demonstrating the accuracy of the approach.

As the results in figure 8 show, the method is very sensitive even for very small beam sizes. Beams with heights down to 8 μm corresponding to a vertical emittance of 3.5 pm rad have been measured.

FEEDBACKS AND FEED FORWARDS

One of the standard application for tune feedbacks is the stabilization of the machine optics while ramping the beam energy. One of the early systems was in use for a short time at ELETTRA. A problem at that time was always the switch from the fast measurement system used during the ramp to the slow, high precision ones used during the storage, so that is was replaced after some time by a feed forward system.

As an example of a light source using top up mode, figure 9 shows the performance of a tune feedback running at the swiss light source SLS. Since there are only very slow drifts in the system, an update rate of one to few samples per minute is sufficient in stabilizing the tune to few times 10^{-4}.

OUTLOOK

Before talking about optimizing the dynamic behaviour of the fluctuations (resp. the stabilization via feedbacks), let us look at current trends in the design of the beam optics.

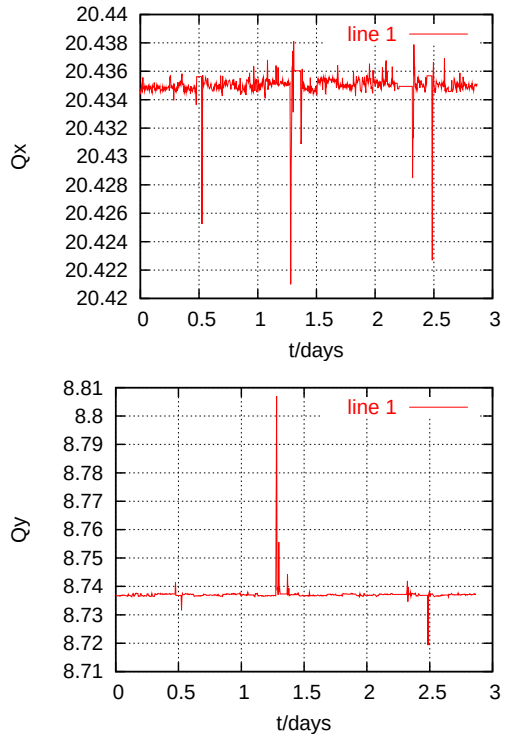

Figure 9: Horizontal and vertical tune at the SLS over a three day period.

Given a certain base line design, further optimization is performed with respect to global and local coupling. The goal is an extremely small vertical beam size allowing small gap insertion devices of a few millimeter height and a small number of halo particles flying at large vertical offsets leading to beam loss inside the device.

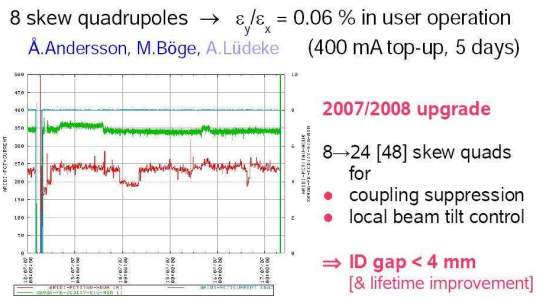

Figure 10: Vertical beam emittance record at SLS due to local control of coupling using skew quadrupoles.

Currently, the SLS employs eight skew quadrupoles to allow this local control of coupling. With these magnets, it was possible to lower the vertical emittance down to a value of 3.5 pm rad (Fig. 10)[8]. For the future, it is planned to go to 24 skew quadrupoles to be able to control coupling and beam tilt in all sectors of the machine.

What does this mean in terms of dynamic stabilization and feedbacks? As the coupling and the vertical emittance goes down, we become more sensitive to fluctuations, which would be invisible otherwise. Machine optimization and performance will get to the point, where feedbacks and/or feed forward will be required despite stable conditions due to features like fast global orbit feedbacks and top up injection. It is less the global parameters, which are of interest, but a local, high precision control of the machine optics, which will drive the development of new dynamic measurement techniques.

REFERENCES

[1] R. Bartolini, priv. communication

[2] M. Böge, U. Flechsig, J. Raabe, T. Schilcher, "Fast Polarization Switching at the SLS Microspectroscopy Beamline POLLUX", proc. EPAC 2006, Edinburgh, Scotland, pp. 3610-3612

[3] G. Rehm, priv. communication

[4] L. Nadolsky, priv. communication

[5] D. Bulfone et al, "Bunch-by-bunch control of instabilities with the ELETTRA/SLS digital feedback systems", proc. ICALEPCS 2003, Gyeongju, Korea, 2003, pp. 32-36.

[6] A. Andersson, "Determination of a small vertical electron beam profi le and emittance at the Swiss light source", submitted to NIM A.

[7] R. Nagaoka et al., "Energy Ramping in ELETTRA", proc. EPAC 1994, 1994, pp. 1812-1814

[8] A. Streun, priv. communication

HERA Proton Transverse Multibunch Feedback with Tune Indicator

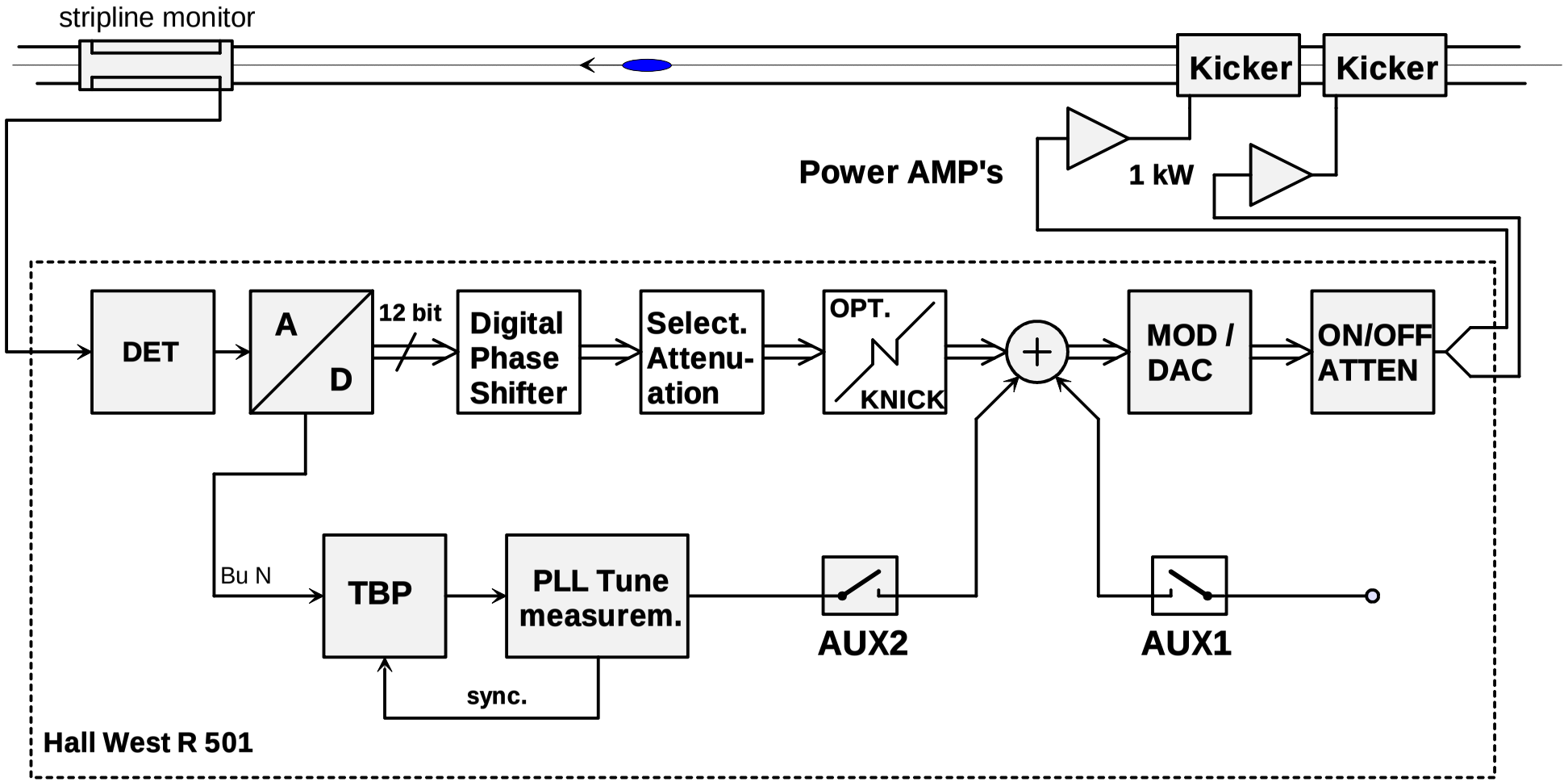

J. Klute, DESY

HERA Proton Tune Indicator

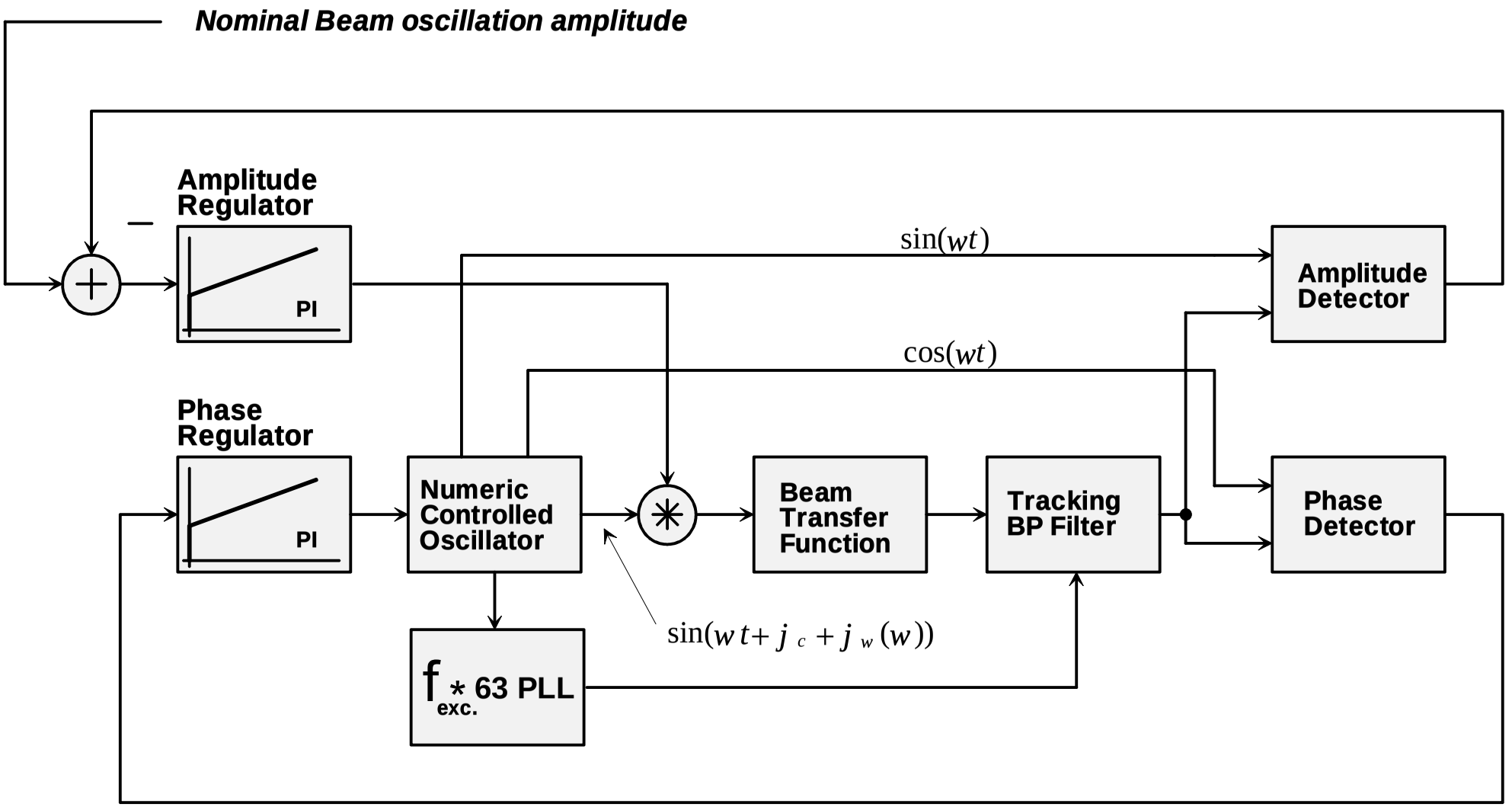

J. Klute, DESY

The Tune Indicator State Machine

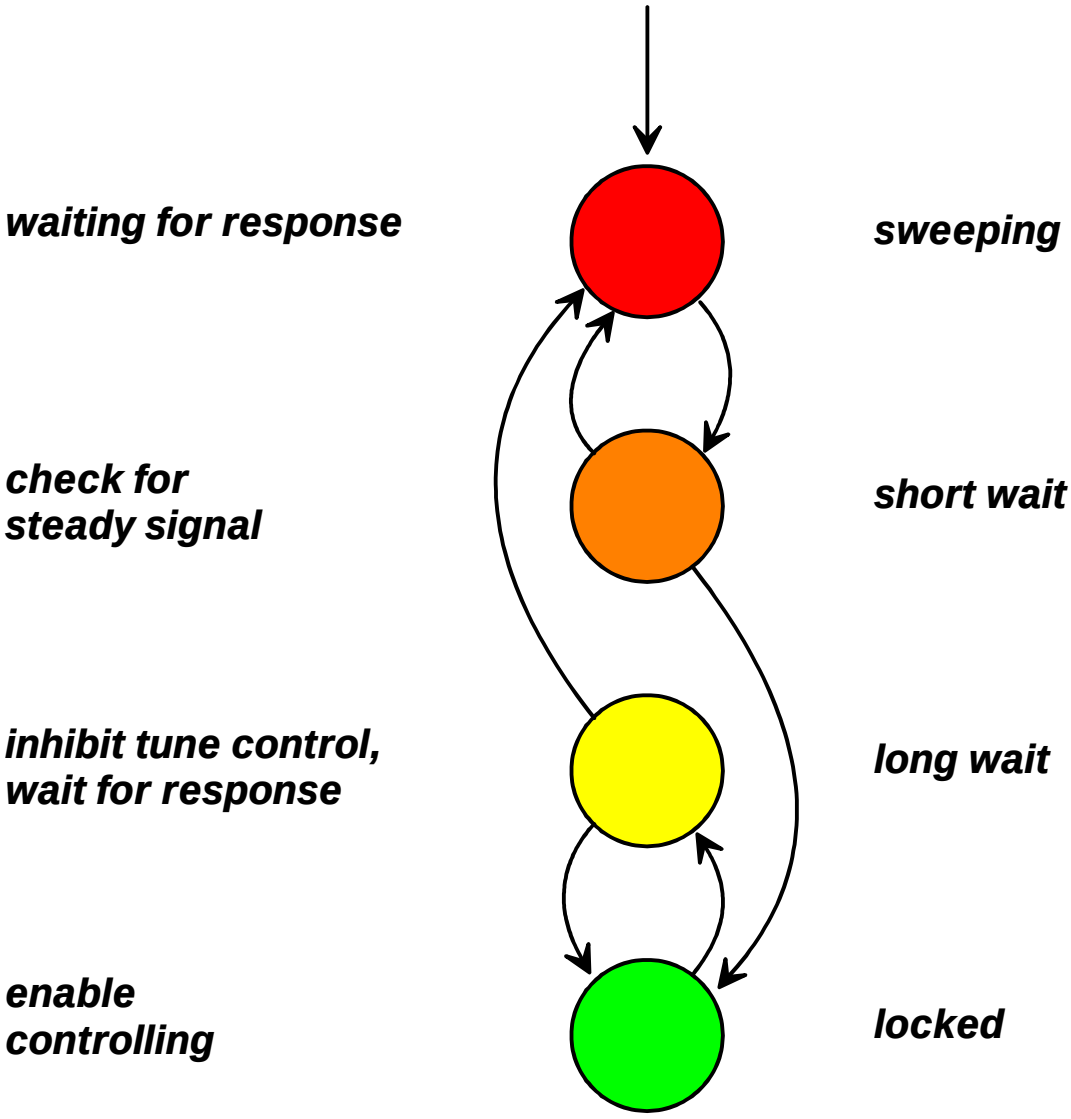

J. Klute, DESY

The noise hole

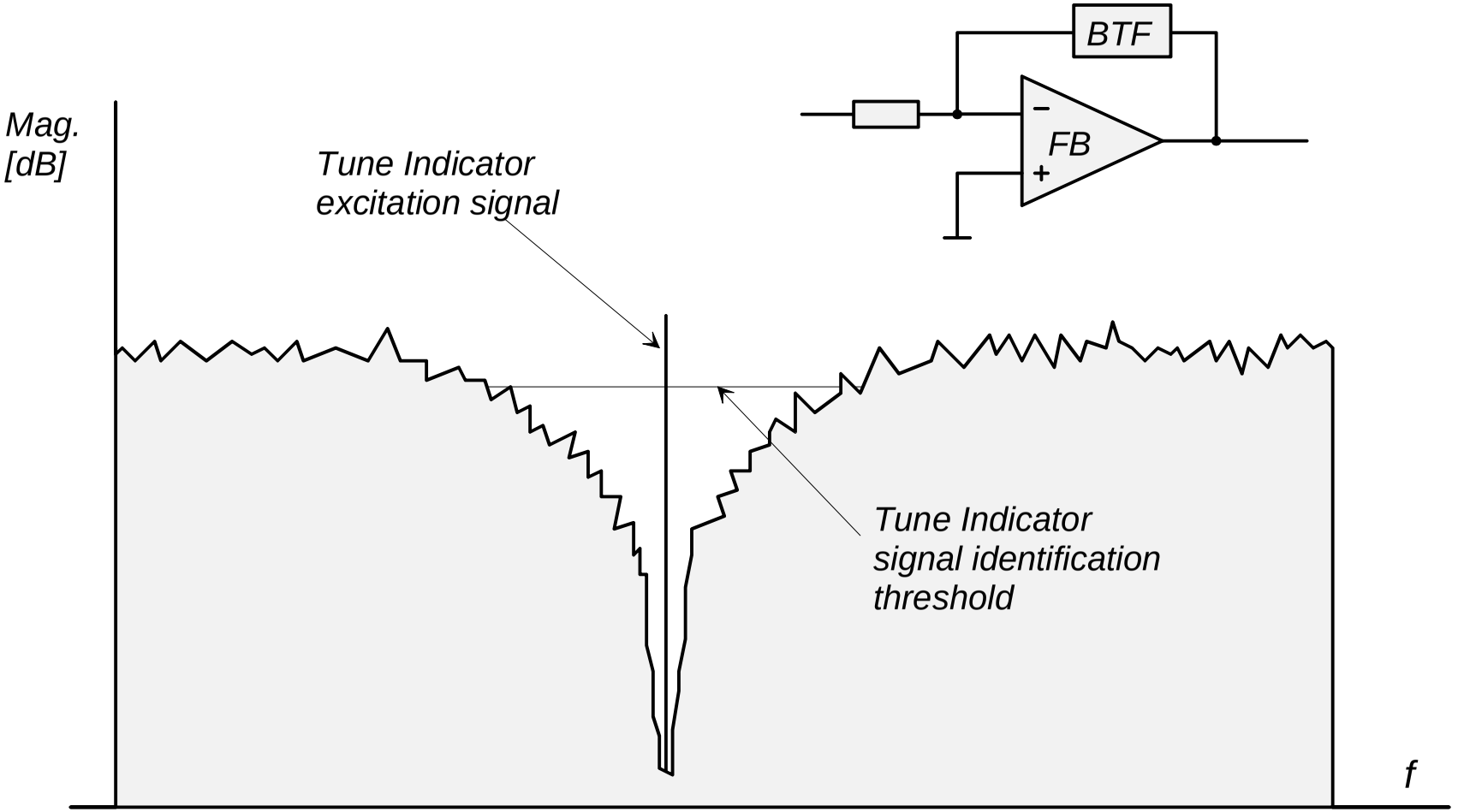

THE LHC PLL SYSTEM FOR Q, Q' AND C MEASUREMENT

A. Boccardi, M.Gasior, O.R.Jones, R.J. Steinhagen, CERN, Geneva, Switzerland

Abstract

A PLL system (QPLL) has been recently developed at CERN for the continuous measurement of LHC tunes, the chromaticity and the coupling parameters. The entire PLL logic has been implemented in an FPGA while the analogue front end is based on the high-sensitivity direct-diode detection technique.

The hardware is virtually identical to that of the standard FFT based tune measurement system developed for the LHC. As a replica of such a system had been tested in 2006 and made operational in 2007 on the SPS it was possible to test the QPLL on this machine by just reconfiguring the FPGA.

During the tests in the SPS with the QPLL it was possible to obtain tune resolution better than 10^{-5} and a resolution of 1 unit for the chromaticity with a radial modulation of $dp/p \sim 2*10^{-5}$ @0.5Hz.

PLL PRINCIPLE

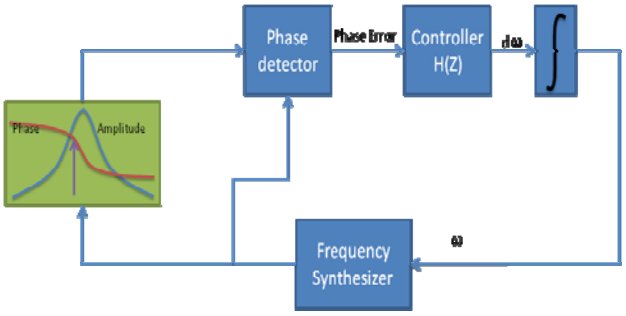

Figure1: PLL functional diagram

The phase difference between sinusoidal excitation and the response of a system to it varies by 180 degrees when moving the excitation frequency across a resonance. This phenomenon is used in a phase locked loop (PLL) system to detect the resonance frequency with high accuracy.

The basic blocks of such systems are a variable frequency tone generator (or frequency synthesizer), a phase detector and a controller of some kind. The generator is used as excitation source for the system for which we want to measure the frequency of resonance. The phase detector measures the phase difference between the generator output and the system's response. This information is used by the controller to modify the frequency of the generator: if the detected phase difference, ignoring an eventual offset, is less than 90 degrees the frequency needs to be increased and if it is more it should be decreased.

Once stability is reached the excitation frequency equals the resonance frequency.

THE HARDWARE CHAIN

The hardware chain of the QPLL is identical to that of the base band, FFT based, tune measurement system (BBQ). Indeed the two can be made into each other just changing the firmware of the FPGA in which the logic is implemented and the front end power PC driver.

In the BBQ system the base band transverse motion of the beam is detected using diodes that detect the envelope of the signal from stripline pickups [1]. This signal, filtered and amplified by an analogue front end, is digitized at a frequency multiple of the revolution frequency using a NIM module equipped with a 24bit audio codec. All the subsequent processing is performed in the FPGA of a general purpose VME board developed at TRIUMF (Canada), the DAB64x. The FPGA logic comprises a digital frequency synthesizer, a phase detector and a controller per plane. The excitation tone, converted to the analogue domain by the codec, is used to

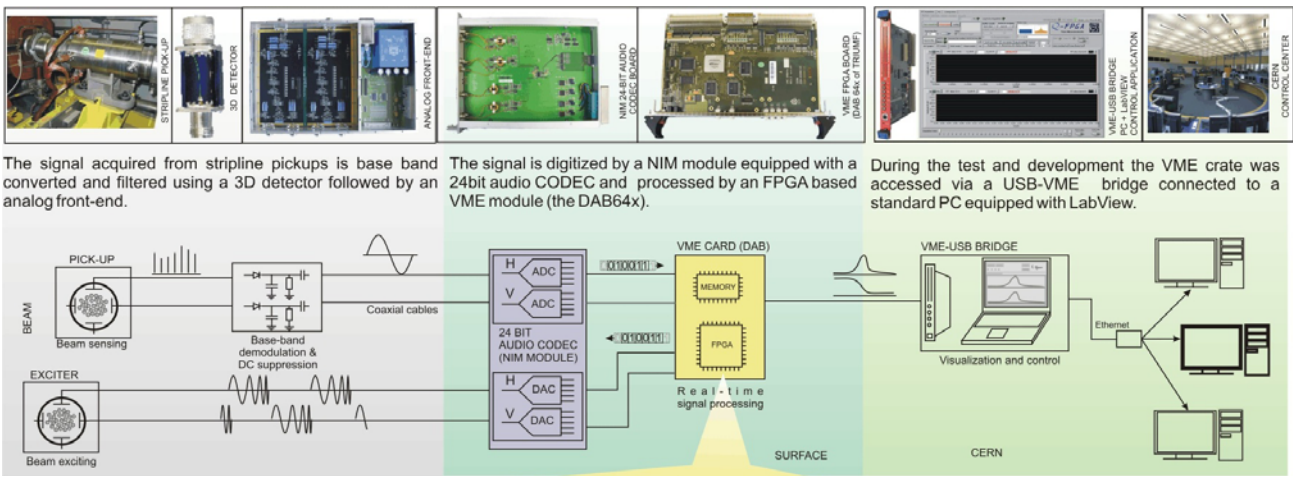

Figure2: The hardware chain

excite the beam using either the excitation channel of the transverse dumper system or a dedicated tickler.

For the lab setup and for the first study of the performances of the system during machine development time (MDs) in the SPS, the QPLL was accessed using a LabView interface running on a standard windows PC. The connection to the VME bus was made possible by a commercial USB to VME bridge and the PC running the front end software was accessed during the MDs using a simple remote desktop connection.

In the final system the standard PC, the LabView software and the USB to VME bridge will be replaced by a power PC sitting directly in the VME crate and running the standard CERN Front End software interface (FESA).

THE QPLL FPGA IMPLEMENTATION

The frequency synthesizer

The main problem in the design of a high precision single tone frequency synthesizer resides in providing sine and cosine values of sufficient accuracy.

The use of a look up table (LUT) to store those values with the required resolution in both amplitude and phase would required an allocated memory space of about 50MB. In terms of silicon space it was therefore more convenient to implement an on line calculator for those values. In particular, as the system is working in base band, the frequency at which those values have to be calculated is orders of magnitude smaller than the clock frequency allowing computation time to be treaded against FPGA space.

The selected algorithm was a coordinate rotation algorithm known as a CORDIC. The sine and cosine values are obtained as the result of the rotation of a vector originally lying on the X-axis. As the rotation can be decomposed into micro rotations of increasing precision the required operation is always the same except for the input vector and the rotation parameters. The same hardware block and silicon space can therefore be reused for all the required steps.

The phase detector

One of the classical phase detection techniques is to multiply the tone for which we want to determine the

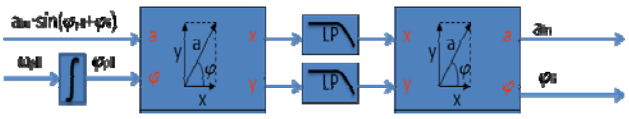

Figure3: the phase detector as a series of rotation

phase by the reference sine and cosine. Once low pass filtered the resulting values are the sine and the cosine of the phase we want to detect, but scaled with the amplitude response value (A_{in}). Those can be considered as the 2 components of a vector whose modulus and phase would be the respectively the amplitude and the phase response of the system. Those values can be extracted by rotating the vector until lies along the X-axis. The x values then represents the modulus while the sum of the rotations required to obtain such a result is the phase.

The implementation of this algorithm can be done using a CORDIC block as for the frequency synthesizer. Indeed even the first sine/cosine multiplication is nothing more than a rotation of a vector whose sole initial component is along the X-axis and is equal to the input value.

This scheme offer a full decoupling of the amplitude and phase information allowing a parameterization of the controller independent of the excitation level and/or beam intensity. It also gives the possibility of adding an additional loop for amplitude control.

The controller

Probably the most common controller is the Proportional/Integral/Differential (PID) controller:

$$D(s) = K_p + K_i \cdot \frac{1}{s} + K_d \cdot \frac{s}{\tau_d s + 1}$$

Where the pole in the differential gain has been added to limit the high frequency noise emphasis introduced by the differentiation.

In the digital domain this can be expressed in its differential form as a simple 2nd order filter:

$$H(Z) = a_0 \frac{(1 - c_1 Z^{-1})(1 - c_2 Z^{-1})}{1 - b_1 Z^{-1}}$$

Indeed it can be proven that for a first order system, or for a first order approximation of it, only the zero linked to c_1 is needed to design an optimal controller, and it is sufficient to match it to the open loop bandwidth [2]. In these conditions the closed loop bandwidth can be steered using just a_0.

Required corrections on the demodulated phase

A simple resonator would have a phase response of about -90 degrees (depending on its quality factor) at its resonance point. Therefore for such a system the detected phase plus 90 degrees would represent the residual phase and could be a suitable input for the controller.

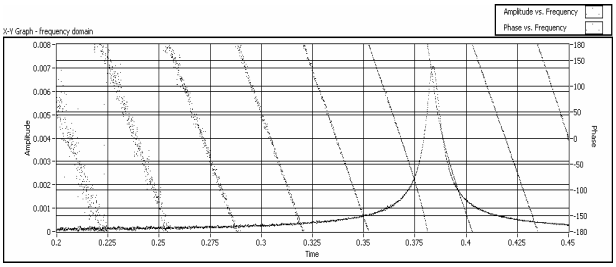

Figure4: a scan of the amplitude and phase response of a simple resonator performed with the QPLL before delay correction

In a real system the phase detected by the phase detector comprises also the effect of the acquisition and excitation chains. In particular the digitalization process can introduce a significant delay and therefore a linear phase shift that is summed to the phase of the resonator. This not only shifts the position of the resonant phase, but

also introduces several artificial phase transitions on which the PLL could erroneously lock. This problem can be easily solved by subtracting a value linearly dependent on the frequency from the detected phase.

The beam is unfortunately not a simple resonator and the presence of resonances other than the betatron tune is possible. Moreover the front end electronics and the exciter are possible sources of phase shift that can also influence the detected phase. It is for this reason that the measured phase must be further corrected with a programmable value that might depend on the working region. Indeed to extend the region in which the PLL can work without a degradation of its precision the constant value should be replaced by a frequency dependent one loaded for example in a look-up table (LUT). The required size of the LUT can be kept small as the residual variations after the delay corrections are small and slow. In the LHC PLL system a 1024 point table is enough to keep the error smaller than 1 degree over the range 0-0.5 frev.

Locking strategies

The locking of the PLL can be critical even after all the applied corrections. The phase transitions due to the synchrotron sidebands are not easy to correct as their location move with the tune and their influence varies with the chromaticity.

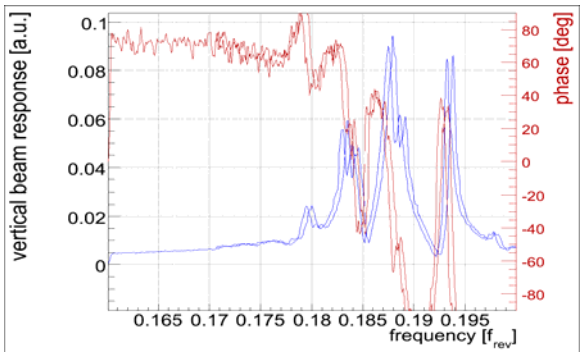

Figure5: a typical Beam Transfer Function (BTF) scan where the synchrotron sidebands are evident and give a phase full phase transition

When such sidebands appear in the beam transfer function as measured by the PLL the PLL can lock on to anyone them or on the central tune peak with no preference. To avoid locking on the wrong resonance a fast BTF scan is first performed for a first rough estimation of the tune position and start the PLL in locking mode at the estimated position. Once locked on the tune peak the PLL will follow it, if its bandwidth is sufficient, and the sidebands will no longer be a problem.

Coupling parameter's measure

The PLL in presence of coupling will detect the eigenmodes of oscillation of the beam on each plane and not the two unperturbed tunes.

Knowledge of the coupling is essential to reconstruct the unperturbed tunes and can be performed starting from the following formulas [3]:

$$\begin{cases} X[n] = A_{1x}\cos[2\pi Q_1(n-1)+\phi_{1x}] + A_{2x}\cos[2\pi Q_2(n-1)+\phi_{2x}] \\ Y[n] = A_{1y}\cos[2\pi Q_1(n-1)+\phi_{1y}] + A_{2y}\cos[2\pi Q_2(n-1)+\phi_{2y}] \end{cases}$$

$$r_1 = \frac{A_{1y}}{A_{1x}} \qquad r_2 = \frac{A_{2x}}{A_{2y}}$$

$$\left|C^-\right| = \left|Q_1 - Q_2\right| \frac{2\sqrt{r_1 r_2}}{1 + r_1 r_2}$$

Where Q1 and Q2 are the eigenmodes and x and y are the oscillations in the horizontal and vertical planes.

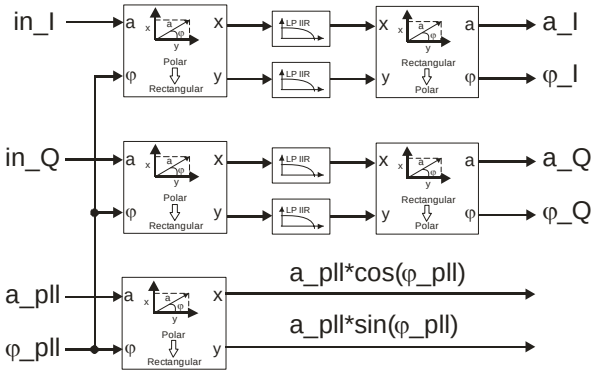

Figure6: block diagram of the QPLL including the coupling parameter extraction (I is the excitation plane and Q the transverse one)

To obtain the 4 amplitudes each PLL needs to demodulate the response from the beam to its excitation on both planes. This method also provides for free the 4 phases, required for coupling feedback [3].

TEST ON THE SPS

During the 2007 SPS run the QPLL was extensively tested. In particular during a machine development run (MD) the QPLL was used to measure chromaticity with the radial modulation method.

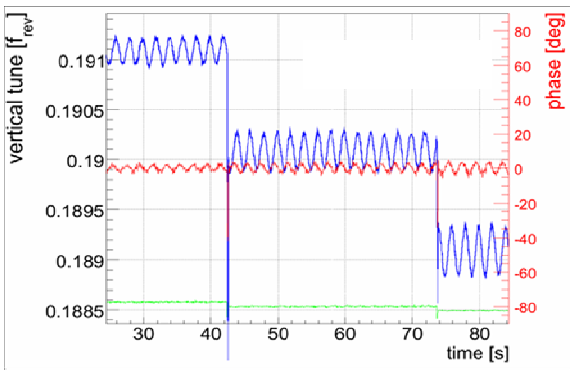

Figure7: part of the tracks of the PLL during the radial modulation test in the SPS. In blue the measured tune, in red the measured phase and in green the amplitude

During the test the PLL was able to achieve a tune resolution of 10^{-5} with the bandwidth set to 2Hz.

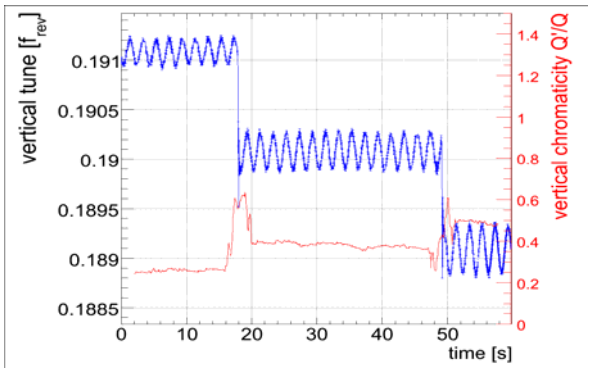

Figure8: part of the tracks of the QPLL. In blue the tune track with the evident modulation and jumps at the change of sextupole strength due to the position offset. In red the estimated relative chromaticity. The chromaticity steps where of 1 absolute unit (Q=26 in the SPS)

This allowed measurement with a modulation depth of just $2*10^{-5}$ dp/p at 0.5Hz while still maintaining a resolution on the chromaticity better than 1 unit as required for the LHC operation.
The tests performed in the SPS proved that the QPLL could also be a valuable tool also for this machine and will therefore be kept as an MD tool in 2008.

REFERENCES

[1] M. Gasior and R. Jones, “High Sensitivity Tune Measurement by Direct Diode Detection”, DIPAC05, Lyon, France, 2005.
[2] Ralph’s paper
[3] Rhodri’s paper